BIOCOMPATIBLE AND SELECTIVE ^{18}F-FLUORINATION REAGENTS FOR THE DEVELOPMENT OF BIOLOGICAL RADIOTRACERS FOR POSITRON EMISSION TOMOGRAPHY

Sofia Otaru

Department of Chemistry
Faculty of Science
University of Helsinki
Finland

DOCTORAL DISSERTATION

To be presented, with the permission of the Faculty of Science of
the University of Helsinki, for public examination in Exactum Auditorium B123
on the 23rd of September 2022 at 1:00 p.m.

Helsinki 2022

Supervisors

Dr. Anu Airaksinen
Professor
Turku PET Centre
Department of Chemistry
University of Turku
Turku, Finland

Dr. Mirkka Sarparanta
Associate Professor
Department of Chemistry
University of Helsinki
Helsinki, Finland

Pre-examiners

Dr. Frederik Cleeren
Assistant Professor
Department of Pharmaceutical and Pharmacological Sciences
Radiopharmaceutical Research
Katholieke Universiteit Leuven
Leuven, Belgium

Dr. Pekka Poutiainen
Head of PET Radiopharmacy
Department of Clinical Physiology and Nuclear Medicine
Kuopio University Hospital
Kuopio, Finland

Dissertation opponent

Dr. Matthias Herth
Associate Professor
Department of Drug Design and Pharmacology
University of Copenhagen
Copenhagen, Denmark

ISNN 0358-7746
ISBN 978-951-51-8503-7 (softcover)
ISBN 978-951-51-8504-4 (PDF)

Unigrafia
Helsinki 2022

The Faculty of Sciences uses the Ouriginal system (plagiarism recognition) to examine all doctoral dissertations.

ABSTRACT

Pathologies that require non-invasive, quantitative, and repeated investigation for treatment follow-up and for patient selection are on the rise due to longer life-expectancy and lifestyle changes. Early treatment and accurate diagnosis are required for curative intervention. Positron emission tomography (PET) offers a non-invasive and quantitative imaging modality for investigating biological processes, namely metabolism and receptor expression in tissues. To achieve the requirements of selectivity and sensitivity, various radiotracers need to be designed, synthesized and evaluated. Anything from small molecules to nanoparticles and biomacromolecules, are utilized as tracers, depending on the imaging target and the kinetics of the process under investigation.

Several tumors over-express on their surface receptors that can be targeted with biomolecules, such as peptides, extremely selectively. Peptides have specific amino acid sequences that interact with the binding site in the receptor, requiring careful design of the radiolabeling modifications in order not to disturb the interaction. Consequently, chemoselective radiolabeling methods are becoming more prevalent in the synthesis of biomolecular radiotracers. Given the high cost of radiopharmaceutical development, the availability of multipurpose, late-stage radiolabeling tools offering rapid radiotracer production from diverse target molecules would lower the development costs and provide wider selection of biological radiotracers for imaging studies.

The aim of this work was to develop fluorine-18-labeled tetrazines for preparing biological radiotracers for PET imaging. The novel tetrazines were studied for their metabolic stability and biological performance and used for *in vitro* radiolabeling of the target biomolecules. Heat sensitive serum albumin protein, and cyclic receptor targeting peptides, were radiolabeled with fast click reactions of the tetrazines providing chemoselective and mild radiofluorination. The first candidate tetrazine, fluorine-18 labeled silicon-fluoride acceptor tetrazine ([^{18}F]SiFA-Tz) with a lipophilic prosthetic group, was found to be metabolically unstable and was further studied for its *in vitro* metabolism pathway in mouse liver microsomes with ultra-high performance liquid chromatography (UHPLC) high-resolution mass spectrometry (HRMS). Structural optimization was done and a metabolically stable and more hydrophilic fluorine-18 labeled alkylammoniomethyltrifluoroborate tetrazine ([^{18}F]AmBF$_3$-Tz) was developed, and evaluated with *in vivo* PET-computed tomography (PET/CT) imaging and *ex vivo* biodistribution studies where it demonstrated excellent stability. [^{18}F]AmBF$_3$-Tz is currently under further investigation for *in vivo* pretargeted PET imaging, due to the highly promising

biological behavior as a standalone radiotracer. [^{18}F]AmBF_3-Tz was subsequently used as a radiofluorination reagent for somatostatin receptor-2 (SSTR2) targeting peptides. The lead peptide tracer was used for PET/CT imaging of preclinical pancreatic carcinoma model, providing clear visualization of the tumor xenografts. The findings presented in this study demonstrate the successful development of a novel radiolabeling tool to produce new biomolecular radiotracers for PET imaging.

ACKNOWLEDGEMENTS

The work presented in this thesis was carried out at the Department of Chemistry, Radiochemistry unit, at University of Helsinki Finland, during years 2017–2020. This study was financially supported by Business Finland, Finnish Society for Nuclear Medicine, Finnish Concordia Fund, and by the Chemistry and Molecular Sciences Doctoral School (CHEMS).

First, I would like to thank my supervisors, Professor Anu Airaksinen and Associate Professor Mirkka Sarparanta for their continuous support, guidance, and vision during this process. I would like to thank Prof. Airaksinen for giving me the opportunity to join TRIM Team. I want to thank you both for the inspiring environment, for keeping an open mind, and for the encouragement towards new ideas. We have shared memorable times together and I have learned so much from you both. The community you have created is amazing and I feel very proud to have been a part of TRIM Team. I wish to thank Associate Professor Matthias Herth for accepting the role of the dissertation opponent. I would also like to acknowledge the pre-examiners of this thesis, Assistant Professor Dr. Frederik Cleeren and Dr. Pekka Poutiainen for reviewing this thesis and for giving valuable and critical comments. I would like to thank Professor Kristiina Wähälä for supervision, mentoring and support during my Master´s thesis in a collaborative research project with Prof. Airaksinen, that concequently led to the start of this journey.

The head of the Radiochemistry unit, Prof. Gareth Law, is thanked for his support, interest in my work, as well as for the great working community created at the unit. I would like to thank my dear friends and colleagues from TRIM Team (past, present, and visitors). Kerttuli Helariutta, Teija Koivula, Ulrika Jakobsson, Surachet Imlimthan, Eliza Lambidis, Dave Lumen, Tiina Ujula, Outi Keinänen, Raymond Li, Andreas Paulus, Sudeep Das, Iida Kuurne, Tatu Martinmäki, Anisa Biti, Alessia Centanni, Kishore Gangangari, Sanjeev Ranjan, Pauline Lang, Chiara Timperanza, Osku Alanen, Marcus Lindgren, Vilma Jallinoja, Isa Coopmans, et al. With you guys all the hard work felt like a vacation and I am so grateful to have made friends like you. So many unforgettable memories, a lot of exciting experiments but also, many fun moments.

I would like to thank my colleagues at Turku PET Centre, University of Turku for the collaboration within this project. Special thanks go to Professor Anne Roivainen, Tatsiana Auchynnikava, Tuula Tolvanen, Helena Virtanen, Heidi Liljenbäck and Aake Honkaniemi.

One of the biggest inspirators during this process has been my dear friend Hanna, whom I admire both as a scientist, as well as a friend. Whenever I needed anything – you were there at any time. It has been priceless to have a friend like you taking this journey together, and then continue our journey beyond together. I would like to thank my friends Outi and Maiju for the priceless support network during these years. I would also like to thank Elisa, Mai, and Suvi for their friendship, support, and all fun times ever since we enrolled in Dept. of Chem. Special thanks go to my family for all their support. My greatest strength comes from this amazing family I am blessed to have; Adebayo, Sirpa, Tero, Niki, Susu, Dansku, Sara, Sirkku, Teuvo, Päivi, and last, but not least Tomi, for taking care of anything and everything required for a normal everyday life whenever needed.

Helsinki, August 2022

Sofia Otaru

TABLE OF CONTENTS

LIST OF ORIGINAL PUBLICATIONS

This thesis is based on the following original publications, which are referred to in the text by their roman numerals.

I **S. Otaru**, S. Imlimthan, M. Sarparanta, K. Helariutta, K. Wähälä, A. J. Airaksinen.
Evaluation of organo[^{18}F]fluorosilicon tetrazine as a prosthetic group for synthesis of PET radiotracers. *Molecules* **2020**, *25*(5), 1208.

II **S. Otaru**, H. Niemikoski, M. Sarparanta, A. J. Airaksinen. Metabolism of a Bioorthogonal PET Tracer Candidate [^{19}F/^{18}F]SiFA-Tetrazine in Mouse Liver Microsomes: Biotransformation Pathways and Defluorination Investigated by UHPLC-HRMS. *Molecular Pharmaceutics* ***2020****, 17, 3106–3115.*

III **S. Otaru**, A. Paulus, S. Imlimthan, I. Kuurne, H. Virtanen, H. Liljenbäck, T. Auchynnikava, T. Tolvanen, A. Roivainen, K. Helariutta, M. Sarparanta, A. J. Airaksinen.
Development of [^{18}F]AmBF$_3$-Tetrazine for the Radiolabeling of Peptides: Preclinical Evaluation and PET Imaging of [^{18}F]AmBF$_3$-PEG$_7$-Tyr^3-octreotide in AR42J Pancreatic Carcinoma Model. *Bioconjugate Chem.* **2022**, *33, 7, 1393–1404.*

IV **S. Otaru**, T. Martinmäki, I. Kuurne, A. Paulus, K. Helariutta, M. Sarparanta, A. J. Airaksinen.
Radiolabeling of Peptides with Inverse electron-demand Diels–Alder reaction: Rapid, Catalyst-free and Mild Conversion of 1,4-Dihydropyridazines to Pyridazines. ***Manuscript (Submitted)***.

AUTHOR CONTRIBUTION IN ORIGINAL PUBLICATIONS

I SO designed and performed the synthesis of the prosthetic group, TCO-modification of albumin protein, radiolabeling, in vitro studies. SO and SI performed the ex vivo studies. SO performed the data analysis and interpretation of results and prepared the figures and wrote the original manuscript and revised it based on comments from co-authors. MS, KH, KW and AA supervised the work.

II SO designed the experimental concept and synthesized of reference compound. SO performed the in vitro studies. SO and HN developed and performed the UHPLC-MS/HRMS experiments, and executed the HRMS and MS/HRMS data analysis and interpretation of results. SO performed the metabolite screening in silico and identification of metabolites. SO prepared the figures, performed the interpretation of the results and wrote the original manuscript and revised it based on comments from co-authors. MS and AA supervised the work.

III SO designed the prosthetic group and its synthesis, designed, and performed the TCO-modifications of octreotide peptides and designed the radiolabeling experiments. SO, AP and IK performed the radiosynthesis and optimization of the radiosynthesis conditions. SO designed and performed the in vitro stability studies and performed the cell-uptake assays. SO, AP and SI performed the ex vivo studies, of which SO and AP performed the ex vivo and radiometabolite analysis. HV, HL and TA performed the PET/CT imaging and ex vivo after PET/CT. TA and HV performed the image analysis of PET/CT images. TT performed the dosimetry calculations. SO prepared the figures, overall data compilation and interpretation of the results, wrote the original manuscript and revised it based on comments from co-authors. AR, KH, MS and AA supervised the work.

IV SO designed and synthesized the novel prosthetic group and designed the experimental concept. IK and TM synthesized together the second prosthetic group used in the study. SO designed and synthesized the TCO compound and the experimental concept. SO developed the TCO-conjugation and together with TM performed the TCO-modification of the peptides. SO, TM, IH and AP executed the radiolabeling

experiments. SO and TM performed the cell uptake assays. SO, TM and AP performed the in vitro studies and optimized the IEDDA conversion conditions. SO performed the data analysis, interpretation of results, prepared the figures, wrote the original manuscript, and revised it based on comments from co-authors. KH, MS and AA supervised the work.

Abbreviations

α-MSH	alpha melanocyte-stimulating hormone
Ac	acetyl
ACN	acetonitrile
A_m	molar activity
$AmBF_3$	alkylammoniomethyltrifluoroborate
$AmBF_3$-TATE	alkylammoniomethyltrifluoroborate octreotate
$AmBF_3$-Tz	alkylammoniomethyltrifluoroborate tetrazine
A_{Oct}	activity in octanol
A_{PBS}	activity in PBS
aq	aqueous
BSA	bovine serum albumin
Bz	benzoyl
COX-2	cyclooxygenase-2
CT	computed tomography
CuAAC	copper-catalyzed azide alkyne cycloaddition
DAD	diode-array-detector
DBPOF	di-tert-butyl-organofluorophosphine
DBPOF-$COOC_6HF_4$	2,3,5,6-tetrafluorophenyl-2-(*tert*-butylfluorophosphoryl)-2-methylpropanoate
DC	decay-corrected
DHP	dihydropyridazine
DOTA	1,4,7,10-tetraazacyclododecane-1,4,7,10-tetraacetic acid
DMSO	dimethyl sulfoxide
[^{18}F]FBA	[^{18}F]fluorobenzaldehyde
[^{18}F]FB-amine	[^{18}F]fluorobenzylamine
[^{18}F]FDG	2-[^{18}F]Fluoro-deoxy-d-glucose
[^{18}F]FDR	5-deoxy-5-[^{18}F]fluoro-d-ribose
[^{18}F]FDG-Tz	[^{18}F]fluorodeoxyglucose tetrazine
[^{18}F]FDR-Tz	[^{18}F]fluorodeoxyribose tetrazine
FET-βAG-TOCA	fluoroethyltriazole-Tyr^3-octreotate
GBq	giga(10^9)becquerel

HetSiFA	heteroaromatic silicon-fluoride acceptor
HCD	higher-energy collisional dissociation
HPLC	high-performance liquid chromatography
HPLC-DAD-ESI-MS	high-performance liquid chromatography-diode-array-detector- electrospray ionization-mass spectrometry
HRMS	high-resolution mass spectrometry
^{18}F-HSA	human serum albumin
HYNIC	hydrazinonicotinic acid
HYNIC-HSA	hydrazinonicotinic acid-functionalized human serum albumin
IE	isotopic exchange
IEDDA	inverse electron-demand Diels-Alder
K2.2.2	kryptofix
LC-MS	liquid chromatography-mass spectrometry
mAbs	monoclonal antibodies
MBq	mega(10^6)becquerel
MC1R	melanocortin 1 receptor
MIP	maximum intensity projection
MLM	mouse liver microsomes
MRI	magnetic resonance imaging
MSA	mouse serum albumin
MS	mass spectrometry
MS/HRMS	high-resolution mass spectrometry fragmentation experiments
MeOH	methanol
MWCO	molecular weight cut-off
N. A.	not applicable
N. D.	not determined
N. C. A.	no-carrier-added
NADPH	nicotinamide adenine dinucleotide phosphate
NEB	NOTA-Evans Blue
NET	neuroendocrine tumor

NHS	N-hydroxysuccinimide
NMR	nuclear magnetic resonance
NODA	1,4,7-triazacyclononane-1,4-diacetate
NOTA	1,4,7-triazacyclononane-N,N-triacetic acid
ox.	oxidized
PBS	phosphate-buffered saline
PET	positron emission tomograpy
ppm	parts per million
QMA	quaternary methylammonium
radio-HPLC	radio-high-performance liquid chromatography
RCY	radiochemical yield
ROI	regions-of-interest
RSA	rat serum albumin
SCID	severe combined immunodeficiency disease
SFB	N-succinimidyl-4-fluorobenzoate
SiFA	silicon-fluoride acceptor
SiFA-Tz	silicon-fluoride acceptor tetrazine
S_N2	bimolecular nucleophilic substitution
S_NAr	nucleophilic aromatic substitution
SPECT	single photon emission computed tomography
SSTR	somatostatin receptor
SSTR2	somatostatin receptor-2
SuFEx	sulfur fluoride exchange
SUV	standardized uptake value
TATE	octreotate
TBAF	tetrabutylammoiumfluoride
TBAOH	tetrabutylammoiumhydroxide
TATE	tyr^3-octreotate
TCO	trans-cyclooctene
TFPE	tetrafluorophenylester
TLC	thin-layer chromatography
TOC	tyr^3-octreotide
Tz	tetrazine

UDPGA	uridine diphosphate glucuronic acid
UHPLC	ultra-high-performance liquid chromatography
UV	ultraviolet

1 INTRODUCTION

Modern imaging modalities have enabled the development of non-invasive detection methods for metabolic disorders, cancer, and central nervous system imaging. Based on recent reports, several types of cancers declining in the older population are on the rise in younger adults, with indications of earlier onset.[1, 2] The development of selectively targeting agents are a prerequisite for accurate and early detection of various cancers, anticipated to have a direct correlation in lowered mortality and better treatment response.[3] Solid tumors often overexpress several receptors, such as the somatostatin receptor (SSTR) subtypes that can be used for targeted delivery of imaging and therapeutic agents to the tumor site.[4, 5] Identifying the subtype of a cancer is critical for selecting the most effective treatment and for maximizing the likelihood of positive clinical outcomes.[6, 7]

Various biomolecules harness an innate and extraordinary potential in their selective targeting capacity towards receptors in the human body. This feature is increasingly utilized in cancer imaging, radioligand therapy, and the development of biomolecule-based radiopharmaceuticals for nuclear medicine in preclinical and clinical research.[8, 9] The exceptional potential of targeting receptors overexpressed on most tumors, offered by biopharmaceutics, requires an accompanying tool, a sensitive and selective diagnostic method to trace the accumulation of the biopharmaceutical at the target site.[9]

Positron emission tomography (PET) imaging offers a non-invasive imaging modality, simultaneously fulfilling those requirements. PET imaging utilizes positron emitting radionuclides bound to a compound, which concequently serve as radiotracers, to track and visualize biological processes or targets.[10] Small molecules, as well as bulkier biomolecules such as monoclonal antibodies (mAbs), their fragments such as fragment antigen-binding regions, as well as peptides and peptidomimetics are used as PET imaging agents. Clinically, the most utilized PET radionuclides are fluorine-18, gallium-68, and carbon-11. The widely available aqueous (aq) nucleophilic [^{18}F]fluoride with ideal nuclear properties, has facilitated efforts in the development of new fluorine-18 imaging agents.[11] [^{18}F]Fluoride can be used in various chemical reactions, and is utilized widely as a radiolabel to date. The radiolabeling of small molecules with [^{18}F]fluoride require sophisticated radiosynthesis apparatus and careful design to avoid altering the desired chemical properties, and hence, the targeting capacity of the compound, as well as designing metabolically the utmost robust radiopharmaceuticals. When radiolabeling compounds aimed to target saturable motifs such as receptors, particular attention must be paid to the radiosynthesis reaction efficacy for maximizing

the signal-to-background ratio by ensuring higher A_m. Furthermore, the degradation of the possible targeting moiety in the biomolecule, or the decomposition of its tertiary and quaternary structures, due to used reaction conditions, is to be naturally avoided. Prosthetic groups or bifunctional chelators are generally utilized as a mild method for incorporating a radionuclide to a complex biomolecule.[12]

The so-called "fluorophilic" elements (Si, B, P, Al) are attracting increasing attention in the development of novel radiotracers, as they offer a rapid incorporation of the [^{18}F]fluoride to the compound by isotopic exchange (IE) or by chelators, as in the case of aluminum.[13-16] These recent advances in the development of fluorophilic prosthetic group bearing compounds, especially of silicon-fluoride acceptor (SiFA) and alkylammoniomethyltrifluoroborates ($AmBF_3$) structures, have demonstrated high promise in preclinical studies and have, just recently, led to clinical trials of highly promising Tyr^3-octreotate (TATE) radiopeptide tracers ^{18}F-SiFA*lin*-TATE,[17-20] and ^{18}F-$AmBF_3$-TATE, both targeting SSTR.[21]

This thesis describes the development and evaluation of two prosthetic groups, fluorine-18 labeled silicon-fluoride acceptor tetrazine ([^{18}F]SiFA-Tz) and fluorine-18 labeled alkylammoniomethyltrifluoroborate tetrazine ([^{18}F]$AmBF_3$-Tz), as universal radiolabeling tools for biological molecules by rapid IE reaction for PET imaging. The purpose of this study was to develop a radiolabeling tool that would provide a radiosynthesis method for sensitive biomolecules, and to evaluate the stability of the prosthetic groups and the developed biological radiotracers *in vitro* and *in vivo*. Serum albumin protein and peptides, neuroendocrine tumor (somatostatin receptor-2; SSTR2) targeting Tyr^3-octreotide (TOC) and a melanoma (melanocortin receptor) targeting alpha melanocyte stimulating hormone (α-MSH) peptide, were radiolabeled with the newly developed prosthetic groups. The influence of the prosthetic groups in the pharmacokinetics and the biological performance of the ^{18}F-labeled biomolecules were evaluated. As a consenquence of the findings in this study, a relevant and previously unreported proposed metabolism pathway participating in defluorination of a SiFA prosthetic group was provided. [^{18}F]$AmBF_3$-Tz, on the other hand, was shown to posess ideal characteristics as a prosthetic group. The novel prosthetic group could also serve as a tool for *in vivo* pretargeting purposes for biomolecules of bulkier size and slow kinetics. Both TOC and α-MSH analogs were used to study the optimal reaction conditions of inverse electron-demand Diels-Alder (IEDDA) cycloaddition for controlling the formed redox products, and a rapid conversion of the reduced dihydropyridazine (DHP) cycloadducts into pyridazine cycloadducts were achieved in mere minutes (10-20 min) and mild conditions (60 °C, ≥95% water). The results described in this study provided a new highly promising and potentially universal tool applicable for *in vitro* radiolabeling of *trans*-cyclooctene (TCO) modified biomolecules, such as

peptides. The relevance of these findings, are closely tied to the currently pressing need for rapid development of novel radiotracers for disease identification, monitoring, and patient selection, especially in oncology.

2 REVIEW OF THE LITERATURE

2.1 POSITRON EMISSION TOMOGRAPHY

2.1.1 PRINCIPLE OF PET IMAGING

PET imaging is a nuclear imaging modality where compounds containing an unstable radioactive nuclide, that decays by positron emission (β^+), are utilized as markers for non-invasive detection of physiological processes using a PET camera. The positron emitted from the nucleus, has a positive charge and a mass equal to a free negatively charged electron, making it the antiparticle of electron.[22] Once positron comes into contact with its counterpart, electron, a subsequent annihilation event takes place, where the two particles are converted into two emitted gammas (511 keV), that are detected on the opposite sides of the detector in a 180° angle. This phenomenon is called the annihilation and the path travelled by the annihilation gammas, the line-of-response.[22] The line-of-response event is detected on opposites sides of the circular row of the scintillation detectors within an accepted time-window. The signals resulting from the annihilation gammas are reconstructed into a 3D-image of the study subject (**Figure 1**). PET imaging is generally accompanied by a complementary imaging modality, such as computed tomography (CT) or magnetic resonance imaging (MRI), for acquiring structural information of the study subject. PET imaging is quantitative and the concentration of the labeled compound, and inversely, the biological process kinetics or concentration, can be measured.

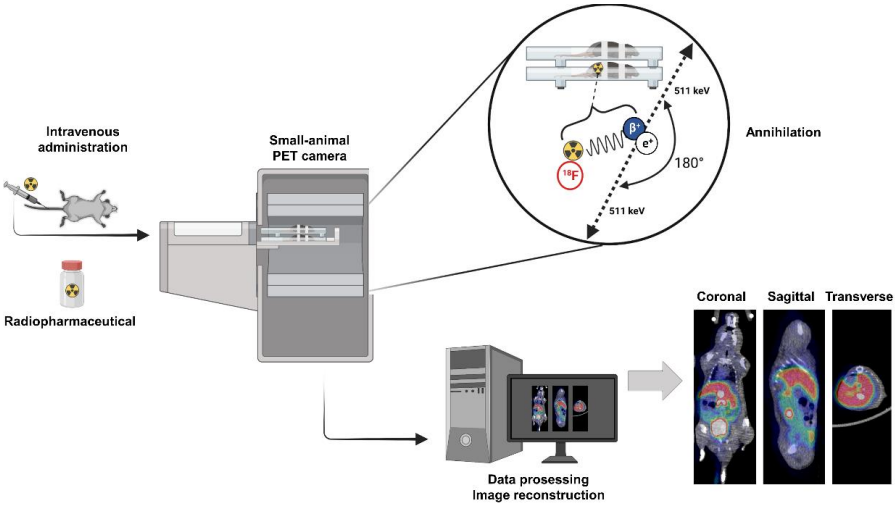

Figure 1. Principle of PET imaging (Graphic created with BioRender, © S. Otaru 2022).

The sensitivity of PET imaging is superior to single photon emission computed tomography (SPECT) imaging, owing to the differences in the detection method.[23] SPECT imaging records individual emitted gamma rays at the decay event with collimators capable of collecting approximately 0.01% of all events, thus exhibiting lower geometric detection capacity. PET, on the other hand, detects the secondary emission, simultaneous gamma rays formed after annihilation without the need for collimators, ruling out individual scattered gamma rays from the image reconstruction.[24] PET imaging has the capability to detect more of the emission events, approximately 1% of all events, offering higher sensitivity for the depiction of the target. In preclinical settings the resolution of SPECT is slightly better than for PET.[23] Unlike in SPECT, the spatial resolution of PET is dependent on the energy at which the positron is emitted from the decaying nucleus. Based on this energy, the positron travels a distance in the tissue, and the distance increases with increasing energy. Soft tissue in the subject body can produce artifacts in the image, that are compensated by attenuation correction, which is relatively easily achieved in PET.[24] Typical SPECT nuclides have longer half-lives, enabling imaging of slower biological processes in the study subject for hours or days after tracer administration. As an advantage, SPECT allows for dual tracer imaging by monitoring multiple energy-windows at the same time, a method not possible with PET detecting only 511-keV gammas, regardless of the radionuclide.

As PET does not detect only structural information of the tissue it travels in, but also its energy metabolism and receptor expression, PET imaging is used for functional, molecular, metabolic, enzyme concentration, and drug-receptor interaction imaging.[10] PET imaging is restricted in capacity to give anatomical information of the study subject and hence, complementary imaging modalities such as CT imaging is used to accurately align the PET data with the CT, conveying the whole study subject structure.

2.1.2 POSITRON EMITTERS IN PET IMAGING

Positron emitters, such as carbon-11, fluorine-18, gallium-68, and oxygen-15 are the most used positron emitters in clinical applications. The wide availability, low positron energy and favorable half-life of fluorine-18, has led to its desirability and extensive utilization in clinical PET imaging. Other longer lived positron emitters, such as zirkonium-89 or iodine-124 can be utilized for imaging processes with slower pharmacokinetics, such as the antibodies that can travel for days until reaching their target and clearing from the blood stream.[25] The selection of appropriate radionuclide depends on the production capabilities, required transportation time, and the process kinetics under investigation. Moreover, the realistically achievable radioactivity per mol of the compound, namely molar activity (A_m), can have a

tremendous influence on the image signal-to-noise outcome, as was demonstrated using [^{18}F]fallypride to image saturable dopamine D2/D3 receptor system.[26]

From the relatively short-lived positron emitters, fluorine-18 has the longest half-life (109.8 min) in comparison to the radioisotopes carbon-11, nitrogen-13, and oxygen-15, all of which have half-lives of 20 minutes or less and ^{68}Ga which has a halflife of 68 minutes. (**Table 1**). Radioisotopes carbon-11, nitrogen-13, oxygen-15 and fluorine-18 are all produced with a cyclotron, while gallium-68 can be produced by cyclotron or by eluting from a generator. The relatively long half-life of fluorine-18 makes complex and multidose synthesis, purification, and quality control of the final product possible, as well as flexible transportation timelines of the radiopharmaceutical, or fluorine-18 itself, from its production location to an off-site imaging center. Positron emitters copper-64 and iodine-124, also produced by cyclotron, with half-lives of hours (12.7 h) to days (4.18 d), respectively, are well suited for the long circulation-time and slow kinetics of biomacromolecules such as antibodies, as well as nanoparticles.[27] Radiometals gallium-68, zirconium-89 and copper-64 offer a facile radiolabeling strategy *via* chelator chemistry, generally applicable to a kit-like radiolabeling setup. Fluorine-18 has the lowest positron energy (0.63 MeV) from the above mentioned (0.65-1.9 MeV) radioisotopes, which results in the positron travelling the shortest distance in the tissue. This short distance of travel before annihilation is the reason for the high resolution of the image (1.5 mm) while utilizing fluorine-18 as the positron emitter.[28] It is often regarded, for the aforementioned reasons, that fluorine-18 indeed has optimal nuclear properties for positron emission tomography. Small animal PET imaging has a resolution capacity of 0.7 mm and clinical PET imaging is at a range of ≥4 mm. The nuclear properties of the most relevant PET radionuclides and most common nuclear reactions for their production are presented in **Table 1**.[27, 29]

The abundance of carbon, oxygen and nitrogen in organic compounds provide optimal vehicles for isotopically labeled compounds, enabling the study of drug metabolism at a single atom level, providing understanding of the stability, soft-spots and behaviour of pharmaceuticals in a biological system. Fluorine only rarely is present in organic compounds and is generally used for substituting a single hydrogen or a hydroxy group, in the structure. A method widely utilized in medicinal chemistry to substitute a hydrogen or hydroxy group present in a compound often alters its stability, biological behaviour and receptor binding, requiring a separate and indepth evaluation of the fluorine-18/fluorine-19 containing analog *in vitro* and *in vivo*.[30]

Table 1. Physical properties of positron emitters. Table adapted from references [25, 29].

Nuclide	$t_{1/2}$	Decay mode and %	$E_{max.}$ [MeV]	$E\beta+_{avg.}$ [keV]	$R_{max.}$ in H_2O [mm]	$R_{avg.}$ in H_2O [mm]	Production
^{11}C	20.4 (min)	99.8 (β^+) 0.2 (EC)	0.96	385	3.8	1	$^{14}N(p,\alpha)^{11}C$
^{13}N	9.97 (min)	99.8 (β^+)	1.19	491	5	1.5	$^{16}O(p,\alpha)^{13}N$
^{15}O	122.2 (s)	99.9 (β^+)	1.73	735	7.6	2.7	$^{14}N(d,n)^{15}O$
^{18}F	109.8 (min)	96.7 (β^+) 3.3 (EC)	0.63	242	2.2	0.3	$^{18}O(p,n)^{18}F$
^{68}Ga	67.7 (min)	89.1 (β^+) 11 (EC)	1.89	740	13.6	3.7	$^{68}Ge/^{68}Ga$ generator
^{64}Cu	12.7 (h)	17.4 (β^+)	0.65	278	2.5	0.7	$^{63}Cu(n,\gamma)^{64}Cu$ $^{64}Ni(p,n)^{64}Cu$
^{89}Zr	78.5 (h)	22.7 (β^+)	0.90	395	3.8	1.3	$^{89}Y(p,n)^{89}Zr$*
^{124}I	4.18 (d)	22.4 (β1+, β2+) (11.7, 10.7)	1.5 (β_1^+) 2.1 (β_2^+)	188	9.7	3	$^{124}Te(p,n)^{124}I$ $^{125}Te(p,2n)^{124}I$ $^{124}Te(d,2n)^{124}I$

avg = average

max = maximum

MeV = megaelectron volt

*=Ref. [31]

2.2 NUCLEOPHILIC [^{18}F]FLUORIDE

2.2.1 PRODUCTION BY ^{18}O(*P*,*N*)^{18}F NUCLEAR REACTION

Fluorine-18 is a cyclotron produced positron emitter with ideal nuclear physical characteristics, which can be produced in its electrophilic [^{18}F]fluorine (F^+) or nucleophilic [^{18}F]fluoride (F^-) form, by $^{18}O_2(p,n)^{18}F$(gas) to produce [^{18}F]fluorine gas or by $H_2{}^{18}O(p,n)^{18}F$(aq) as [^{18}F]fluoride anion in aqueous solution.[11] Production of [^{18}F]fluoride by $^{18}O(p,n)^{18}F$ nuclear reaction utilizes highly isotopically enriched (≥98%) oxygen-18 water ($H_2{}^{18}O$) as a liquid target, which is bombarded with a proton beam, substituting and subsequently ejecting a neutron from the nucleus, thus forming an unstable ^{18}F-nucleus comprising 9 neutrons (*n*) and 9 protons (*p*). This unstable ^{18}F-nucleus is the lightest unstable nucleus with even *p* to *n* number, which decays by positron emission (97%) and electron capture (3%), and has a halflife of 109.7 min.

No-carrier-added (n.c.a.) [^{18}F]fluoride offers the optimal starting point for producing radiopharmaceuticals with high A_m. This makes [^{18}F]fluoride well suited for radiolabeling of compounds used to image even saturable targets such as receptors. N.c.a. [^{18}F]fluoride is a prerequisite for radiolabeling by isotopic exchange for ensuring adequate A_m, due to the stable isotopic fluorine (^{19}F) already present in the non-labeled compound substrate, called the precursor. Furthermore, stable fluorine-19 is often also leached to the system generally from the Teflon transportation lines leading to the synthesis unit. The nucleophilific [^{18}F]fluoride can be utilized in a plethora of radiolabeling reactions with a variety of requirements for reaction conditions.[11] The radiolabeling of small molecules with [^{18}F]fluoride require planning to avoid altering the chemical characteristics by, for example uncontrolled substitution to unintended positions.[32] When radiolabeling larger compounds, such as peptides, particular attention must be paid to the radiolabeling efficiency for maximizing the signal-to-background ratio and receptor visualization with higher A_m,[26] and to avoiding the degradation of the possible targeting moiety in the biomolecule due to reaction conditions.

2.2.2 NUCLEOPHILIC RADIOFLUORINATION (S_N2 AND S_NAR)

[^{18}F]Fluoride anion is hydrated by water molecules in aqueous solution,[33] dramatically decreasing its reactivity, and thus needs to be rendered more nucleophilic for nucleophilic aromatic substitution (S_NAr) and bimolecular nucleophilic substitution (S_N2) reactions, by introducing a bulky counterion.

Conventionally, tetrabutylammoiumhydroxide (TBAOH) is used to form tetrabutylammoniumfluoride (TBAF), and Kryptofix 2.2.2 (K2.2.2) crown ether, together with K_2CO_3, rendering reactive and highly nucleophilic but alkaline formulations of "naked" [^{18}F]fluoride. The bulky counterion makes the [^{18}F]fluoride extremely nucleophilic, and accelerates the radiofluorination reaction speed. Prior to radiolabeling, the water that contains the [^{18}F]fluoride anion, is azeotropically distilled out together with acetonitrile (ACN), leaving a dry [^{18}F]fluoride-Kryptofix complex residue ready for radiolabeling. This way the fluoride is rendered more reactive towards nucleophilic substitution reactions requiring anhydrous conditions.[34] The chemical structures of nucleophilic [^{18}F]fluoride as a potassiumcarbonate kryptofix complex (K^+/K2.2.2/^{18}F-) and as a "free" anion in aqeuous solution coordinated to four water molecules by F-HOH bonds ($F[H_2O]_4$), are presented in **Figure 2**.

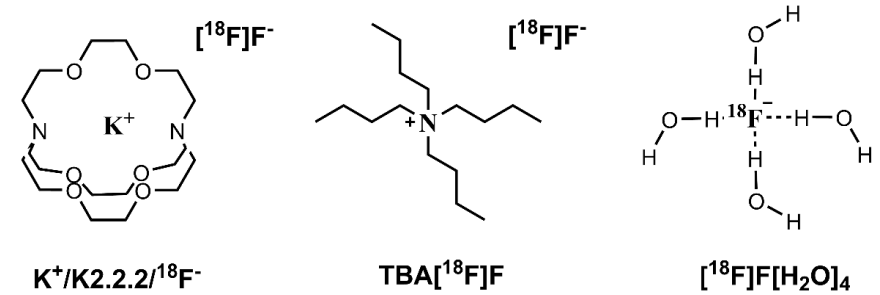

Figure 2. Chemical structures of K^+/K2.2.2-complex of [^{18}F]fluoride, TBA[^{18}F]F and hydrated "inert" [^{18}F]F[H_2O]$_4$ in aqueous solution.

[^{18}F]Fluoride, as n.c.a., is used in various aliphatic and aromatic nucleophilic substitution reactions to produce radiotracers of high A_m. For recovering the nucleophilicity of the [^{18}F]fluoride hydrated in the aqueous solution, radiolabeling is generally preceded by azeotropic removal of residual target water and the nucleophilic reaction subsequently takes place in aprotic polar solvents. The aforementioned phase transfer catalyst systems K^+/K2.2.2/^{18}F- or TBA[^{18}F]F are the gold standard for traditional formulation of [^{18}F]fluoride for nucleophilic subsitutions. Due to the alkaline conditions of radiofluorinations by nucleophilic substitution in organic solvents, compounds containing base or solvent intolerant structures need more sensitive radiolabeling methods. There are several alternatives for modifying the nucleophilic radiofluorination conditions more suitable for base sensitive motifs.[35] Eluting the [^{18}F]fluoride trapped to an anion exchange cartridge in the opposite direction to the target water flow, in so called "minimalistic approach, with an ionic precursor in methanol (MeOH) results in reduced base content in the reaction mixture. Using non-basic mesylate anions for both preconditioning the cartridge and elution of [^{18}F]fluoride, enables the addition of predetermined amount of base to the reaction mixture, increasing expected radiochemical yields (RCYs). Also, a combination of using mesylate ions for

preconditioning and for elution of [^{18}F]fluoride, *tert*-butanol as the reaction solvent, together with a mixture with dimethyl sulfoxide (DMSO) or ACN (16%v/v), resulted in high incorporation yields for base sensitive motifs, such as a tetrazine.[36] Prosthetic groups, such as 2-deoxy-2-[^{18}F]fluoro-d-glucose ([^{18}F]FDG) and 5-deoxy-5-[^{18}F]fluoro-d-ribose ([^{18}F]FDR) can be used for mild radiolabeling of base sensitive tetrazines, providing glycoconjugates [^{18}F]fluorodeoxyribose tetrazine ([^{18}F]FDR-Tz) and [^{18}F]fluorodeoxyglucose tetrazine ([^{18}F]FDG-Tz).[37, 38] Furthermore, the [^{18}F]fluoride from the target water can be converted into volatile [^{18}F]HF in acidic reaction media and transported by distillation to the reaction vessel containing phosphazine base, that traps the [^{18}F]fluoride and is ready for S_N2 radiofluorinations as phosphazene base trapped *N*-onium hydrofluoride [^{18}F]P_2Et·HF.[35] General depiction of aliphatic S_N2 (A) and aromatic S_NAr (B) substitution reaction mechanism are presented in **Scheme 1**.

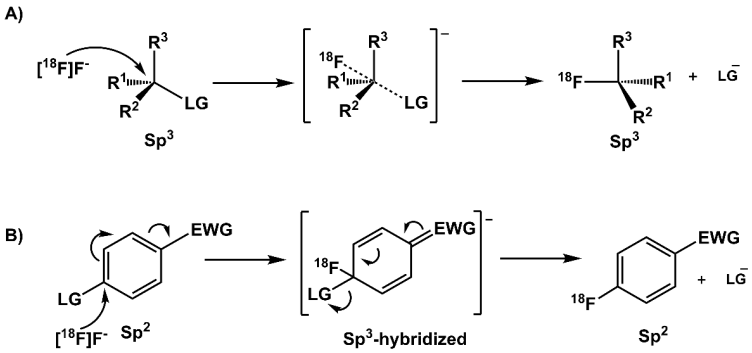

Scheme 1. Reaction mechanism of S_N2 (**A**) and S_NAr (**B**) substitution reactions. R^1-R^3; general substituents, LG; leaving group, EWG; electron withdrawing group.

[^{18}F]FDG is one of the most prevailing imaging agents in nuclear medicine, with PET imaging applications ranging from oncology to inflammation. [^{18}F]FDG is taken up by cells with rapid glucose metabolism, accumulating into the cells, which cannot expell the modified sugar analogue out, blocking the natural metabolism route of glucose, due to the substitution of the hydroxy group at 2-position with [^{18}F]fluorine. Upregulated glucose metabolism is a known marker of cancer, making [^{18}F]FDG an ideal candidate for evaluating alarming alterations in cellular glucose uptake and metabolism. The radiosynthesis of [^{18}F]FDG is executed by typical S_N2 reaction, starting with the glucose analog precursor, mannose triflate, protected with acetyl (Ac) groups. The nucleophilic substitution takes place by the attack of the kryptofix complex-bound [^{18}F]fluoride (K^+/K2.2.2/$^{18}F^-$) at the base of the 2-triflate leaving group, at 85 °C in few minutes. During the nucleophilic attack, the stereochemistry at the 2-position inverts, as the leaving group and the attacking group are on opposite orientations of the molecule. The radiolabeling is followed by either acid or base hydrolysis of the acetyl groups.

The base catalyzed deprotection takes place at room temperature in minutes, while the acid catalyzed deprotection requires elevated temperatures. An example of the radiosynthesis of [^{18}F]FDG is presented in **Scheme 2**.[39]

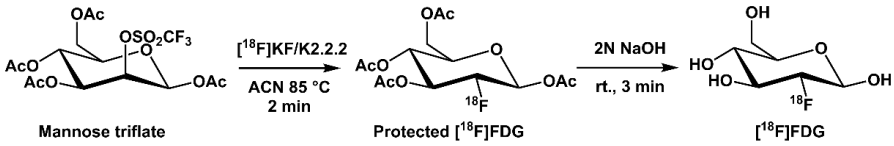

Scheme 2. FDG radiosynthesis by aliphatic nucleophilic substitution and base catalyzed deprotection. K2.2.2; kryptofix crown ether, ACN, rt.; room temperature, Ac; acetyl protecting groups.

2.2.3 ISOTOPIC EXCHANGE RADIOFLUORINATIONS

2.2.3.1 Fluorophilic elements

IE in radiofluorinations utilizes an existing fluorine atom in the compound, which is replaced by exchanging it with chemically identical isotope, resulting in isotopologue [^{19}F/^{18}F]-compounds. The maximum theoretical A_m is directly influenced by [^{19}F]fluorine in the substrate itself, requiring the radiolabeling method to provide rapid and efficient incorporation of [^{18}F]fluoride to the compound, low fluoride contamination from synthesis equipment, and the use of as low amount as possible of the precursor compound itself.[26] Aluminum, boron, sulfur and silicon posess low activation energies for forming a bond with fluorine, and high bond entalphy with fluorine atom, facilitating their use as radiopharmaceuticals.[13, 40, 41] The bond formed with fluorine is generally stable, with certain exceptions, and prevents its elimination by substitution with a hydroxy group in solution. Characteristics of the chemical bonds of common elements with fluorine are presented in **Table 2**.

Table 2. Chemical characteristics of commonly used bonds in radiofluorinations and examples of their application in PET tracer development.[13]

Bond	Dissociation energy (kJ/mol)	Bond length (pm)	Example radiotracer	Application in PET	Ref.
C-F	513.8 ± 10	135	[^{18}F]FDG	Glucose uptake, cancer imaging	[39]
Si-F	576.4 ± 17	160	[^{18}F]SiFA	Prosthetic group	[42]
B-F	732	130	[^{18}F]AmBF$_3$	Prosthetic group	[43]
P-F	≤405	154	[^{18}F]DBPOF-COOC$_6$HF$_4$	Prosthetic group	[16]
Al-F	675	163	[^{18}F]AlF-NOTA-Bz-TFTE	Prosthetic group	[44]
S-F	284	156	H-Tyr([^{18}F]FS)-OMe	amino acid transporter or brain tumor imaging	[45]

DBPOF; di-*tert*-butyl-organofluorophosphine

2.2.3.2 Organosiliconfluoride acceptor (SiFA)

SiFA radiolabeling offers a rapid incorporation of [^{18}F]fluoride by [^{19}F/^{18}F]-IE reaction, with remarkable, near quantitative incorporation or RCYs of [^{18}F]fluoride to the prosthetic group or the compound of interest.[15] SiFA-radiolabeling proceeds traditionally in alkaline solution with a Kryptofix complex K^+/K2.2.2/^{18}F- carrying the nucleophilic fluoride, and attacks the silicon central atom, expelling the stable isotope [^{19}F]fluoride (**Scheme 3 A**). [^{18}F]SiFA-based prosthetic groups were obtained in a kit-like radiolabeling setup with and incorporation yield of 40-60% in 5 min and with A_m of 11-34 GBq/µmol, analyzed with radio-high-performance liquid chromatography (radio-HPLC).[42] A limitation of Si-F radiolabeling chemistry is the requirement of generally alkaline conditions, resulting from the traditionally used counter anions, carbonate (CO_3^{2-}) of hydroxy (-OH), in conditions that might not be suitable for all target molecules. Münich method was developed for a kit-like radiolabeling obviating the use of azeotropic distillation, where [^{18}F]fluoride is trapped in a strong anion exchange cartridge and eluted with anhydrous solution of K^+/K2.2.2/OH^- in ACN, providing a solution ready for fluorinations as such.[46, 47] Tremendous amount of investigation has gone to develop stable SiFA-derivates comprising the most stable di-*tert*-butylphenylsilane, applicable to protein and peptide radiolabeling when hydrophilic auxialiries are added to lower the lipophilicity of the resulting biomolecule tracer.[48] The advances in structural optimization and promising results of successful SiFA-derivatized biomolecules are pawing the way for clinical translation.[15] As a down-fall, the bulky *tert*-butyl groups of SiFA-compounds result often in an increase in the lipophilicity of the radiolabeled end-product tracer, influencing the pharmacokinetics of specifially smaller biomolecules, such as peptides.

The chemical structures of the most relevant SiFA-prosthetic groups reported to date, SiFA (R; -SH or -CHO), SiFA*lin* and heteroaromatic silicon-fluoride acceptor (HetSiFA™), are presented in **Scheme 3 B**.

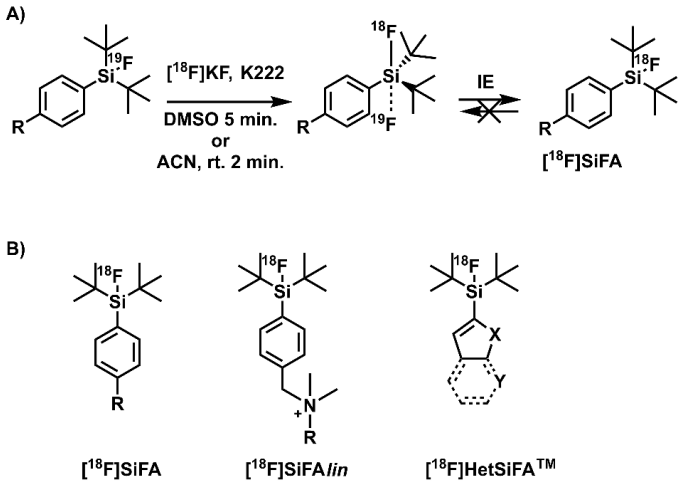

Scheme 3. A) Radiolabeling of a silicon-fluoride acceptor (SiFA) prosthetic group with isotopic exchange (IE).[42] **B)** Chemical structures of [^{18}F]SiFA, [^{18}F]SiFA*lin* and [^{18}F]HetSiFA™. **X**; S, O, NMe_2, $N(CH_2Ph_2)$ and **Y**; CH, N.

2.2.3.3 Organotrifluoroborate fluoride acceptor (BF_3)

Alkylammniomethyltrifluoroborate ($AmBF_3$) was introduced as the first truly efficient fluorophilic prosthetic group tolerant of substantial quantities of water during radiofluorination by IE.[43] Due to the enhanced hydrophilicity of the zwitterionic structure, the trifluoroborate moiety provides beneficial characteristics, when renal clearance is preferred, to the radiolabeled target molecule.[49] $AmBF_3$ chemistry is utilized overwhelmingly in one-step radiolabeling protocols, where the $AmBF_3$-alkyne is conjugated to a compound of interest by copper-catalyzed azide alkyne cycloaddition (CuAAC), prior to radiolabeling the whole target structure, generally omitting its use in 2-step method as a prosthetic group.

In $AmBF_3$-based radiolabeling the nucleophilic [^{18}F]fluoride is used for in aqueous solution, generally detrimental to (radio)fluorination, due to the "inertness" of the hydrated form of [^{18}F]fluoride. The radiolabeling conditions require heating in acidic conditions (pH 2-2.5), and hence rules out compounds extremely sensitive to heat or acid.[43] $AmBF_3$-bioconjugates are obtained in decay-corrected (DC) RCYs of approximately 30% with A_m of >111 GBq/μmol within 30 min, when performed at 80 °C in a pyridazine HCl buffer at pH 2.5 (**Scheme 4 A**). The acid catalyzed deprotection of the pinacol ester and the proposed mechanism of radiofluorination are presented in **Scheme 4 B**.[49] Radiofluorination follows the same reaction mechanism, and adding carrier-fluoride, for example KHF_2, would thus lower the RCY(%).

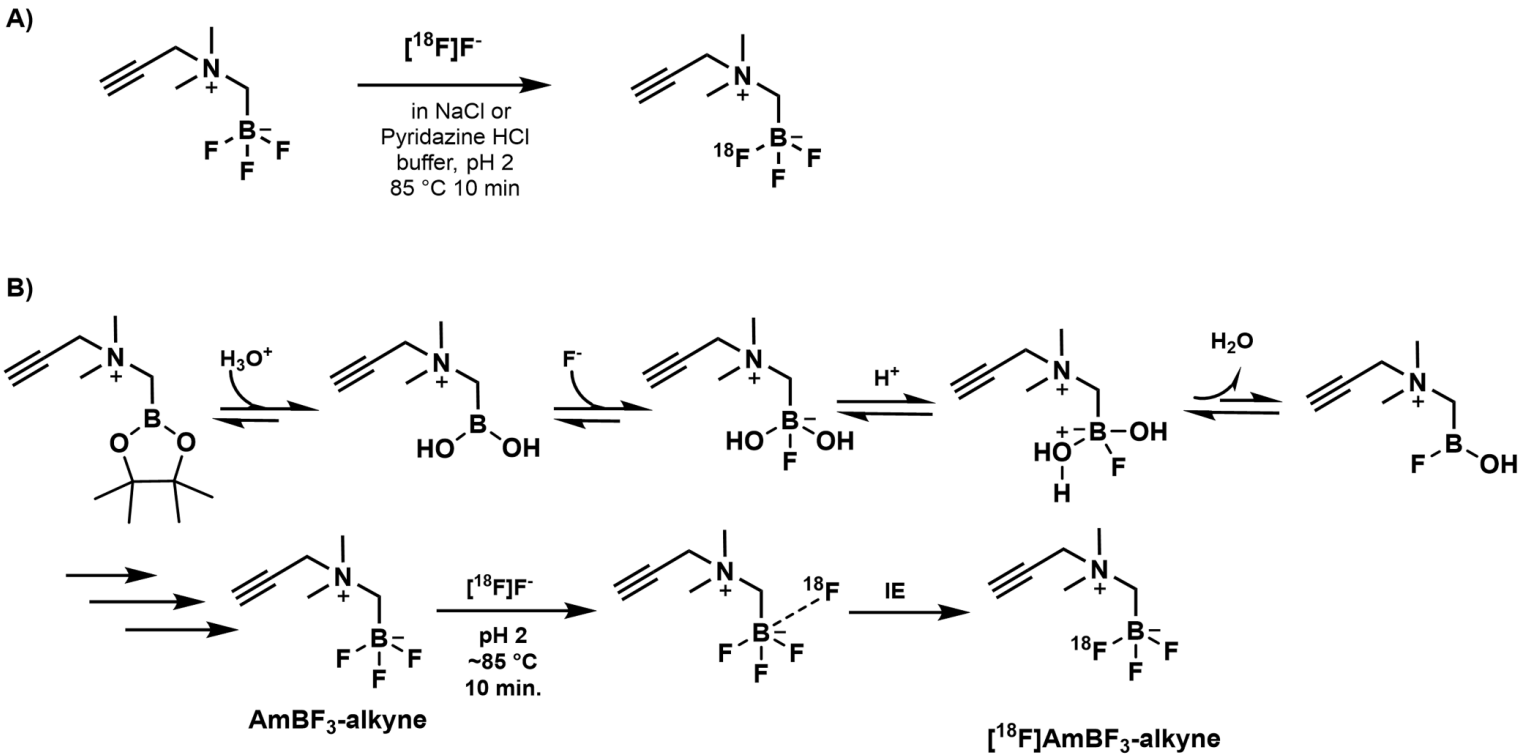

Scheme 4. **A**) Radiolabeling of $AmBF_3$-alkyne with [^{18}F]fluoride by isotopic exchange (IE). **B**) Proposed reaction mechanism of $AmBF_3$ fluorination by Perrin.[49] After acid catalyzed deprotection of the pinacol ester, the fluorination afforded the trifluoroborate, subsequently radiolabeled with isotopic exchange (IE) with [^{18}F]fluoride in aqueous acidic solution

2.2.3.4 Di-tert-butyl-organofluorophosphine (DBPOF)

Recently a new IE prosthetic group, di-*tert*-butyl-organofluorophosphine (DBPOF) fluoride acceptor has been reported.[16] The DBPOF prosthetic groups are radiolabeled by reacting hydrophosphine oxides with fluoride in good yields even at room temperature in various combinations of water-organic solvent such as DMSO. The radiosynthesis is well compatible with aqueous solutions and applicable to biomolecule radiolabeling. [^{19}F/^{18}F]di-*tert*-butyl-organofluorophosphine and its derivatives, organophosphine fluoride acceptors exhibit excellent stability *in vivo*. RCY of an astonishing >97% was achieved in DMSO when heated at 75 °C for 5-15 min, and A_m of 0.37-1.85 GBq/μmol for the lead prosthetic group ^{18}F-DBPOF, using precursor amounts of 1 – 3 μmol. The chemical structures and general radiosynthesis conditions of DBPOF-derivatives are presented in (**Scheme 5**).

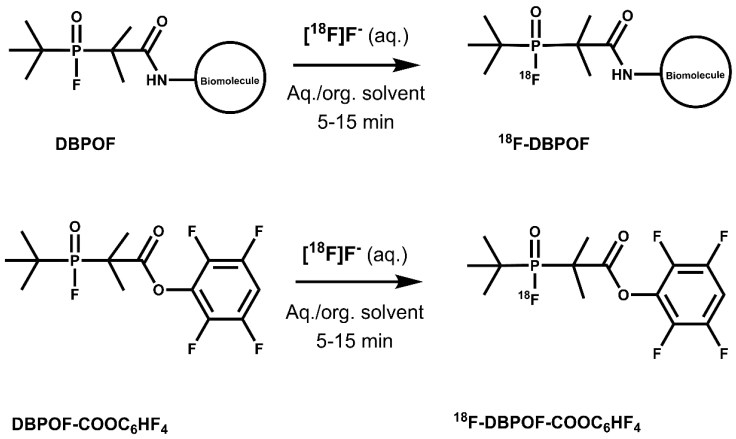

Scheme 5. Radiosynthesis conditions of radiolabeling DBPOF-derivatized prosthetic groups in aqueous (aq) or organic solvent (for example DMSO) or their mixtures.[16]

2.2.3.5 Organosulfur(VI)fluoride exchange (SuFEx)

An emerging isotopic exchange based on sulfur(IV)fluoride exchange (SuFEx) has been recently reported, enabling radiofluorination by ultrafast click chemistry in mild conditions.[50, 51] The aryl and heteroaryl fluorosulfate-based probes were obtained in 83-100% RCY (radio-HPLC) and in A_m of 103-280 GBq/μmol in amazing 30 seconds to minutes at or near room temperature.[50] Zheng et al. reported extremelty high RCYs (≈99%, radio-HPLC) in mere 30 sec at room temperature, using potassium fluoride salt (K[^{18}F]F) together with K2.2.2 in ACN (**Scheme 6 A**).[50] Later, Walter et al., reported lower RCYs using similar method in their hands, but successfully applied a modified method using organic salts in MeOH for eluting [^{18}F]fluoride, of which the best performing salt was benzyltriethylammonium chloride ($BnEt_3NCl$), yielding radiochemical conversions of 65–93% in mild reaction conditions (23–40 °C), with reaction times of 3–5 min.[45] A general depiction of reaction conditions in radiolabeling [^{18}F]F-SuFEx (**Scheme 6 A** and **Scheme 6 B**), together with proposed reaction mechanism of fluoride exchange (**Scheme 6 C**), is presented in **Scheme 6**.[45]

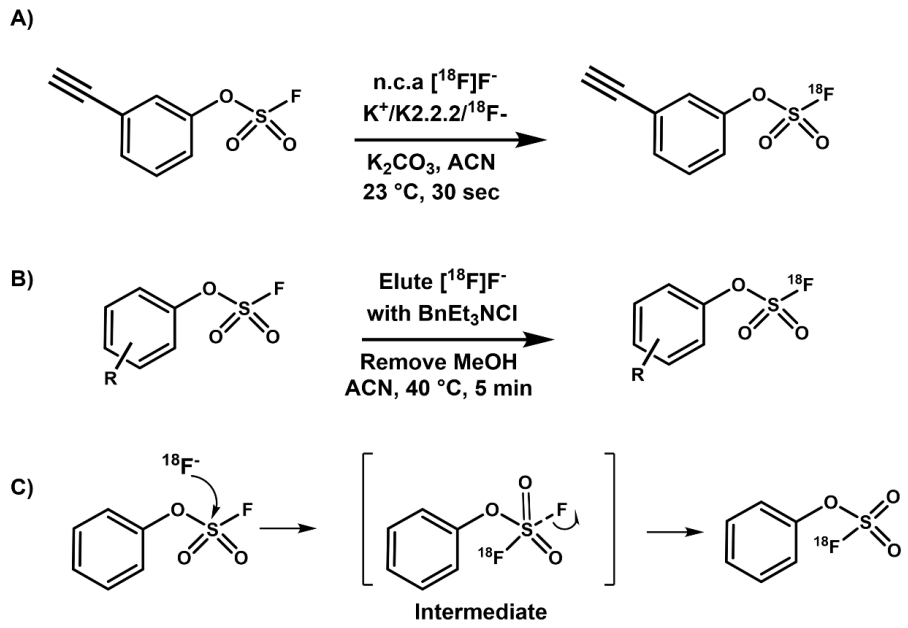

Scheme 6. Sulfonyl-fluoride exchange (SuFEx) radiolabeling with [^{18}F]fluoride by isotopic exchange (IE).[50] **A** and **B**) Radiolabeling conditions used in SuFEx reaction, and **C**) mechanism of incorporation of fluoride into the structure by isotopic exchange [45, 50]

2.2.4 PROSTHETIC GROUPS IN RADIOFLUORINATION

Prosthetic groups are generally utilized to deliver a radiolabel, to more sensitive compounds intolerant of direct radiolabeling. The use of prosthetic groups is especially important for those substrates, that are pH, solvent, or heat sensitive, such as serum albumin proteins used for blood pool imaging. There is an array of functional groups that can be utilized for targeting biomolecules containing free -NH_2, -SH and -OH. Several prosthetic groups for radiolabeling SSTR targeting peptides or serum albumin proteins have been developed, either to target naturally abundant moieties or synthetically added functionalities.

Prosthetic groups can be used to radiolabel a variety of compounds from small molecules to biomacromolecules with n.c.a [^{18}F]fluoride.[52] As an example of a prosthetic group-based labeling of a receptor –targeted small molecule, [^{18}F]fluorobenzylamine ([^{18}F]FB-amine) has been used to radiolabel a selection of cyclooxygenase-2 (COX-2) inhibitors in 20 min at elevated (95 °C) temperature, with methylsulfonyl (-SOO_2Me) as the leaving group while the free amine attacks.[53] These relatively harsh reaction conditions are suitable for robust small molecules. [^{18}F]fluorobenzaldehyde ([^{18}F]FBA) was used to radiolabel serum albumin protein chemoselectively, *via* the conjugation of the [^{18}F]FBA to a hydrazinonicotinic acid (HYNIC), in mild reaction conditions in 30 min, where 60 °C afforded the highest radiolabeling yield of fluorine-18 labeled human serum albumin (^{18}F-HSA), from the tested conditions. For this method the albumin protein was functionalized with HYNIC moieties from lysine residual free amines.[54] *N*-succinimidyl-4-[^{18}F]fluorobenzoate ([^{18}F]SFB) was [^{18}F]fluorinated with a traditional S_N2 reaction, and developed for radiolabeling biomolecules, such as serum albumin, *via* reaction between an activated *N*-hydroxysuccinimide (NHS) ester with the lysine amines residues.[55] [^{18}F]SiFA-SH was radiolabeled in alkaline conditions at room temperature *via* isotopic exchange, and designed to radiolabel proteins, such as serum albumin by the reaction of the thiol with a preconjugated maleimide present in the albumin.[42] In **Figure 3** and **Table 3** are presented typical prosthetic groups, some of which have been used to radiolabel proteins such as serum albumins.

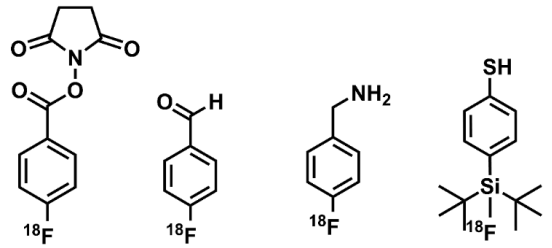

Figure 3. Examples of prosthetic groups used to radiolabel for example biomolecules in mild conditions. [42, 53-55]

Table 3. Typical prosthetic groups, their RCYs and examples of their use in radiolabeling or biologically relevant molecules and serum albumin proteins.

Prosthetic group	Labeling efficiency (%)	Reactive functional groups	^{18}F-Compound	**Ref.**
[^{18}F]SFB	30–35	NHS ester to NH_2	[^{18}F]HSA	[44]
[^{18}F]FBA	67 ± 15.7	CHO to HYNIC	[^{18}F]HSA	[54]
[^{18}F]FP-Amine	27 ± 11	NH_2 to SOO_2Me	^{18}F-labeled COX-2 inhibitors	[53]
[^{18}F]SiFA-SH	40−60	thiol to maleimide	[^{18}F]SiFA-RSA	[42]

*HSA; human serum albumin, RSA; rat serum albumin

2.3 INVERSE ELECTRON-DEMAND DIELS-ALDER CYCLOADDITION

IEDDA is a bioorthogonal cycloaddition reaction where an electron poor tetrazine and an electron-rich alkyne or alkene, such a TCO, react rapidly and catalyst-free. IEDDA reaction harnesses the high reactivity of a tetrazine (Tz) while it reacts with a strained TCO and forms a bicyclic compound as a product, a concept first proposed by Carboni and Lindsay.[56] The initial cycloadduct DHP products are slowly oxidized into pyridazines, creating a product mixture. The Tz-TCO ligation is the fastest IEDDA-reaction reported to date,[57] and the reaction rate is dependent on the used tetrazine. IEDDA possesses excellent reaction kinetics and reactivity even in low concentrations, and is efficient, mild and chemoselective, and has attracted utmost interest in the fields of chemical biology, nuclear imaging, and radiotracer development. These characteristics make IEDDA suitable for a plethora of radiolabeling strategies, from *in vitro* to *in vivo* pretargeting.

Initially during IEDDA cycloaddition, 4,5-DHPs are formed, which isomerize into 1,4-DHPs, reduces (+2 H) cycloaddition products (**Scheme 7**).[57] The

metastable 1,4-DHP is subsequently oxidized (–2 H) or aromatized into a stable pyridazine form. IEDDA is not stereoselective and produces diastereomers by reacting head-to-head or head-to-tail between the reactive pair if no steric hindrance is present in the structures. Accelerating the oxidation process of the DHPs have been attempted with for example applying ultraviolet irradiation under air atmosphere.[58]

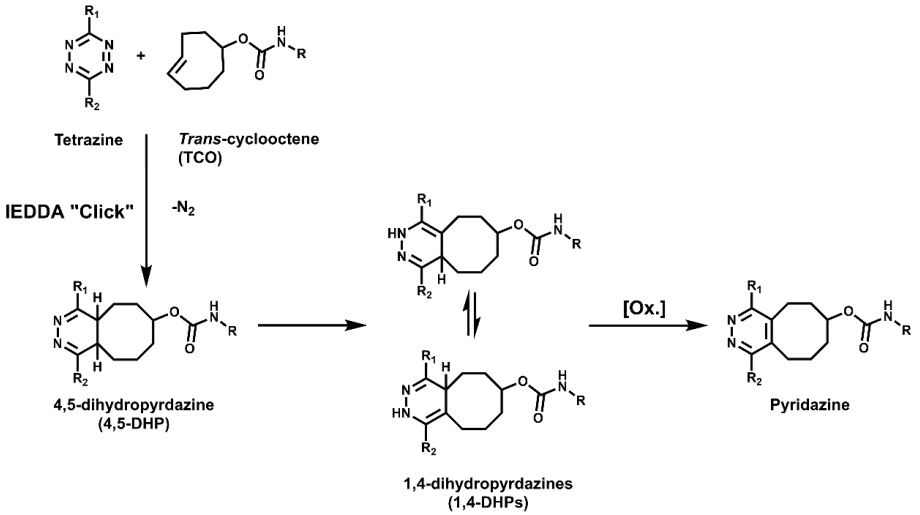

Scheme 7. General depiction of IEDDA cycloaddtion reaction between a phenyltetrazine and a TCO.[57]

In comparison to other click-based methodologies, the exquisite reaction rate ($k \approx 10^6\ M^{-1}\ s^{-1}$),[57, 59] and the biocompatibility of IEDDA, has made it the focal point of click chemistry-based developments for pretargeted PET-imaging.[60] Pretargeted imaging, where the targeting vector is traced *in vivo* with a radionuclide bearing compound, has found exceptional utility with imaging agents of slow pharmacokinetics, such as antibodies, which when directly radiolabeled would require the use of long-lived radioisotopes, such as ^{89}Zr or ^{111}In, both with ~3-day physical half-lives, to track their biodistribution *in vivo*. In the pretargeted approach by IEDDA, the targeting vector, such as an immunoglobulin G antibody, is first modified with one of the IEDDA reactants and allowed to distribute in the body after administration. Next, the location of the modified antibody is tracked using the other reactant radiolabeled with a short-lived radioisotope, providing improved image contrast and lower radiation burden to the subject.[60] Recently increasing efforts have concequently been targeted towards *in vivo* pretargeting with IEDDA, to visualize biological processes by radiolabeling the targeting vector inside the study subject. The radiolabeling of biomolecules such as antibodies or nanoparticles with a short lived radionuclide *in vitro* would likely result in poor image contrast in a reasonable timeframe given the half-life of fluorine-18 and would require *in vitro* radiolabeling with a longer-

lived radionuclide. Therefore, to optimize the image contrast, while simultaneously lowering the radiation dose to the study subject, pretargeting *in vivo* after antibody accumulation to the target site would likely result in best outcome. The generally applied method in pretargeting is to use TCO as the targeting vector accumulating on the tissue surface, and a radiolabeled Tz as the tracer, due to the higher lipophilicity of TCOs and the isomerization of reactive TCO *in vivo* by copper-containing proteins to unreactive *cis*-cyclooctene, that would result in the cirulation of radiolabeled unreactive and lipophilic TCO analog in background tissues.[61] If TCO was used as the tracer instead of Tz, a dominantly hepatobiliary elimination of radioactivity would be expected, instead of elimination *via* urinary route due to the higher lipophilicity of TCOs and a lower image contrast due to higher liver and intestine uptake could be expected, if no hydrophilic linkers are used. The timing between the administration of the antibody or a nanoparticle and of the tracer is a balancing act between TCOs *trans-to-cis* isomerization *in vivo* and of the possible tumor internalization rate of the macromolecule. Additionally, after antibody accumulation to the target site, pull-down reagents, a third molecule containing the reactive part of the complementary IEDDA component, can be used to scavenge the excess of the unbound antibody from the circulation prior to tracer administration, thus lowering the target tissue to background contrast, after administration of the rapidly eliminatin radiotracer.[62] The use of pull-down reagents is valuable in imaging and importantly can result in significantly lower non-target radiation burden when used in for example targeted radionuclide therapy applications. Although IEDDA gives high promise as a powerful tool for pretargeting *in vivo*, specific requirements, such as low calculated lipophilicity (clog$D_{7.4}$ – 3 or below) of the tetrazine was shown to have strong correlation with the *in vivo* performance in pretargeting TCO-modified CC49 mAb.[63] Applying IEDDA for *in vitro* radiolabeling is best suited for relatively small compounds with rapid kinetics, such as peptides or immunoconjugates of lower M_w, to ensure adequate clearance from background tissue and good image contrast. There are exceptions, such as blood pool imaging with biomacromolecules, such as serum albumin, where long circulation and radioactivity retention in the blood pool is preferred.

2.4 EXAMPLES OF SELECTED ^{18}F-LABELED BIOMOLECULES

2.4.1 ^{18}F-SERUM ALBUMIN TRACERS

Serum albumin is a negatively charged 66.5 kDa plasma protein, that is sensitive to heat and many organic solvents, in which the protein loses its

ordered structure, resulting in so called denaturation of the protein construct. Serum albumin retains cations such as sodium (Na^+), simultaneously retaining water, maintains adequate pressure in blood vessels, and is solely responsible for around 80% of the plasma osmotic pressure.[47] Serum albumin transports drugs, vitamins, and hormones, among other compounds and ions, as well as scanvenges reactive oxygen species in the body.[64, 65] Serum albumin can be utilized for imaging for example blood pool or heart function. Radiolabeling such important biomolecules would require a relatively sensitive and targeted radiolabeling strategy, avoiding compromising the structure and biological function of the biomacromolecule. The specificity of the pre-modification of the biomolecule with for example TCO, can have a significant impact on the performance of the resulting biological radiotracer in addition to the influence of the radiolabeling conditions. As biomolecules have a conciderable amount of amino acid residues available, the most straight forward conjugation strategy is using chemical coupling methods targeting abundant groups such as lysine residues with NHS esters for delivering the TCO to the biomolecule. This method results in heterogenious conjugation in the biomolecule structure often both by conjugation-site and conjugate-number, even though the conjugation is amino acid specific. An alternative strategy is to use enzymes such as transglutaminases for catalyzing the generally unreactive γ-carboxamide group of glutamine to react with primary amine group of lysine, forming a stable isopeptide amide bond. This method results in site-specific conjugation and subsequently homogenious end-products with better performance in-comparison to their chemically modified analogs, as has been demonstrated with antibodies.[66] The site-specific conjugation is driven by the enzymes capability to recognize the glutamine residue at a sterically non-hindered location.[66, 67] Several prosthetic groups have been developed in the attempt to radiolabel serum albumins in mild conditions *in vitro* or by pretargeting *in vivo*, as demonstrated by [^{18}F]AlF-labeled 1,4,7-triazacyclononane-N,N',N''-triacetic acid (NOTA) NOTA-Evans Blue (NEB) conjugated probe ^{18}F-AlF-NEB.[68] ^{18}F-AlF-NEB was used as an albumin-binding radiotracer for radiolabeling serum albumin *in vivo*, where its pharmacokinetics closely resembled the *in vitro* labeled mouse serum albumin (MSA), used as control.[68]

N-succinimidyl 4-[^{18}F]fluorobenzoate ([^{18}F]SFB) is a prosthetic group widely used for radiolabeling of proteins and peptides for PET imaging. [^{18}F]SFB can be produced by a nucleophilic attack of the trimethylammonium group in 4-formyl-*N*,*N*,*N*-trimethyl benzenaminium trifluoromethane sulfonate, forming 4-[^{18}F]-fluorobenzaldehyde, which is oxidated in alkaline conditions, yielding 4-[^{18}F]-fluorobenzoic acid intermediate, and converthed to *N*-succinimidyl 4-[^{18}F]fluorobenzoate ([^{18}F]SFB) with *N*,*N*-disuccinimidyl carbonate. [^{18}F]SFB targets free lysine residues on the albumin protein and is used as such to radiolabel serum albumins.[44] A thiol (-SH) functionalized SiFA (SiFA-SH)

is produced by isotopic exchange radiofluorination, forming the radiolabeling agent [^{18}F]SiFA-SH, that reacts with the maleimido functionalized rat serum albumin (RSA), resulting in overall RCY of 12% rapidly in 20-30 minutes, providing a blood pool imaging agent [^{18}F]SiFA-RSA (purity >97%, radio-size-exclusion-chromatography-HPLC, or radio-SEC-HPLC), with a calculated A_m of 11-34 GBq/μmol.[42] [^{18}F]Fluorobenzaldehyde ([^{18}F]FBA) was developed to react with hydrazinonicotinic acid-functionalized human serum albumin (HYNIC-HSA) via hydrazone formation. [^{18}F]FBA was produced from 4-trimethylammonium benzaldehyde triflate with tetrabutylammonium bicarbonate in DMSO at 100 °C in 6 min and conjugated to the HYNIC modified human serum albumin at pH 7.5 with mild heating, producing ^{18}F-HSA in 30 min.[54] An organofluorophosphine fluoride acceptor, 2,3,5,6-tetrafluorophenyl-2-(*tert*-butylfluorophosphoryl)-2-methylpropanoate (DBPOF-$COOC_6HF_4$), was used to radiolabel human serum albumin (HSA) with [^{18}F]fluoride by IE, after incorporation of DBPOF prosthetic group through conjugation to the lysine residues, resulting in ^{18}F-DBPOF-HSA.[69] A radiometallated RSA analogue was radiolabeled using the same conjugation strategy to the protein, by first radiolabeling the 1,4,7-triazacyclononane-1,4-diacetate (NODA) tetrafluorophenylester (TFPE) containing a benzoyl (Bz) linker (NODA-Bz-TFPE) with [^{18}F]fluoride by aluminum-NODA complexation, which was followed by conjugation to RSA *via* lysine residues, providing [^{18}F]RSA-AlF.[44]

2.4.2 ^{18}F-LABELED SOMATOSTATIN DERIVATIVES AND A-MELANOCYTE-STIMULATING HORMONE PEPTIDE

Small, radiolabeled biomolecules such as peptides, offer potential as highly selective vehicles for delivering drugs and imaging agents to the target site. Receptors overexpressed by tumors act as desirable targets for radiolabeled peptides in nuclear imaging. Majority of melanomas overexpress melanocortin 1 receptor (MC1R), which has low expression in healthy tissue. α-MSH peptide, secreted primarily by the pituitary gland, is responsible for melanocyte control and pigment production in pigmented cells and binds to MC1R with high affinity.[70, 71] Synthetic cyclic derivatives of α-MSH resist *in vivo* degradation and have been synthesized with click-based chemistry utilizing IE radiolabeling strategy for radiofluorination. The developed [^{18}F]$AmBF_3$-derivatized α-MSH peptides resulted in high affinity tracers and provided high-contrast PET images in C57BL/6J mice bearing B16-F10 tumors,[72] indicating the [^{18}F]$AmBF_3$-alkyne coupled to the α-MSH-azide peptide were well tolerated in the cyclic peptide structure and in the peptide-receptor binding process. SSTR family comprises of five subtype receptors SSTR1 – SSTR5, which are found in several organs, such as the brain and gastrointestinal tract, where they secrete gastrin, histamine, and stomach acid. As well as found in normal tissue, SSTRs are overexpressed in several tumors,

and approximately 80% of neuroendocrine tumors (NETs) overexpress SSTR2, making it an important target for imaging and therapeutic purposes.[73] Hence the development of peptide-based radiotracers targeting SSTR2 with TOC and TATE, synthetic analogues of somatostatin, that expresses strong affinity to SSTR2, are under intense investigation. Several radiometallated 1,4,7,10-tetraazacyclododecane-1,4,7,10-tetraacetic acid (DOTA) chelated derivatives of TOC/TATE have been developed for clinical theranostic purposes as ^{177}Lu/^{68}Ga-DOTATOC and ^{177}Lu/^{68}Ga-DOTATATE pairs.[74] Continuing attempts for introducing a positron emitter with near optimal nuclear properties, such as longer half-life and shorter positron range than gallium-68, has led to the development of ^{18}F-SiFA*lin*-TATE and ^{18}F-AmBF$_3$-TATE, which have both entered clinical trials. AmBF$_3$-alkyne has been used to functionalize and then radiolabel several biomolecules such as Tyr^3-octrotate and for example α-melanocyte stimulating hormone peptides.[75] The peptides were radiolabeled with good RCYs (20 – 25%,), A_m (111 GBq/μmol, 79 GBq/μmol) and demonstrated high and specific tumor uptake 60 minutes p. i. (AR42J baseline 10.11 ± 1.76 %ID/g vs. blocked 0.32 ± 0.21 %ID/g, and B16/F10 baseline 7.80 ± 1.77 %ID/g vs. blocked 1.97 ± 0.60 %ID/g), respectively, verifying the prosthetic group, and radiolabeling conditions did not compromise the structural integrity of the peptides.[49, 76, 77] A fluorine-18 radiolabeled SSTR2 targeting peptide, ^{18}F-fluoroethyltriazole-Tyr^3-octreotate (^{18}F-FET-βAG-TOCA), was radiolabeled with the 2-[^{18}F]fluoroethylazide prosthetic group using click chemistry by CuAAC, and when evaluated in humans for neuroendocrine imaging, provided high tumor-to-background contrast images.[78] In addition to the clinically tested ^{18}F-FET-βAG-TOCA, one of the most prevalent competitors for SiFA and AmBF$_3$ -derivatized fluorine-18 radiolabeled TATE/TOC tracers is using a macrocyclic chelator, typically NODA or NOTA, to bind [^{18}F]fluoride with aluminum, where first [^{18}F]AlF is formed and then bound to the precursor *via* the chelator. This method has been used successfully in producing [^{18}F]AlF-NOTA-octreotide in good RCYs for preclinical evaluations (RCY 50 ± 2%), in good manufacturing practices compliant setup (RCY 26.1 ± 3.6%), and with radiolabeling efficiency reaching up to 83 ± 19% in optimized conditions at 60 °C.[79-81] The compatibility of the AlF-chelator approach with aqueous reaction conditions, the resulting high yields and A_m of the final peptide tracer and the suitability to a kit-based setup, make [^{18}F]AlF a strong competitor for radiopeptide production with fluorine-18. The elevated temperatures (100 – 120 °C) required for forming the [^{18}F]AlF-NOTA complex can be circumvented and the required chelating temperature lowered (40 °C) by changing the used macrocyclic chelator to an acyclic one when radiolabeling heat sensitive biomolecules.[82] Optionally a two-step method can be applied, as demonstrated in the RSA radiolabeling with [^{18}F]AlF-NODA-Bz-TFPE.[44] The small structural difference of TOC and TATE, from alcohol to carboxylic acid group, results in quite dramatic change in receptor affinity, the tenfold

higher affinity of TATE *in vitro* to SSTR2 (**Figure 4**). In **Table 4** is presented relevant data TOC and TATE analogues evaluated *in vivo* to date.

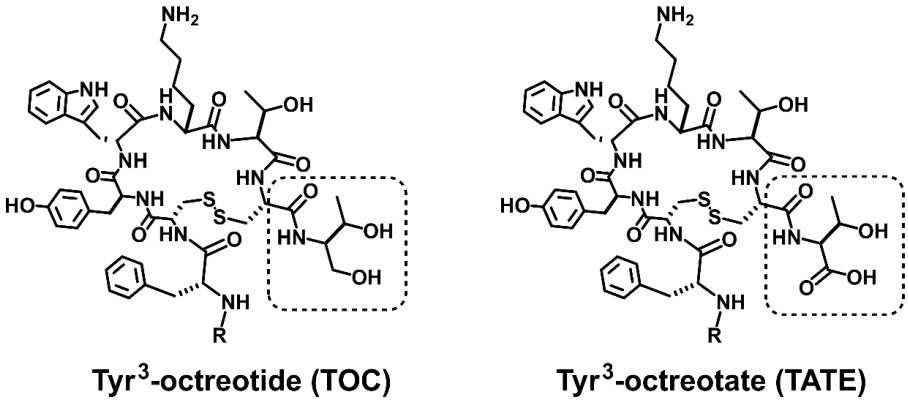

Figure 4. Chemical structures SSTR2 targeting TOC and TATE octapeptides.

Table 4. [^{18}F]Fluorinated TOC and TATE-based peptide tracers developed for SSTR2 imaging and their comparison *ex vivo*.

Radiopeptide	Synthesis time (min)	A_m (GBq/μmol)	Binding affinity (nM)	Tumor *t*=60 min (%ID/g)	Tumor/Blood *t*=60 min (%ID/g)	Tumor/Muscle *t*=60 min (%ID/g)	Ref.
^{18}F-FETE-PEG-TOCA	90	5.9	12	5.14	24.15	23.47	[83]
^{18}F-FETE-βAG-TOCA	90	3.9	4.7	8.23	13.47	24.12	[83]
^{18}F-FETE-βAG-[W-c-K]	90	12.3	220	0.11	1.10	0.65	[83]
[^{18}F]FGlc-TATE	70	32-106	4.2	5.62	9-17	-	[84]
^{18}F-AmBF$_3$-TATE	<30	111	0.14	10.11	25.10	88.96	[76]
^{18}F-SiFAlin-Glc-Asp$_2$-PEG$_1$TATE	20-25	44-63	3.67 ± 1.09	18.51 ± 4.89	57.58 ± 35.89	211.05 ± 143.38	[20]
[^{18}F]AlF-NOTA-octreotide	40 ± 3	27	3.6 ± 0.6	-	-	-	[80]
^{18}F-IMP466	45	48	3.6 ± 0.6	28.3 ± 5.2 (*t*=120 min)	300 ± 90 (*t*=120 min)	- -	[79, 81]

2.5 METABOLIC STABILITY OF FLUORINE-18 IN RADIOPHARMACEUTICALS

2.5.1 FLUORINE IN ORGANIC COMPOUNDS

In drug design, the incorporation of fluorine into a compound traditionally serves several purposes, such as tailoring the elimination route, distribution, target binding and metabolism of the compound.[32] By substituting selected metabolically sensitive substituents at a labile position in a compound with fluorine, can enhance its metabolic behaviour by deactivating or blocking a possible hydroxylation site. A hydrogen or a hydroxy group is generally substituted with fluorine, due to the expected minimal steric effect, arising from the similarity of van der Waals radiuses (fluorine; 147 pm, hydrogen; 120 pm, oxygen; 157 pm) of the functionalities, simultaneously providing enhanced stability. The metabolic stability of C-F bond can in part be explained by one of the highest bond strengths of carbon-to-heteroatom available (C-H; 99 kcal/mol, vs. C-F; 116 kcal/mol).[30] By substituting a hydrogen with fluorine in a compound can result in changes in electronic properties that alter the *p*Ka, in metabolism, and in target binding of the molecule, features that require investigating after the hydrogen-to-fluorine exchange.

2.5.2 ANALYSIS METHODS IN DRUG METABOLISM STUDIES

The identification of metabolites that form after administration of a pharmaceutical compound, is an avenue towards understanding the *in vivo* behaviour, anticipated accumulation sites and elimination route of the pharmaceutical. Computational drug discovery is used to find or to optimize the lead candidates prior to metabolism studies, thus reducing the time, labour and cost of the drug development process.[85] Metabolism studies are crucial for understanding the elimination of the pharmaceutical and for the development of more robust and metabolically stable drugs. Isotopically labeled compounds, whether labeled with stable or radioactive nuclides aid in this quest.[86] Understanding the weaknesses and strengths in a drug compound structure, enable the optimization of their pharmacokinetics, *in vivo* stability, receptor binding and elucidating their mechanism of toxicity.

The metabolism of a drug candidate is screened by *in vitro* methods, such as incubation in hepatocytes, microsomes or S9 fraction. The formed metabolites are then analyzed with liquid chromatographic methods using a variety of detectors (ultraviolet; UV, diode-array-detector; DAD, and mass spectrometry; MS) for assessing the metabolites quantitatively.[87] high-

resolution mass spectrometry (HRMS) provides a robust tool for studying the chemical structures of the parent compound and its formed metabolites in detail, providing information of exact mass and of the elemental composition of the compounds and structural information by generated fragment ions. The superior resolving power of HRMS coupled to ultra-high performance liquid chromatography (UHPLC) techniques, compared to other mass spectrometry-based methods, provide the possibility to gain such detailed information.[88] Together with nuclear magnetic resonance (NMR) spectrometry, positional isomers, in addition to substitution sites, in example on an aromatic ring, can be verified.

In addition to these gold-standard methods, radiolabeled isotopes provides an avenue towards complementary evaluation by radiodetection methods (radio-HPLC) of the stability of a certain atomic position, with chemically identical isotopes such as carbon or tritium.[89] The stable isotopes (carbon-12, hydrogen) found in the studied compound can be substituted with stable carbon-13 or deuterium, or with a radioactive analogue (carbon-14, tritium) for rapid evaluation of the elimination and biotransformation of the compound in physiological conditions *in vitro* or *in vivo*. Radiopharmaceuticals are subject to certain analysis methods providing information specifically of the radionuclides faith. Radionuclides with long half-lives, carbon-14 ($t_{1/2}$ = 5730 y) and tritium ($t_{1/2}$ = 12.4 y) are applied for studying target binding and biotransformation in drug development, utilizing autoradiography, a quantitative *ex vivo* method able to localize the radioactivity distribution over a tissue section.[86, 89] Radiodetection methods such as radio-thin-layer chromatography (TLC) and radio-HPLC are also applied for metabolite studies by quantitating the radioactivity distribution, indicative of the number of radioactive compounds present.[90] Radiodetection methods such as gamma counting and PET or SPECT imaging, provide information on the stability (for example bone uptake), distribution and receptor binding of the radiolabeled compound as a distribution of the radioactivity, without information of the chemical structure of the radioactive compound, making the aforementioned methods highly complementary.

2.5.3 DEFLUORINATION OF ^{18}F-LABELED RADIOTRACERS

Oxidative defluorination belongs to phase I metabolic transformation pathway and is typical for organofluorine compounds bearing aromatic and aliphatic functionalities. Organofluorine compounds exhibit high stability and thus generally persist in the environment. In cytochrome P450 (CYP450) mediated oxidations monooxygenases transfer one oxygen atom to the substrate and nicotinamide adenine dinucleotide phosphate (NADPH) functions as the electron donor, while simultaneously one water molecule is cleaved off the oxygen molecule.[91] CYP450 monooxygenase catalyzed defluorination of fluoroaromatics has been widely studied and a generally accepted mechanism involves electrophilic attack of iron(IV)oxide on the substrate, generation of a quinone, which can be reduced to a phenol, and the fluoride releases while the iron oxide bond is cleaved.[92] Aromatic C(sp^2) and primary aliphatic C(sp^3)

C-H bond dissociation energies are nearly equally high (aromatic; 473 kJ/mol, aliphatic 424 kJ/mol), but they proceed via different mechanisms, explaining the tendency of a substrate to oxidize at the aromatic ring, if available. It is hypothesized that the hydroxylation of a sp^3-carbon takes place by a homolytic cleavage, where each departing component harbours one electron, forming two radicals, whereas aromatic oxidation proceeds via the quinone intermediate. The bond dissociation energy is determined by the carbon radical stability.[91]

Radiodefluorination is a phase I metabolism reaction mediated by CYP450 isoenzyme 2E1 by the liver microsomes.[93] Defluorination of a radiotracer leading to the subsequent accumulation of [^{18}F]fluoride to the bone hydroxyapatite *in vivo*,[94] is highly undesirable, resulting in lower image contrast, higher radiation burden and even oxidative stress to bone and bone marrow. In radiotracers administered at "trace amounts", [^{18}F]fluoride is released at nanomolar scale, and most likely causes no long-term adverse effects, and mainly causes concern due to radiation burden off-target and by disrupting the background-to-contrast ratio of the PET image.

SiFA-derivatized compounds, have been vastly studied for the ^{18}F-hydrolysis phenomenon and several structural alterations for SiFA-derivates have been executed and higher stability has been achieved.[95, 96] The studies around the substituent effect on the silicon-central atom and fluoride stability, has led to the shift from diphenyl substituents, *via* dipropyl substituents all the way to the most stable *di*-tert-butyl analogues extensively used currently.[97] In a study by Schirrmacher *et al*, mono-*tert*-butyl[^{18}F]triorganofluorosilane exhibited faster defluorination, detected as bone uptake, than the di-*tert*-butyl substituted analog, di-*tert*-butyl[^{18}F]triorganofluorosilane, evaluated by PET imaging (**Figure 5 B**, **C**).[96] The introduction of the more stable di-*tert*-butyl-SiFA derivatives motivated further efforts to develop various silicon-fluoride acceptors as radiolabeling tools. HetSiFAs were developed as alternatives for traditional SiFA building blocks, with lower lipophilicity.[16] The chemical structures of SiFA-derivates, DBPOF-derivate and trifluoroborate $ArBF_3$-derivative, together with their bone uptake values, demonstrating both high and lower *in vivo* stability of the radiolabel in the tracer, are presented in **Figure 5**.

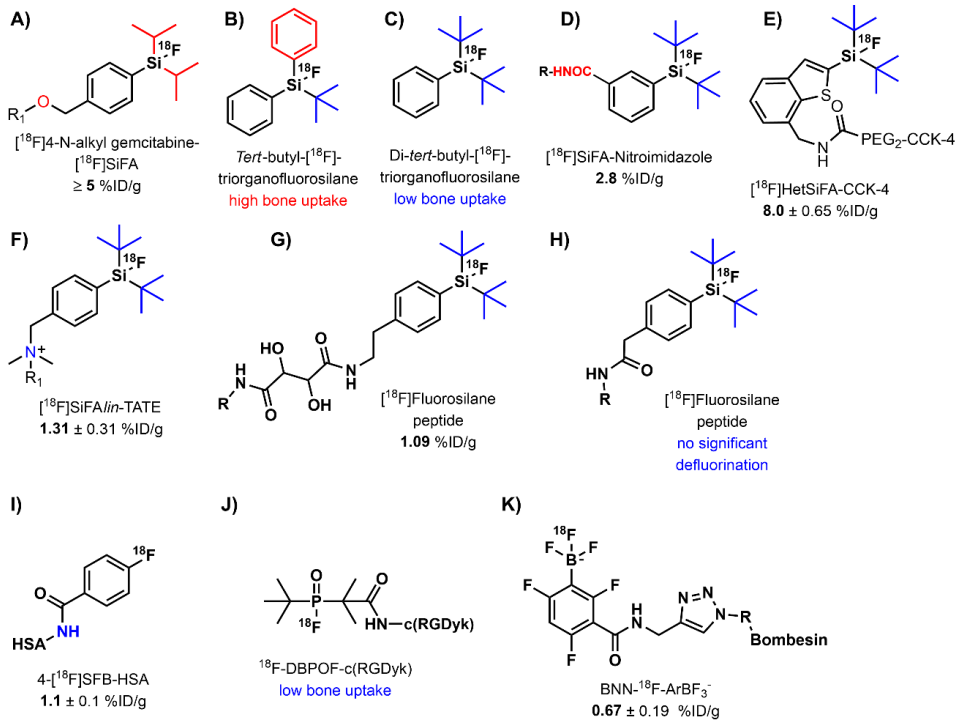

Figure 5. Chemical structures of relevant radiolabeled prosthetic groups and their bone uptakes presented as percentage per injected dose per gram of tissue (%ID/g) or as high/ low defluorination. Beneficial functionalities are depicted in blue and metabolically unfavorable functionalities are depicted and red. **A**) [^{18}F]4-N-alkyl gemcitabine-SiFA [98], **B**) *tert*-butyl-[^{18}F]triorganofluorosilan [96], **C**) di-*tert*-butyl-[^{18}F]triorganofluorosilan [96], **D**) [^{18}F]SiFA-nitroimidazole [99], **E**) [^{18}F]HetSiFA-CCK-4 [99], **F**) [^{18}F]SiFA*lin*-TATE [100], **G**) [^{18}F]Fluorosilane peptide [95], **H**) [^{18}F]Fluorosilane peptide [95] .**I**) 4-[^{18}F]SFB-HSA [54], **J**) ^{18}F-DBPOF-c(RGDyk) [16], **K**) BNN-^{18}F-ArBF$_3$ [101].

The hydrolytic cleavage of fluoride from the siliconfluoride acceptor has been hypothesized to follow the same path as a general S_N2 reaction. Due to the larger covalent radius, the nucleophilic substitution is more favored in silicon compared to a carbon central atom, and bulkier steric substituents are required to shield the SiFA-group from defluorination by nucleophilic substitution, hence the introduction of the *tert*-butyl groups. The proposed hydrolysis of a silicon-fluoride acceptor, leading to defluorination, is presented in **Scheme 8**.[97]

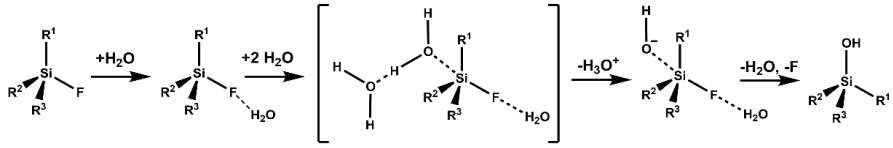

Scheme 8. Proposed hydrolysis mechanism leading to defluorination of an organofluorosilane by S_N2 reaction.[97]

3 AIMS OF THE STUDY

The primary objective of this study was to develop chemoselective fluorine-18 radiofluorination reagents for mild radiolabeling of sensitive biomolecules, to evaluate the stability of the radiolabeling reagents and the performance of the radiolabeled biomolecules *in vivo*. The aims were devided into the following subprojects:

(I) **Develop** prosthetic groups suitable for radiolabeling by isotopic exchange and use them to radiolabel serum albumin and SSTR2 targeting TOC by IEDDA

(II) **Investigate** the stability of the prosthetic group and the radiolabeled biomolecules *in vitro*

(III) **Evaluate** the performance, stability and biodistribution of [^{18}F]F-prosthetic groups and, [^{18}F]fluoroalbumin and Tyr^3-octreotide analogs utilizing *ex vivo* biodistribution methods and PET/CT imaging

(IV) **Investigate** *the in vitro* radiolabeling conditions by IEDDA and to convert the DHP cycloadducts to pyridazines using Tyr^3-octreotide analogs

4 MATERIALS AND METHODS

4.1 EQUIPMENT, REAGENTS AND CONSUMABLES

All reagents were purchased from commercial vendors and used as such without further purification unless otherwise noted. Ultrapure water (18.0 MΩ, at 25 °C, 2 parts per billion of total organic carbon) was produced with a Milli-Q Integral Water Purification System (Merck Millipore, Burlington, MA, USA). Detailed descriptions of chemicals, reagents, consumables, instrumentation, methods, chemical synthesis, radiosynthesis *in vitro*, *ex vivo*, *in vivo* evaluations and other study details are reported in the original publications (**I**-**IV**).

Prosthetic groups and reference compounds for radiolabeled tracers were synthesized at the Department of Chemistry, University of Helsinki, Finland (**I**, **III**, **IV**). The synthesized compounds were characterized with NMR spectroscopy and mass spectrometric methods. NMR measurements were carried out with Varian 300 MHz NMR (I), Bruker Avance NEO 400 NMR spectrometer (**III**, **IV**), Varian Unity Inova 500 NMR spectrometer (**I**) or Bruker Avance NEO 600 NMR spectrometer (**I**). Chemical shifts were referenced to tetramethyl silane (TMS) at δ = 0.0 ppm or to the deuterated solvent residue signal.

Mass spectrometric measurements were conducted with three different instruments. A Bruker Micro TOF with electro spray ionization (ESI) was used in study **I**. HPLC-DAD-ESI-MS analysis was done using Agilent Technologies 1260 Infinity HPLC-DAD system, equipped with Waters Atlantis® T3 3 µm C18 100 Å, LC Column (4.6 × 150 mm), together with Agilent Technologies 6120 Quadruple LC/MS detector with heated electrospray ionization (HESI) on positive ion mode and scan range of 100-2000 *m/z* (**III**, **IV**). UHPLC-HRMS analysis was done using Orbitrap fusion UHPLC Thermo Scientific Dionex Ultimate 3000 ultrahigh performance liquid chromatography (Germering, Germany), equipped with a Waters ACQUITY UPLC BEH C18 column (2.1 × 50 mm, 1.7 µm), and coupled to Thermo Scientific Orbitrap Fusion mass spectrometer (San Jose, CA, USA) using HESI in the positive or negative ion mode and scan range of 70–2000 *m/z* depending on the study (**II**-**IV**). High-performance liquid chromatography was carried out using a Shimadzu HPLC DGU-20A degasser unit, an LC-20AD UPLC LC unit, a SIL-20A HT autosampler, a CTO20 AC column oven, a CBM 20A communications bus module, a Scionix Holland scintillation detector with a 51 BP 51/2 NaI(Tl) crystal and a SPD-M20A diode array detector (**I**-**IV**). The chromatographic separations with HPLC were executed with Waters Symmetry semi-

preparative C18 column (300 × 7.8 mm, 7 μm) (**I**), Phenomenex BioSep SEC s3000 size exclusion column (**I**), Phenomenex Kinetex® 5 μm C18 100 Å, LC Column 250 × 10.0 mm (**III**, **IV**), HiChrom (Alltech) Alltima® 5 μm C18 100 Å, LC Column 250 × 10.0 mm

No-carrier-added [^{18}F]fluoride was produced in-house from ^{18}O-enriched water ([^{18}O]H_2O) with (*p*,*n*) reaction by bombarding $H_2{}^{18}O$ with 10 MeV protons on an IBA Cyclone 10/5 (Louvain-la-Neuve, Belgium) medical cyclotron at the Radiochemistry Unit at the Department of Chemistry, University of Helsinki (**I**, **III**, **IV**). The ^{18}O-enriched water, Hyox-18 (isotopic purity ≥98%) or Water-O18 (isotopic purity ≥97%), were purchased from Rotem Industries Limited (Arava, Israel) and Campro Scientific (Berlin, Germany), respectively. The preclinical radiotracer formulations for PET imaging were produced at the Radiochemistry Unit at the Department of Chemistry, University of Helsinki and the PET image acquisitions were executed at Turku PET Centre at the Department of Chemistry at University of Turku (**III**).

4.2 SYNTHESIS OF PRECURSORS AND REFERENCE COMPOUNDS

The tetrazine prosthetic groups were synthesized in-house from commercially available reagents (**I**, **III**). Bovine serum albumin was used as received and modified with TCO-PEG_4-NHS ester from free lysine residues. Aminooxy-modified TOC and *α*-MSH peptides were purchased as a custom synthesis service from CSBio (Kelly Ct, Menlo Park, CA), and further modified in-house with TCO-aldehydes (**III**, **IV**). Detailed descriptions of synthesis, purifications and characterization of the compounds can be found in original publications **I**-**IV**.

4.2.1 PROSTHETIC GROUPS

SiFA-Tz (**I**) was synthesized with a synthesis route described in **Scheme 9**.

Tetrazine amine (**9.1**) was coupled to the *t*-butoxycarbonyl (*t*-boc) protected carboxylic acid (**9.2**) using HATU as the coupling reagent, purified with liguid-liguid extraction and silica gel column chromatography. The product **9.3** was analyzed with ^{1}H NMR and ^{13}C NMR. The *t*-boc protected tetrazine derivative (**9.3**) was deprotected with 1 M HCl in MeOH and diethylether at +4 ◦C, evaporated to dryness and the deprotected tetrazine oxyamine (**9.4**) was used as such in an oxime-bond formation between a SiFA-aldehyde (**9.5**) to form SiFA-Tz (**9.6**), which was purified with two Sep-Pak C_{18} Light cartridges and by HPLC. Compound **9.6** was analyzed with ^{1}H NMR, ^{13}C NMR, ^{19}F NMR, ESI-TOF MS and UHPLC-HRMS. Detailed descriptions of characterization are found in study **I**.

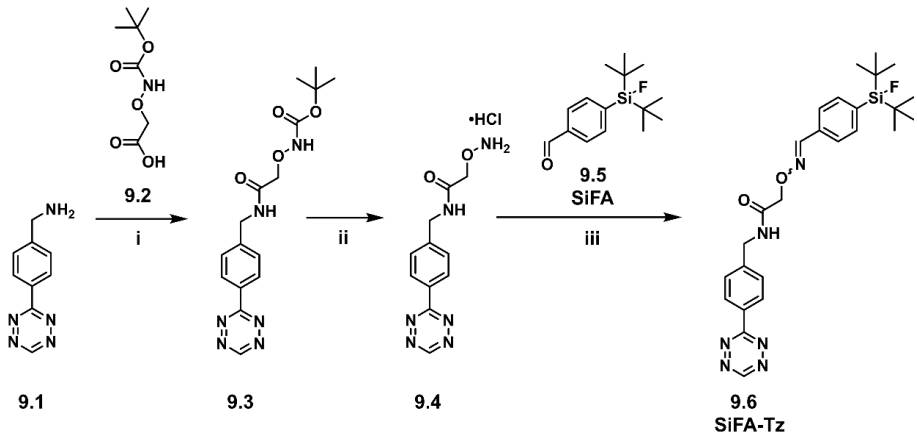

Scheme 9. Synthesis of SiFA-Tz. Reaction conditions used: i) HATU, DIPEA, DMF, 20 h, argon, ii) 1 M HCl Et_2O 25 °C, 24 h, MeOH and iii) aniliniumacetate-buffer pH 4.6, 25 °C, 15 min.

$AmBF_3$-Tz (**III**) was synthesized with a stepwise protocol depicted in **Scheme 10**.

Tetrazine NHS (**10.1**) ester was coupled to 1,2-dimethylethylene diamine (**10.2**) under argon. The resulting product **10.3** was purified with a Sep-Pak C_{18} Plus short cartridge (Waters, MA, USA) and analyzed with ^{1}H NMR. Compound **10.3** was reacted with iodoboron pinacole ester (**10.4**), again under argon overnight, washed with diethyl ether to remove excess pinacol ester, evaporated to dryness and analyzed with ^{1}H NMR. The resulting compound (**10.5**) was heated to 70 °C for 30 min for fluorination of the pinacol, forming a trifluoroborate tetrazine (**10.6**), which was purified with two parallel SPE C_{18} Plus cartridges.

Compound **10.6** was analyzed with ^{1}H NMR, ^{11}B NMR, ^{13}C NMR, ^{19}F NMR and UHPLC-HRMS. Detailed descriptions of characterization are found in study **III**.

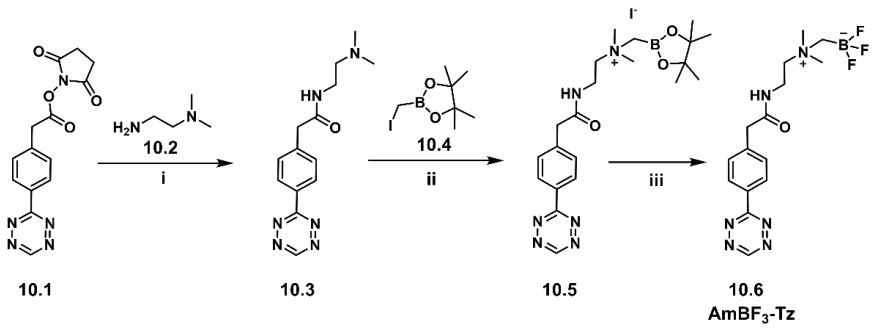

Scheme 10. Synthesis of $AmBF_3$-Tz. Reaction conditions used: i) DCM, argon, ii) ACN, argon, and iii) 1153 µL of DMF, 387 µL of water, 577 µL of 4 M HCl, 577 µL of 3 M KHF_2, 70 °C for 30 min.

$AmBF_3$-PEG_4-mTz was synthesized as a comparison compound in radiolabeling of TOCs, and was earlier developed originally by Liu, and its synthesis starting from $AmBF_3$-alkyne has been earlier reported in the M. Sc. thesises of Iida Kuurne (neé Hirsso) and Tatu Martinmäki and in original publication **IV**. $AmBF_3$-PEG_4-mTz was synthesized in-house and used for radiolabeling with TCO-modified TOC peptide (**IV**).

4.2.2 *TRANS*-CYCLOOCTENE-FUNCTIONALIZED BIOMOLECULES

The biomolecules were purchased from commercial vendors and used as such (Bovine Serum Albumin, study **I**) or ordered custom made (aminooxy-PEG_3-peptides, studies **III**-**IV**). Albumin was modified from lysine residues on the protein structure with TCO-PEG_4-NHS ester and characterized with MALDI-MS (**11.5**, **I**). The custom modified peptides were purchased with a PEG-linker and an aminooxy-functionality for a rapid and mild oxime bond formation with the selected aldehydes. The TCO-aldehydes were either purchased from commercial vendors (TCO-PEG_3-aldehyde **11.4**, commercial) or synthesized in-house (TCO-aldehyde **11.3**, TCO-CHO, synthesized in-house, **III**). Aminooxy-functionalized peptides were further modified, TOC with TCO-CHO (**11.3**) or TCO-PEG_3-aldehyde (**11.4**, **III**, **IV**), and α-MSH with TCO-PEG_3-aldehyde (**11.4**, unpublished data) in 0.3 M anilinium acetate buffer at pH 4.6 (**Scheme 11**), followed by analysis with mass spectrometric methods. The details of synthesis, purification and characterization are found in original publications **III-IV**.

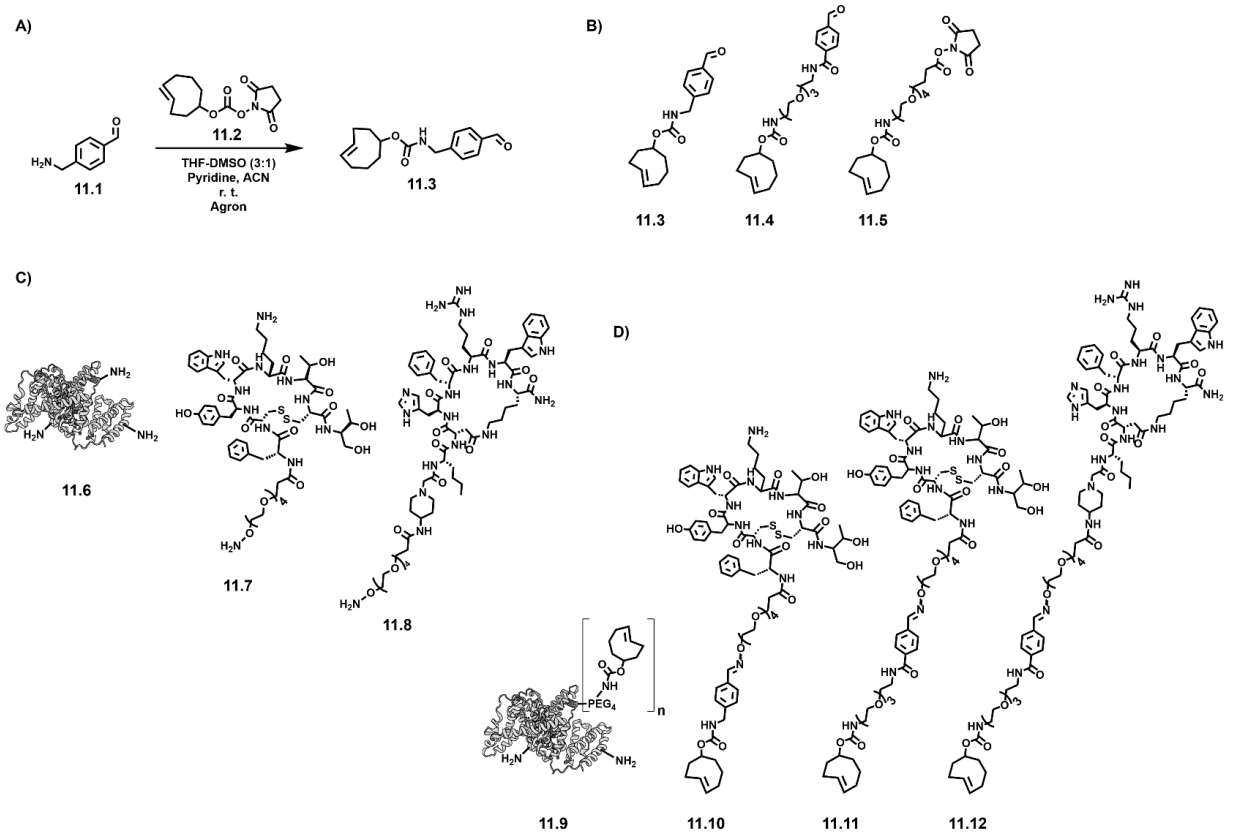

Scheme 11. Synthesis of **A**) TCO-CHO and shemical structures of **B**) TCOs used for bioconjugation, **C**) serum albumin and aminooxy peptides, and **D**) TCO-functionalized biomolecules.

4.2.3 BIOCONJUGATION WITH IEDDA

The TCO-modified biomolecules were conjugated with the selected tetrazines as reference compounds for the radiolabeled biomolecules. TCO modified bovine serum albumin (BSA), albumin-TCO (**11.9**) was conjugated with SiFA-Tz (**9.6**) as a reference compound for the radiolabeled analogue, and the albumin-conjugate (**12.1**) was analyzed with size-exclusion-chromatography (SEC) by HPLC-DAD (**I**). TCO-peptides (**11.10**, **11.11**, and **11.12**) were conjugated with $AmBF_3$-Tz (**10.6**) in aqueous (≥95% water) solution, for producing the peptide-conjugates $AmBF_3$-PEG_4-TOC (**12.2**), $AmBF_3$-PEG_7-TOC (**12.3**), and α-MSH-PEG_7-TOC (**12.4**) as reference compounds (**Scheme 12**). The formed peptide conjugates were analyzed with HPLC-DAD-ESI-MS or UHPLC-HRMS (**III**, **IV**).

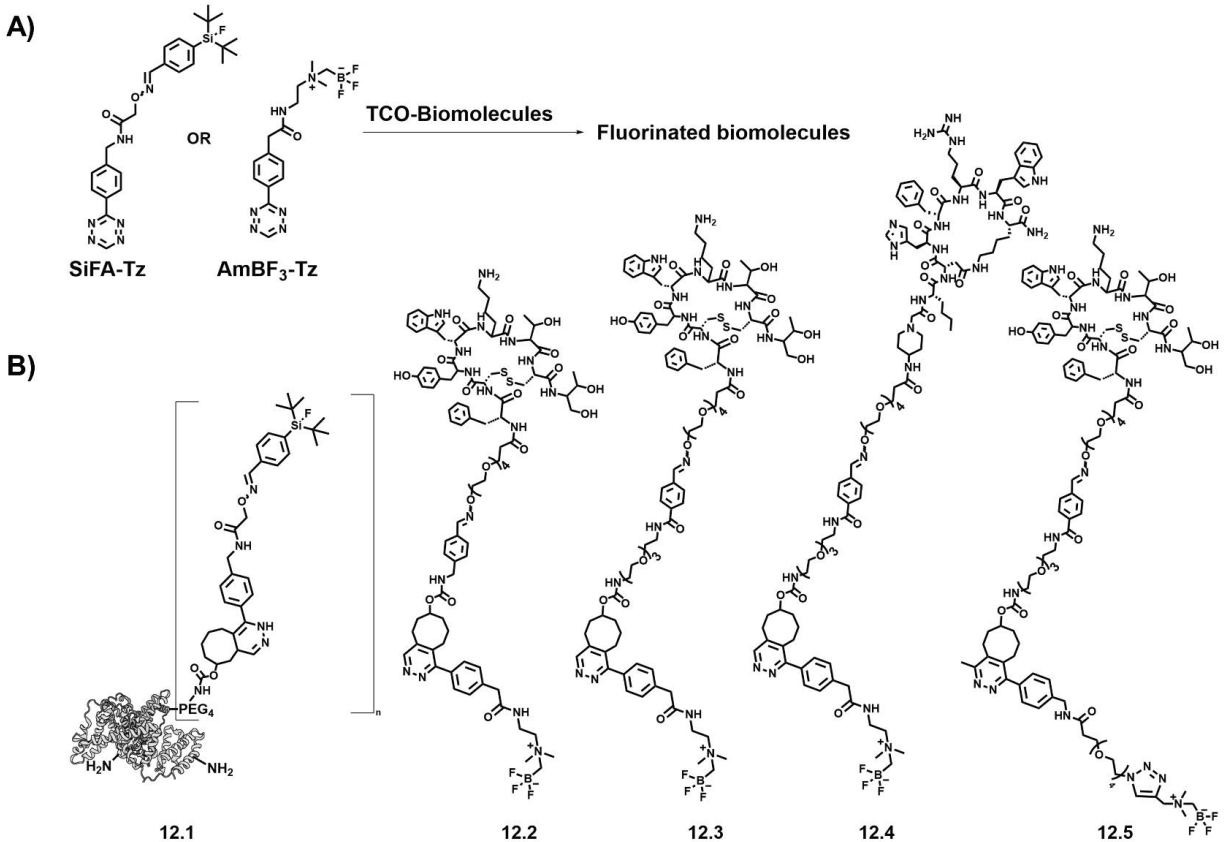

Scheme 12. **A**) Schematic depiction of teterazines used for IEDDA cycloaddition in this study. **B**) Fluorinated biomolecules formed after IEDDA cycloaddition between TCO-biomolecules and tetrazines (**I**, **III**, **IV**).

4.3 RADIOLABELING

4.3.1 PROSTHETIC GROUPS WITH ISOTOPIC EXCHANGE

[^{18}F]Fluoride (no-carrier-added) was produced with Cyclone 10/5 cyclotron (IBA, Louvain-la-Neuve, Belgium) in-house with a $^{18}O(p,n)^{18}F$ nuclear reaction, by bombarding oxygen-18 enriched target water ($H_2{}^{18}O$) with 10 MeV protons. All radiosynthesis was carried out inside a semiautomatic synthesis unit (DM Automation), integrated to a preparative HPLC system. SiFA-Tz (**9.6**) and $AmBF_3$-Tz (**10.6**) were radiolabeled by IE providing the corresponding radiolabeled prosthetic groups [^{18}F]SiFA-Tz ([^{18}F]**9.6**) and [^{18}F]$AmBF_3$-Tz ([^{18}F]**10.6**) (**Scheme 13**).

[^{18}F]SiFA-Tz ([^{18}F]**9.6**). The radiosynthesis was tested in two different methods, by one-step and two-step protocols. For the radiosynthesis of [^{18}F]SiFA-Tz, the nucleophilic [^{18}F]fluoride trapped with a quaternary methylammonium (QMA) Light ion-exchange cartridge was eluted with alkaline K^+/K2.2.2/[^{18}F]F^--complex solution, and evaporated azeotropically to dryness with anhydrous ACN. The one-step method comprised of radiolabeling **SiFA-Tz** (**9.6**, 500 µg, 1.0 µmol) in 500 µL of anhydrous ACN by incubating for 2 min (25 °C), and the reaction was quenched by diluting with anhydroys ACN (500 µL). The two-step method comprised of radiolabeling the prosthetic group **SiFA** (**9.5**, 280-350 µg, 1.0-1.3 µmol) in anhydrous ACN (0.5 mL incubated for 2 min, 25 °C), followed by the oxime bond formation between **SiFA** (**9.5**) and the tetrazine oxyamine (**9.4**, 700 µg, 2.4 µmol) in 0.3 M anilinium acetate buffer pH 4.6 (200 µL) and ACN (50 µL), at room temperature in 15 min. [^{18}F]**9.6** was purified with preparative HPLC coupled to the semi-automated synthesis unit inside the hotcell.

[^{18}F]$AmBF_3$-Tz ([^{18}F]**10.6**). The radiosynthesis was conducted in acidic aqueous solution with nucleophilic [^{18}F]fluoride. [^{18}F]fluoride was trapped on a Chromafix 154 PS-HCO_3 ion-exchange cartridge. Two solvents were tested for eluting the trapped [^{18}F]fluoride from the resin; 1) 0.9% NaCl (150 µL) or 2) pyridazine HCl buffer, pH 2.0 (100 µL), into the tube containing the tetrazine. 0.9% NaCl was concentrated at 125 °C under argon gas flow until 10-25 µL reaction volume was reached. Tetrazine (100 nmol) in 5 µL of ACN was added into a polypropylene tube containing 10 µL of pyridazine HCl buffer (pH 2.0). The reaction mixture was heated for an additional 10 minutes at 85 °C and quenched with 600 uL of H_2O:EtOH (50:50). When using the buffer, the mixture of **10.6** and pyridazine HCl buffer was concentrated by heating at 85 °C and under argon gas flow (20 mL/min), facilitating the radiolabeling when reaction volume reached tens of microliters. After 15 minutes the crude reaction mixture was quenched with water (600 µL) and purified with a Sep-Pak

C_{18} Light cartridge. The chemical structures of the prosthetic groups together with the radiolabeling conditions are depicted in **Scheme 13**.

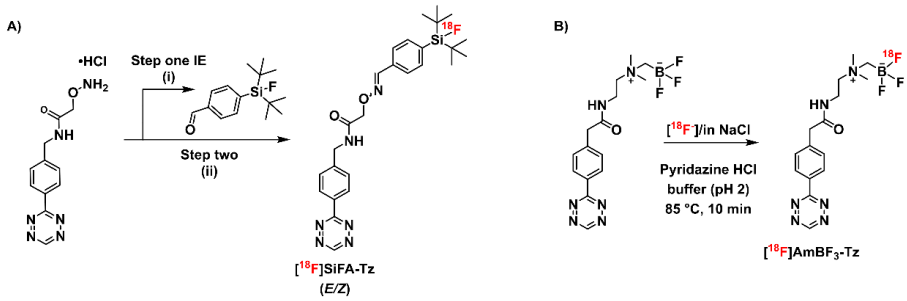

Scheme 13. **A**) Radiosynthesis of [^{18}F]SiFA-Tz was executed in two steps; isotopic exchange (IE), followed by oxime bond formation. i) ACN, K^+/K2.2.2/$^{18}F^-$, 25 °C, 2 min ii) 4 + Anilinium acetate buffer pH 4.6 at 25 °C, 15 min. **B**) Radiosynthesis of [^{18}F]AmBF$_3$-Tz was done in one step using acidic conditions and elevated temperature.

4.3.2 BIOCONJUGATION WITH IEDDA

[^{18}F]SiFA-Tz ([^{18}F]**9.6**) and [^{18}F]AmBF$_3$-Tz ([^{18}F]**10.6**) were used as prosthetic groups for radiofluorination of TCO-biomolecules in mild conditions.

[^{18}F]Fluoroalbumin ([^{18}F]**12.1**). HPLC purified [^{18}F]SiFA-Tz ([^{18}F]**9.6**) was added to the lyophilized albumin-TCO (350 µg, 4.3 nmol) and incubated at room temperature for 15 min. The produced [^{18}F]**12.1** was purified by ultrafiltration (10 000 *g*, Eppendorf Centrifuge 5430, Ag, Hamburg) with molecular weight cut-off (MWCO) filters (30K, VWR® Radnor, PA, USA) with 0.01 M phosphate-buffered saline (PBS) as the eluent.

A general procedure for radiosynthesis of peptide tracers [^{18}F]AmBF$_3$-PEG$_4$-TOC ([^{18}F]**12.2**)**, [^{18}F]AmBF$_3$-PEG$_7$-TOC,** ([^{18}F]**12.3**) **[^{18}F]AmBF$_3$-PEG$_7$-α-MSH** ([^{18}F]**12.4**) **and [^{18}F]AmBF$_3$-PEG$_{11}$-mTOC** ([^{18}F]**12.5**). TCO functionalized peptide (50 nmol in 20-50 µL of water) was added into the reaction mixture (20 µL) of the radiolabeled tetrazine and heated at 60 °C for 15 minutes. The reaction mixture was diluted with water and purified with two C18 cartridges by washing with ultrapure water and by eluted with ethanol (150 µL), followed by 0.01 M PBS (200 µL). The purified peptide solution was diluted with 0.01 M PBS to constitute ≤ 5% ethanol for intravenous administration.

An example of radiolabeling with IEDDA executed in this study is presented in **Scheme 14** between TCO-PEG$_7$-TOC (**11.11**) and [^{18}F]AmBF$_3$-Tz ([^{18}F]**10.6**), affording [^{18}F]AmBF$_3$-PEG$_7$-TOC (**12.3**) in full conversion.

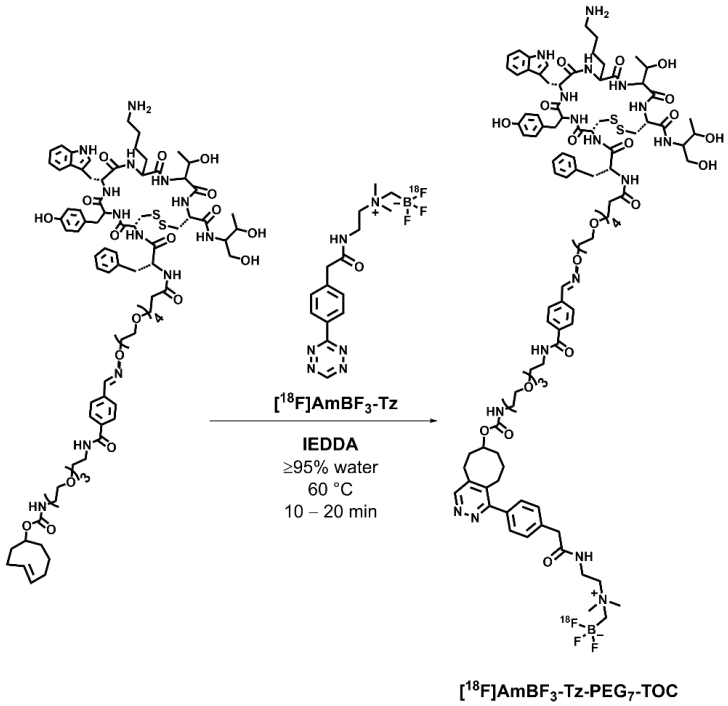

Scheme 14. General depiction of radiolabeling of TCO-modified TOC with [^{18}F]AmBF$_3$-Tz ([^{18}F]**10.6**) IEDDA providing [^{18}F]AmBF$_3$-PEG$_7$-TOC ([^{18}F]**12.3**).

4.3.3 CONVERSION OF DHPS TO PYRIDAZINES DURING IEDDA

The tetrazine (100 nmol) was radiolabeled with the general method described earlied (**III**, **IV**). After radiolabeling, the temperature of the reaction mixture was adjusted to 60 °C and the TCO-modified peptide (50 nmol, in 500 µL of water) was added to the reaction vial containing the crude radiolabeled tetrazine. The reaction mixture was heated for maximum 20 minutes at 60 °C in aqueous solutions (95:5 %v/v of H_2O:ACN), diluted with 8 mL of water, and inserted to two SPE C_{18} cartridges assembled parallel. The cartridges were washed with water (40 mL), then 20% EtOH (3 mL) and the radiolabeled peptide was eluted with ethanol (400 µL) and 10 × PBS (400 µL) pH=7.4. The purified product was diluted with water to constitute 1 × PBS and analyzed with radio-HPLC (**IV**).

4.4 IN VITRO EVALUATION

In vitro evaluation of the radiotracer stability was conducted with hydrolytic stability studies in its injection formulation or in 1 × PBS. Enzymatic stabilities were studied with human or mouse plasma incubation experiments. The specific binding to SSTR2 of novel TOC radiotracers were additionally evaluated in SSTR2-overexpressing AR42J tumor cell line. The radioactive samples were analyzed with either radio-TLC, radio-HPLC or gamma counting methods. The stable isotope (^{19}F) containing samples from the mouse liver microsome (MLM) mediated metabolism studies were analyzed with HRMS.

4.4.1 LIPOPHILICITY AND IN VITRO STABILITY

The Log$D_{7.4}$ values were determined by shake-flask method as a distribution profile between octanol and PBS. The distribution of the radiotraces between octanol and PBS was calculated according to equation

$$\mathrm{Log}D_{7.4} = \mathrm{Log}\,\frac{\mathrm{A_{OCT}}}{\mathrm{A_{PBS}}}$$

where A_{oct}=activity of octanol and A_{PBS}=activity of PBS in the sample. The detailed description of the Log$D_{7.4}$ determination is described in original publication **I**, **III** and **IV**.

In order to evaluate the hydrolytic stability, the selected radiotracer was incubated in 1 × PBS at ambient temperature in a microtube with shaking (400 rpm). At selected time points samples were analyzed with radio-HPLC or TLC for analysis methods (**I**, **III**).

The enzymatic stability of selected radiotracers was studied by incubating in 50% human plasma-PBS (**I**, **III**) or mouse plasma (**I**) at 37 °C. The human plasma was received from Finnish Red Cross Blood Service, Helsinki, Finland (anonymous donor FFP-24, permission 33/2018). Mouse whole blood from healthy CD-1 mice was collected from a cardiac puncture after Co_2 asphyxiation and cervical dislocation. Mouse plasma was separated from mouse blood cells by centrifugation (1000 × g, 10 min). At selected time points a sample was diluted with twice its volume of cold ACN and centrifuged (10 000 × g, 5 min). The radioactivity distribution between the precipitated pellet (*protein-bound fraction*) and the supernatant (*free fraction*) were measured with a gamma counter, after which a sample from the supernatant was analyzed with radio-HPLC.

4.4.2 MOUSE LIVER MICROSOMAL STABILITY

4.4.2.1 Study outline

Phase I and phase II metabolites of the cold reference compound SiFA–Tz were generated *in vitro* in mouse liver microsomes (MLMs), that contain several enzymes needed for metabolism of compounds *in vivo* (**II**). The microsomal solutions were prepared abiding the manufacturer instructions (Liver microsomes prepared from a pool of male CD-1 mice, 20 mg/ml, Gibco, Thermo Fisher Scientific, Waltham, MA, USA). Phase I metabolites were generated in a suspension of MLMs in 100 mM potassium phosphate buffer containing the cold reference and in the presence of 20 mM NADPH at 37 °C. Phase II metabolite suspensions contained the cold reference, $MgCl_2$, MLMs, alamethicin (5 mg/mL) in DMSO, uridine diphosphate glucuronic acid (UDPGA) and NADPH and the samples were incubated at 37 °C. Phase I and phase II reagents and co-factors are presented in **Table 5**. For negative controls the following samples were prepared: samples with all co-factors for 0 min. (*control 1*), samples without SiFA–Tz and UDPGA for 0 min (*control 2*), samples without NADPH for 240 min (*control 3*), and samples without microsomes for 240 min (*control 4*). The reactions were terminated with equal volume of cold ACN, vortexed, centrifuged (3000 *rpm*, 5 min), supernatants separated from the pellet and filtered (0.22 µm PVDF sterile filter) prior UHPLC-HRMS separation and analysis.

Table 5. Mouse liver microsome preparations used for phase I and II metabolite generation.

Reagent	Phase I	Phase II
SiFA-Tz (**9.6**) in ACN	2 µL	2 µL
MLMs (20 mg/mL solution)	5 µL	5 µL
100 mM potassium phosphate buffer pH 7.4	183 µL	n.a.
100 mM potassium phosphate buffer pH 7.4 (cont. 1 mM of $MgCl_2$)	n.a.	173 µL
NADPH (20 mM)	10 µL	10 µL
UDPGA (20 mM)	n.a.	10 µL or 15 µL*
Alamethicin (5 mg/mL in DMSO)	n.a.	1 µL

n.a.; not applicable

*10 µL for 5 min and 60 min samples, 15 µL for 120 min and 240 min samples.

4.4.2.2 UHPLC HRMS method

The HRMS experiments were conducted with UHPLC Thermo Scientific Dionex Ultimate 3000 ultra-high performance liquid chromatography (Germering, Germany) coupled to Thermo Scientific Orbitrap Fusion mass spectrometer (San Jose, CA, USA).

UHPLC separation was executed with Waters ACQUITY UPLC BEH C18 column (2.1×50 mm, 1.7 µm, 130Å) at 40 °C using gradient of 0.1% formic acid in water (A) and 0.1% formic acid in ACN (B). The flow rate was 0.5 mL/min, and the injection volume was 2.5–5.0 µL. The ionization was done using heated electrospray ionization (HESI) in the positive ion mode at resolution of 120,000. Mass accuracy of the instrument using internal calibration was specified to be ≤ 3 ppm. The samples were analyzed in full scan mode with nontargeted screening method, and the raw data was filtered with Compound Discoverer (3.0 and 3.1 by Thermo Fisher Scientific, Waltham, MA, USA) for phase I and phase II transformation reactions. The structure elucidation of formed metabolites was done using MS/HRMS technique, and fragmentation of the protonated molecules was executed with higher-energy collisional dissociation (HCD), with selected collision energies for different detected proposed metabolites. The identification criteria for the LC-MS analysis state that the retention time (t_R) of the identified compound corresponds to the reference compound with a tolerance of ±2.5% and the mass difference between the measured and theoretical mass has to be ≤ 2.5 ppm. Detailed description of the study can be found in original publication **II**.

4.4.2.3 Metabolite identification and structure elucidation

The structures of the detected proposed metabolites were elucidated by applying MS/HRMS using HCD (at 30%) for generating fragment ions of protonated molecules. The samples were analyzed with nontargeted HRMS method and the metabolites, in addition to the isomers of SiFA–Tz and SiFA–H_2Tz, were screened with Xcalibur (Thermo Fisher Scientific, Waltham, MA, USA), Compound Discoverer (3.0 and 3.1 by Thermo Fisher Scientific, Waltham, MA, USA), and MassFrontier softwares (7.0 and 8.0, Thermo Fisher Scientific, Waltham, MA, USA). A metabolic pathway was proposed based on the results (**II**).

4.4.3 CELLULAR UPTAKE STUDY

Rat pancreatic tumor cell line AR42J (ATCC CRL-1492), that expresses SSTR2, was obtained from American Type Culture Collection (Manassas, VA, USA). AR42J cells were cultured at 37 °C in an incubator with relative humidity of 95% containing 5% CO_2. Cells were grown to >90% confluence and one million cells/well were seeded overnight on 6-well plates. The growth media was removed and the radiotracer containing medium was added. A set of cells were co-incubated in the presence of 220-fold excess unmodified octreotide to study the specificity of the cell uptake. At the designated time-points, the cell media was removed and collected to a scintillation tube, cells

washed with cold 0.01 M PBS, and the supernatant collected into the same scintillation tube (*free fraction*). Ice-cold glycine buffer was added on the cells, incubated on ice (5 min), supernatant removed, the procedure repeated once more, cells washed with ice-cold 0.01 M PBS, and collected to the same scintillation tube (*membrane-bound fraction*). 1 M NaOH was added on the cells and left incubating at ambient temperature (10 min). The supernatant was removed, the wells washed 2 × with cold 0.01 M PBS, and the supernatants collected into the same microtube (*internalized fraction*). The three fractions were measured with a gamma counter, the counts per minute (CPM) of each fraction (n = 3) were determined, and the internalization presented in percent (%) normalized to the radioactivity in all three fractions (**III**-**IV**).

4.5 BIOLOGICAL EVALUATION

4.5.1 *EX VIVO* BIODISTRIBUTION

The animal experiment were conducted under a project license approved by National Board of Animal Experimentation in Finland (license number ESAVI/12132/04.10.07/2017). Female CD-1 mice, female C57BL/6JRj, male severe combined immunodeficiency disease (SCID) mice and nude NMRI mice were purchaced from Charles River. Mice were group-housed in a HEPA-filtered housing unit (SCID and nude mice) in polycarbonate cages on aspen bedding in HEPA-filtered housing units. Envigo Teklad Global Diet food and tap water were available *ad libitum*. Housing conditions were maintained at 21 ± 1 ◦C and a relative humidity of 55 ± 15% with a 12:12 hour light-dark cycle. The radiotracers, in their corresponding injection formulations, were administered to awake mice *via* the lateral tail vein. The mice were euthanized at predetermined time-points with CO_2 asphyxiation followed by cervical dislocation. Selected organs and tissue samples were collected, washed with water, blotted dry, measured with a gamma counter, and weighted after decay of radioactivity. After PET/CT imaging, the organs were collected, measured with a gamma counter, and weighted. The detailed descriptions of the studies are described in original publications (**I**, **III**).

4.5.2 *EX VIVO* TISSUE PREPARATIONS

4.5.2.1 Mouse liver homogenate for metabolite screening

Livers of CD-1 mice (female, n = 2) were harvested during *ex vivo* studies after intravenous administration of [^{18}F]SiFA–Tz ([^{18}F]**9.6**), weighted, measured with a gamma counter, and stored at -20 °C. The livers were thawed, homogenized once at room temperature with a VDI 12 homogenizer in cold ACN-water (80:20) mixture, centrifuged (10 000 × g, 10 min), and the separated supernatants were filtered with 0.22 μm syringe filter. The filtered supernatants were analyzed with UHPLC-HRMS to screen for parent compound and possible metabolites.

4.5.2.2 Mouse blood and urine sample treatment

Samples of blood and urine were collected after *ex vivo* biodistribution studies for evaluation of the biological stability of the radiotracers. Selected small radiotraces were analyzed to evaluate whether the tracer was found intact in the biological fluids and to determine if any decomposition occurred. The plasma protein, [^{18}F]fluoroalbumin ([^{18}F]**12.1**) was sampled from mouse blood to evaluate the size-distribution of the radiolabeled species found in blood. The aim was to determine if a change in the apparent size (molecular weight) of radiolabeled species was detected as a function of time (**I**). After administration of [^{18}F]fluoroalbumin, the plasma was separated from the blood cells containing pellet fractionated with a 30 kDa MWCO centrifugal filter, to separate over 30 kDa [^{18}F]F-molecules from below 30 kDa ^{18}F-labeled molecules. Based on the distribution of radioactivity, the percentage ratio was determined. Over 30 kDa molecules were accounted as [^{18}F]fluoroalbumin protein (m_W ca. 82 kDa). MWCO filtering and separation protocol is depicted in **Scheme 15** and in origical publication **I**. After administration of TOC-analog [^{18}F]AmBF$_3$-PEG$_4$-TOC ([^{18}F]**12.2**), mouse blood and urine were collected after *ex vivo* biodistribution study and centrifuged (1000 × g, 10 min) to separate the supernatant from the cell -containing pellet (blood; red blood cells, urine; red and white blood cells, and epithelial cells). The pellet and supernatants were separated, measured with a gamma counter, and the supernatants were analyzed to evaluate the stability of [^{18}F]**12.2** *in vivo* (**III**). For small compounds and peptides, cold ACN (2 × the volume of plasma) was added to the plasma and centrifuged (10 000 × g, 5 min) to precipitate the proteins in the biological fluids. After measuring the radioactivities in the fractions, a sample (4 μL) was applied on a silica TLC and after elution, analyzed with digital autoradiography. Detailed description of the protocol is found in original publications **I** and **III**.

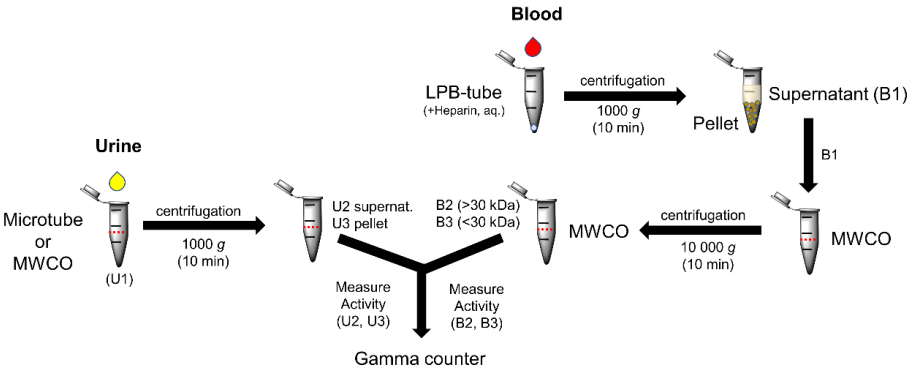

Scheme 15. General depiction of sample preparation of *ex vivo* mouse plasma sample for separating below and over 30 kDa ^{18}F-molecules after intravenous administration of [^{18}F]fluoroalbumin ([^{18}F]**12.1,** study **I**), together with depiction of urine pretreatment after administration of TOC radiotracer ([^{18}F]**12.2**, study **III**). LPB; low protein binding, MWCO; molecular weight cut-off filter-containing microtubes, ACN, U;urine, B;blood, rpm;revolutions per minute. © S. Otaru 2022

4.6 PET/CT IMAGING AND DOSIMETRY

The radiotracers were formulated and administered to selected mouse models for *in vivo* evaluation of their biological behaviour. [^{18}F]AmBF$_3$-Tz ([^{18}F]**10.6**) in 10% ethanol-0.01 M PBS was administered intravenously to male SCID mice (CB.17 SCID) 11.0 ± 0.5 MBq, 150 µL, n = 4) and healthy female C57BL/6JRj mice (11.3 ± 0.3 MBq, 150 µL, n = 4) under 2% isoflurane anesthesia. A dynamic PET/CT image was acquired with Inveon PET/CT from 0-60 min after administration followed by a 15 min static scan at 4 hours after administration. [^{18}F]AmBF$_3$-PEG$_7$-TOC in 4% ethanol-0.01 M PBS was administered intravenously (0.80 ± 0.30 MBq, 0.2 nmol, 150 µL, n = 4) to AR42J tumor bearing Rj:NMRI-*Foxn1*$^{nu/nu}$ mice under 2% isoflurane anesthesia. PET/CT images were acquired with Molecubes PET (β-CUBE) coupled with a CT (X-CUBE) (MOLECUBES NV, Ghent, Belgium).

Standardized uptake values (SUVs) were determined from the PET image by drawing regions-of-interest (ROI) around selected organs (heart, liver, kidney, lung, muscle, bladder). The ratio of radioactivity per unit volume of the ROIs normalized to the injected dose were measured with Carimas software. After the second PET imaging (t = 270 ± 1.9 min, n = 4), the organs were harvested, weighed, the radioactivity in each tissue sample measured with a γ-counter and reported as percentage of injected radioactivity dose per gram of tissue (%ID/g).

Based on the dynamic preclinical PET-scan (Molecubes), region of interest (ROI) were drawn around heart, kidneys, liver and lungs, and the time-activity curves (TAC) in the selected organs were converted from mouse to human TACs with the equation;

$$TAC_{organ,h} = TAC_{organ,m} \times \frac{{}^{m_{organ,h}}/_{WB_h}}{{}^{m_{organ,m}}/_{WB_m}}$$

where;
$m_{organ,h}$ = human whole-body mass
$m_{organ,m}$ = mouse whole-body mass
WB_h = human whole-body mass
WB_m = mouse whole-body mass

The TACs were normalized to 1 MBq injection and the decay correction was removed, and the TACs extrapolated into 3000 minutes. The input for OLINDA/EXM (version 2.1, Vanderbilt University, 2012) dosimetry software was the number of disintegrations in source organs as TAC from time 0 to 3000 minutes.

4.7 STATISTICAL METHODS

The graphs were plotted with GraphPad Prism software (GraphPad Software, San Diego, CA, USA) and the statistical significance between the groups were evaluated using unpaired *t*-test (Welch's correction) with GraphPad Prism software version 9.1.1 (III, IV), version 8.0 (II) and version 8.0.1 (I). $P < 0.05$ was regarded as statistically significant. The significances (p-value) were $*p < 0.05$, $**p < 0.01$, and $***p < 0.001$.(**III**) Statistical significance was set at $*p < 0.05$, $**p < 0.005$, $***p < 0.001$, $****p < 0.0001$).(**IV**) The graphs with statistics are presented as mean ± standard deviation (SD).

5 RESULTS AND DISCUSSION

5.1 SYNTHESIS

In this study precursors were designed to contain *three* main features:

I. apply a fluorophilic heteroatom nucleus in the structure enabling $^{19}F/^{18}F$ **isotopic exchange**
II. include a **tetrazine** tag ensuring chemoselective delivery of the radiolabel to the *trans*-cyclooctene modified biomolecule
III. tailor the pharmacokinetics of the prosthetic group or the final biomolecular radiotracer by adding **PEG linkers**

5.1.1 SYNTHESIS OF TETRAZINE PROSTHETIC GROUPS

SiFA-Tz (**9.6**) was synthesized in three steps. The first step provided the *t*-Boc protected aminooxy tetrazine (**9.3**) in 65% yield. In the second step the aminooxy **9.3** was deprotected affording the tetrazine oxyamine (**9.4**) hydrochloride salt, also in 65% yield, ready for use in the next step as such. The third step between the SiFA-aldehyde (**9.5**) and tetrazine oxyamine (**9.4**) hydrochloride provided the final prosthetic group SiFA-Tz (**9.6**) as *E*- and *Z*-isomers, arising from the formed oxime bond, with a yield of 90%.

The first step of the synthesis of $AmBF_3$-Tz (**10.6**) comprised of an amide formation between tetrazine NHS ester (**10.1**) and 1,2-dimethylethylene diamine (**10.2**) in 68 ± 26% (n = 3) yield. The formed tetrazine dimethylamine (**10.3**) was alkylated with an iodoboronpinacol ester (**10.4**) in 58 ± 31% (n = 3) yield providing compound (**10.5**). In the third step the pinacol ester tetrazine (**10.5**) was deprotected and fluorinated in acid catalyzed conditions affording the trifluoroborate tetrazine (**10.6**) in 90% yield. The third step included heating the tetrazine in 70 °C. The formation of the fluorinated product was monitored carefully by HPLC-DAD (254 nm, 534 nm). The ^{1}H NMR of **10.6** revealed characteristic proton signal at the para-position of the Tz ring at 10 ppm, and the presence of the Tz ring was verified by HPLC-DAD with the characteristic absorbance of a tetrazine detected above 500 nm wavelength. In the ^{19}F NMR spectra of **10.6** the splitting of the fluorine signal coupled to the trifluoroborate ^{11}B, and the boron-11 coupling to fluorine-19 seen in the ^{11}B NMR spectra, as a split quartet signal, verified the formation of a trifluoroborate. Compound **10.6** eluted at t_R = 4.59 minutes on UHPLC-HRMS with a mass peak corresponding to the calculated protonated molecule ion $[M+H]^+$.

5.1.2 TCO MODIFICATION OF BIOMOLECULES AND BIOCONJUGATION WITH IEDDA

All model biomolecules were specifically selected due to their extensively studied characteristics to evaluate the influence of the prosthetic group and the bionconjugation strategy on the *in vivo* behaviour of the well-known biomolecules. The biomacromolecular model protein, bovine serum albumin was functionalized with TCO, for rapid and mild incorporation of [^{18}F]fluoride in mild conditions. Albumin-TCO (1 mg) was dissolved in 1 mL of ultrapure water and analyzed with MALDI-TOF-MS (calculated for bovine serum albumin 66.338 kDa, measured for albumin-TCO 82.039-82.265 kDa), corresponding to 40 TCOs per albumin protein molecule. The imaging targets, reactive groups, and measured masses of the modified biomolecules are presented in **Table 6**. SSTR2 targeting cyclic TOC peptide and cyclic α-MSH peptide, selected as model biomolecules to represent biomolecules of lower molecular weight in the study, were functionalized with a linker and TCO for mild fluorine-18 radiolabeling (**IV**, unpublished data).

Table 6. Results of TCO-modification and IEDDA cycloaddition between synthesized tetrazines and TCO-modified TOCs and serum albumin.

Compound	Measured and calculated mass	Elemental composition	Imaging target	Study
TCO-PEG$_4$-Tyr^3-octreotide (**11.10**)	$[M+2H]^{2+}$= meas. 784.7, calc. 784.4	$C_{77}H_{108}N_{12}O_{19}S_2^{2+}$	SSTR2 receptor	**III**
TCO-PEG$_7$-Tyr^3-octreotide (**11.11**)	$[M+3H]^{3+}$ = meas. 586.61316, calc. 586.61454 (Δ = -2.35545 ppm) $[M+2H]^2$ = meas. 879.41663, calc. 879.41817 (Δ = -1.75922 ppm)	$C_{85}H_{125}O_{23}N_{13}S_2^{3+}$ $C_{85}H_{124}O_{23}N_{13}S_2^{2+}$	SSTR2 receptor	**III**
AmBF$_3$-PEG$_4$-Tyr^3-octreotide (**12.2**)	$[M+3H]^{3+}$ = meas. 636.6, calc. 636.6 $[M+2H]^{2+}$ = meas. 953.9, calc. 953.9 $[M+H]^+$ = meas. 1907.6, calc. 1907.9	$C_{92}H_{127}BF_3N_{16}O_{20}S_2^{3+}$ $C_{92}H_{126}BF_3N_{16}O_{20}S_2^{2+}$ $C_{92}H_{125}BF_3N_{16}O_{20}S_2^{+}$	SSTR2 receptor	**III**, **IV**
AmBF$_3$-PEG$_7$-Tyr^3-octreotide (**12.3**)	$[M+3H]^{3+}$ = meas. 698.99744, calc. 698.99612 (Δ = 1.87679 ppm) $[M+2H]^{2+}$ = meas. 1047.99207, calc. 1047.99055 (Δ = 1.44731 ppm)	$C_{100}H_{142}BF_3O_{24}N_{17}S_2^{3+}$ $C_{100}H_{141}BF_3O_{24}N_{17}S_2^{2+}$	SSTR2 receptor	**III**, **IV**
AmBF$_3$-PEG$_{11}$-m-Tyr^3-octreotide (**12.5**)	$[M+2H]^{2+}$ = meas 1184.06909, calc. (Δ = -1.66578 ppm)	$C_{112}H_{163}O_{28}N_{20}BF_3S_2^{2+}$	SSTR2 receptor	**IV**
Albumin-TCO (**11.9**)	82039-82265	n.d.	Blood pool/vasculature	**I**
Fluoroalbumin (**12.1**)	n. a.	n.d.	Blood pool/vasculature	**I**

For high-resolution mass spectrometry measurement, mass errors are given in parts per million (ppm).

5.2 RADIOLABELING

5.2.1 PROSTHETIC GROUPS

In this study, nucleophilic [^{18}F]fluoride was pretreated in two different ways prior radiolabeling, in order to utilize it for the radiolabeling of both SiFA-Tz (**9.6**) and AmBF$_3$-Tz (**10.6**) by isotopic exchange reactions (**I**, **III**). These prosthetic groups had two different radiolabeling approaches rendering them useful in a varying circumstances.

SiFA-Tz (**9.6**) was radiolabeling was tested with two methods: 1) a two–step method where the SiFA-aldehyde moiety (**9.5**) was radiolabeled prior to the oxime formation with the tetrazine (**9.4**), and 2) a one–step direct radiolabeling of SiFA-Tz (**9.6**) after the oxime-bond formation (**I**). The two-step approach provided a higher RCY, while in the one-step approach, the RCY of the product was observed to decrease rapidly as a function of time, due to the decomposition of the precursor in the alkaline reaction mixture. No further optimizations or repetitions was done for the one-step method. Radio-TLC analysis of [^{18}F]SiFA-Tz ([^{18}F]**9.6**) revealed the formation of two isomers arising from the formed oxime bond, with *E*-isomer as the predominant isomer and the *Z*-isomer detected only in 1.5 ± 0.4% (n = 16). A later analysis with HRMS revealed that the dominating *E*-isomer was present in 92 ± 0.7% (n = 2). The significant difference in the ratio of the *E*- and *Z*-isomers is likely attributed to the sterical hindrance provided by the bulky *tert*-butyl groups bound to the silicon atom (**I**, **II**). An earlier attempt to provide a fluorine-18 labeled SiFA-derivatized tetrazine-derivative, [^{18}F]-SiFA-OTz for bioorthogonal radiochemistry, has been reported, which provided the prosthetic group in decay-corrected RCY 78 ± 5% within 25 min, with A_m of 7.1–8.6 GBq/μmol.[102]

AmBF$_3$-Tz (**10.6**) was radiolabeled in acidic (pH 2) buffered solution in elevated temperature (**III**). The [^{18}F]fluoride eluent was modified more suitable for our use, ensuring repeatable radiolabeling yields (20.8 ± 10.3%, n = 7) in microliter volumes (optimal volume = 10–20 μL). The RCYs correlated with previously reported yields for AmBF$_3$-tracers, reaching approximately 16–35%.[103-106] Decreasing the reaction volume 2.5 times increased the yield 6 times at 85 °C using 0.9% NaCl for the elution with 200 nmol of **10.6**. For eluting adequate amounts of [^{18}F]fluoride, a minimum 20–30 μL of 0.9% NaCl was required. Hence, we chose to substitute aqueous 0.9% NaCl as [^{18}F]fluoride eluent with pyridazine HCl eluent formulation, which we modified from the recipe reported by Liu et al.

The [^{18}F]fluoride release efficiency from the cartridge remained high (93 ± 2%, n = 3) with the new buffer formulation, providing a suitable reaction media for radiolabeling directly after rapid concentration (~10 min), decreasing the evaporation time from 45 minutes (100 µL 0.9% NaCl as the eluent) to 10 minutes. Kwon *et al* reported utilization of pyridazine HCl buffer for the elution of [^{18}F]fluoride from the ion exchange cartridge,[107] a method also applied in this study (**III**). [^{18}F]Fluoride was trapped to a µQMA cartridge and eluted with the reaction media buffer, since elution with the buffer (93 ± 2%, n = 3), provided equally good [^{18}F]F^- release to 0.9% NaCl but with shorter concentration time of the aqueous [^{18}F]F^- to appropriate volumes and a suitable reaction media for radiolabeling directly after rapid concentration (~10 min). Good A_m (15.4 ± 9.2 GBq/µmol) and DCY (20.8 ± 10.3% (n = 7) was obtained.

Both novel prosthetic groups [^{18}F]**9.6** and [^{18}F]**10.6** would benefit from further experiments to optimize the used tracer amount in the radiolabeling and comparison of the resulting A_m to the reported ones. Lowering the used amount of tracer while increasing the starting activity would likely increase A_m and would have a direct influence on the image quality of the resulting receptor targeted biological radiotracers. The RCY (%), RCP (%) and A_m of the prosthetic groups (**I, III**) are presented in **Table 7**.

Table 7. Radiolabeling results of prosthetic groups [^{18}F]SiFA-Tz ([^{18}F]**9.6**) and [^{18}F]AmBF$_3$-Tz ([^{18}F]**10.6**).

Radiotracer	RCY (%)	RCP (%)	A_m (GBq/µmol)	Study
[^{18}F]SiFA ([^{18}F]**9.5**)	89-99.6% (inc.yield)*	≥89%**	n. d.	**I**
[^{18}F]SiFA-Tz ([^{18}F]**9.6**) (*one-step*)	21% (inc. yield)*	n. d.	n. d.	**I**
[^{18}F]SiFA-Tz ([^{18}F]**9.6)** (*two-step*)	42.7 ± 14.2% (n = 8)	>98%	5.0	**I**
[^{18}F]AmBF$_3$-Tz ([^{18}F]**10.6**)	29.8 ± 15.0% (n = 8)	>98%	15.4 ± 9.2	**III**

*Incorporation yield = inc. yield determined by radio-TLC

**Not purified, crude mixture of the first step prior oxime formation, radio-TLC, the only impurity was free [^{18}F]fluoride

5.2.2 RADIOFLUORINATED BIOMOLECULES

[^{18}F]**9.6** was used as a prosthetic group to chemoselectively radiolabel the TCO-functionalized albumin *in vitro*, producing the [^{18}F]fluoroalbumin ([^{18}F]**12.1**) at 99.1 ± 0.2% RCY (n = 3) and a A_m of 1.1 ± 0.2 GBq/μmol (n = 2).(**I**) The incorporation yield of [^{18}F]fluoroalbumin was high, owing to the abundance of available TCO-functionalities in one TCO-albumin molecule. The A_m of [^{18}F]**12.1** (1.1 GBq/μmol) of protein at EOS, providing the blood pool imaging tracer with comparable A_m to the comparison albumin tracers labeled with IE. Serum albumin tracer for blood pool imaging, ^{18}F-DBPOF-HSA, was radiolabeled with >5% RCY and in a A_m of 1.11 GBq/μmol.[16] The radiochemical purities (RCP), the decay corrected yield (DCY) corrected to end-of-synthesis (EOS) and the A_m were determined, and the details of the measurements are described in detail in studies **I**, **III** and **IV**.

The obtained A_m of the TOC radiotracers were moderate, ranging from 2.8 ± 1.8 GBq/μmol (n = 3), 6.0 ± 3.4 GBq/μmol (n = 13), and 0.7 GBq/μmol presented here by increasing PEG-chain length. The isolated RCYs (1%, 3% and 5% from [^{18}F]fluoride), were low likely due to two reasons; 1) the synthesis time of >60 minutes for all tracers, ranging from 70-130 minutes, and 2) the prosthetic group **10.6** capturing near 30% of the initial [^{18}F]fluoride that was used further in the second step in approximately 2 × molar excess that the used TCO-peptide.(**III**, **IV**) The isolated yield from [^{18}F]**10.6** in the cycloaddition step, radiolabeled by the prosthetic group, resulted in RCYs of around 20%. Generally radiolabeling by IEDDA cycloaddition, the incorporation yield is high, but as in this study, the radiolabeled prosthetic group [^{18}F]**10.6** was used in higher molar ratio (minimum 2 × equivalent) than the TCO-biomolecule, the maximum expected incorporation yield in the second step would be 50%. This was a premeditated compromise, in order to consume all the cold peptide from the reaction mixture, and to leave as little of the non-labeled competitor in the final formulation, capable of binding to the tumor receptors. The radiolabeling results of the biomolecules are presented in **Table 8**.

Table 8. Radiolabeling results of radiolabeled biomolecules.

Biomolecule	Radiolabeled biomolecule	RCY (%)	RCP (%)	A_m (GBq/μmol)	Study
BSA-TCO (**10.9**)	[^{18}F]Fluoroalbumin ([^{18}F]**12.1**)	inc. ≥99*	≥99	1.1	**I**
α-MSH-PEG$_7$-TCO (**10.12**) (*one-step*)	[^{18}F]AmBF$_3$-PEG$_7$-α-MSH ([^{18}F]**12.4**)	n. d.	≥99	n. d.	unpublished
TOC-PEG$_4$-TCO (**10.10**) (*two-step*)	[^{18}F]AmBF$_3$-PEG$_4$-TOC ([^{18}F]**12.2**)	5.1 ± 3.4% (n = 5)	>98%	2.8 ± 1.8	**III**
TOC-PEG$_7$-TCO (**10.11**)	[^{18}F]AmBF$_3$-PEG$_7$-TOC ([^{18}F]**12.3**)	3.3 ± 1.7% (n = 3)	>98%	6.0 ± 3.4	**III**

*Incorporation yield of fluorine-18 in the form of [^{18}F]SiFA-Tz ([^{18}F]**9.6**).

5.3 IEDDA AND REDUCTION-OXIDATION OF CYCLOADDUCT

IEDDA cycloaddition produces initially 4,5-DHPs, that rearrange to metastable 1,4-DHPs, which demonstrate relatively good stability, if no oxidants are used.[108] The generation of several chemical species during the cycloaddition results in the need for evaluating all formed compounds *in vitro* and *in vivo*, specifically when using small biomolecules, such as peptides. This is to rule out the influence of even small chemical differences in the structure in the pharmacokinetics or stability of the radiotracer. In this study, the cycloaddition products of [^{18}F]**10.6** and a peptide (α-MSH or Tyr^3-octreotide) was shown to futher oxidize spontaneously, losing two protons (unpublished data, **IV**). The oxidation process kinetics for these peptide derivatives was slow enough to enable the detection of both forms simultaneously (**Figure 6**). The full conversion of DHPs often requires oxidative reagents for obtaining the pyridazine as the primary product, meanwhile requiring an additional step for the removal of the oxidant. In this study, it was shown that if the reduced analogs (**Figure 6**, **B**) were separated from the oxidized form (**Figure 6**, **A**), the oxidized form was again detected in the sample, after approximately 1 hour from the separation (**IV**). When separating the oxidized form, no other radiochemical species were detected for at least 9 hours in the formulated radiotracer solution, as demonstrated for the ^{18}F-labeled TOC-analog (**III**). This corroborated the hypothesis, that the oxidized form was the most stable one.

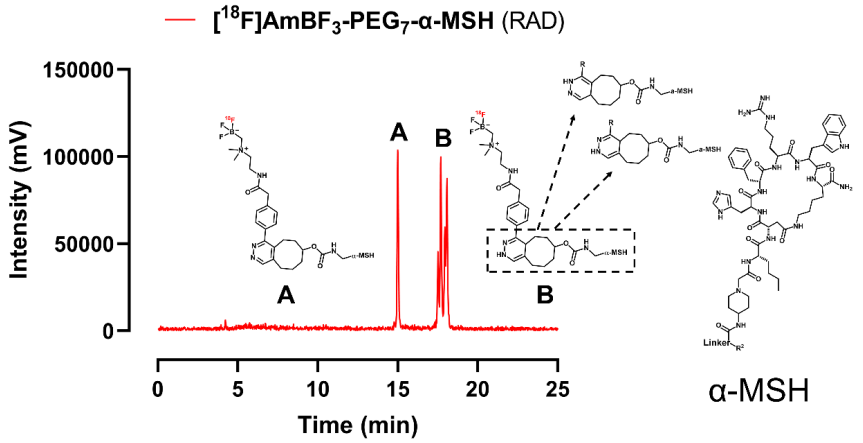

Figure 6. Radio-HPLC chromatogram of SPE purified [^{18}F]AmBF$_3$-PEG$_7$-α-MSH ([^{18}F]**12.4**) showing **A**) the oxidized (t_R = 15.0 min) and **B**) the reduced (t_R =17.3-18.2 min) DHP forms of the peptide.

In this study, the oxidation of the 1,4-DHPs to the pyridazine was accelerated in aqueous solution (≥95% water) by heating the reaction mixture mildly (60 °C, 10–20 min), without a need for a separate oxidant or special apparatus (**Figure 7**).(**IV**) In a previous study the oxidization was accelerated by UV light in the presence of atmospheric air, when applied for several DHP derivatives, yielding the transformation in approximately 5 hours.[58] The reaction between 3,6-di(2-pyridyl)-1,2,4,5-tetrazine and a TCO yielded the pyridazine in 76% conversion in CH_2Cl_2 under LED light (λ=365 nm).[58] The conversion of DHPs to pyridazine in 96% was completed in 7 hours, while subjected to atmospheric air and kept dark in CH_2Cl_2. The hypothetical reaction mechanism proceeded by a singlet oxygen reacting with 1,4-DHP, yielding hydrogen peroxide and pyridazine. Mechanistically a similar phenomenon was described for phenylboronic acid converting into phenol in the presence of an amine by photoirradiation, with air as the oxidant.[109] The conversion took place in minimum of 4 hours. The oxidation of the DHP by air has been applied in a post-polymerization modification, and the oxidation of DHP by air provided full conversion in aqueous solution (D_2O) at 37 °C after 2 hours compared to incubation in d_6-DMSO. It is apparent that high aqueous solvent content in the reaction media beneficially influences the full conversion, although the underlying mechanism is unknown and needs to be investigated. The same phenomenon was presented in detail on HPLC, where the DHP and aromatized forms were well separated and both were present 120 minutes into incubation in PBS, yielding a conversion of 1:2.5 (Ox:DHP).[110] As IEDDA-mediated cycloaddition is extensively used in radiolabeling, and when used for short lived radionuclides *in vitro*, IEDDA requires rapid conversion.

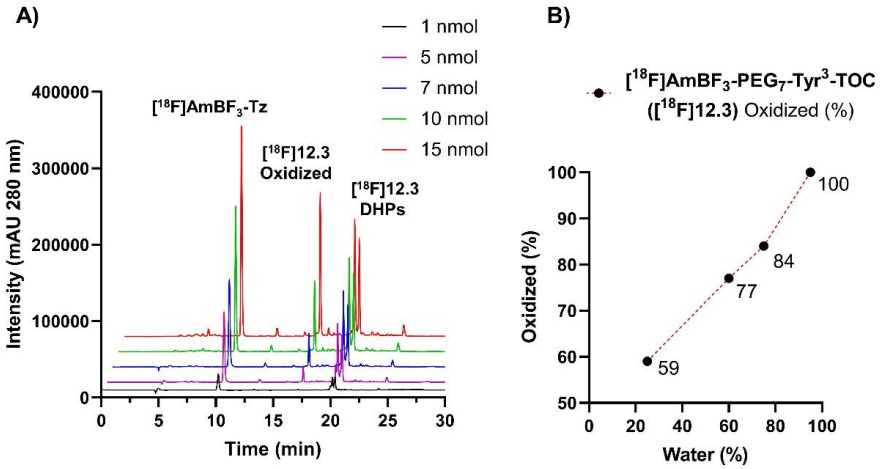

Figure 7. **A**) HPLC-DAD chromatogram of IEDDA cycloaddition reaction micture demonstrating unreacted [^{18}F]AmBF$_3$-Tz ([^{18}F]**10.6**, t_R = 10 min), and formed Tyr^3-octreotide peptide conjugate [^{18}F]AmBF$_3$-PEG$_7$-TOC ([^{18}F]**12.3**) as reduced DHPs (t_R = 20.2–20.6 min) and oxidized (t_R = 17 min) forms. **B**) The correlation of water content (%v/v) and conversion efficiency of DHPs to oxidized peptide analog at 60 °C.

5.4 IN VITRO EVALUATION

5.4.1 IN VITRO STABILITY AND LIPOPHILICITY

The *in vitro* stability of [^{18}F]**9.6** was studied in 1 × PBS, 50-human and 50%-mouse plasma in plasma–PBS (pH 7.4). [^{18}F]**9.6** demonstrated excellent stability in 1 × PBS (pH 7.4), with only minimal defluorination (<1%) during the 90-minute incubation. While incubated in human plasma (37 °C), [^{18}F]**9.6** demonstrated decent stability (94.9 ± 1.6 % intact tracer, n = 2) with up to 6% of free [^{18}F]fluoride detected over the 180 minute study, due to hypothesized defluorination by ^{18}F-hydrolysis, based on radio-TLC. [^{18}F]**9.6** (n = 3) revealed in human and mouse plasma, that approximately 58% of the radiotracer was in the free fraction and the rest bound to plasma proteins. The results indicated that initially relatively high percentage (63 ± 3.0%) of [^{18}F]**9.6** resided in free fraction, which shifted towards plasma protein binding as a function of time, resulting in 46.5 ± 7.1% free tracer at 120 min. [^{18}F]**10.6** demonstrated excellent hydrolytic stability in 1 × PBS (≥ 99% intact at t = 3 h). The peptide radiotracer [^{18}F]AmBF$_3$-PEG$_7$-TOC ([^{18}F]**12.3**) in its reduced form [^{18}F]AmBF$_3$-PEG$_7$-TOC(Ox.) ([^{18}F]**12.3(ox.)**) exhibited good stability in human plasma (≥95%), while the shorter PEGylated analog, [^{18}F]AmBF$_3$-PEG$_4$-TOC(Ox.) ([^{18}F]**12.2(ox.)**), had the lowest stability with up to 20% of radioactivity accounted for a polar metabolite and around 80% intact tracer 3 hours into the study (**Figure 8 A**).

The distribution constant Log$D_{7.4}$, indicative of the lipophilicity of the radiotracers at pH$_{7.4}$ were determined by the shake-flask method. The most lipophilic tracer [^{18}F]**9.6** demonstrated desirable lipophilicity for blood-brain-barrier permeability based on its Log$D_{7.4}$ (1.56 ± 0.2, n = 5). Lipophilic compounds generally exhibit a higher plasma-protein binding, as was also found for [^{18}F]**9.6**. [^{18}F]**10.6** was designed as a more hydrophilic tetrazine, and it indeed demonstrated a more desirable hydrophilicity for the *in vitro* IEDDA labeling strategy based on its Log$D_{7.4}$ value (0.13 ± 0.06, n = 4).

The Log$D_{7.4}$ values oh the oxidized and reduced PEG$_7$-modified TOC analogs of [^{18}F]**12.3** were evaluated after HPLC separation. The *E*- and *Z*-isomers of the reduced [^{18}F]AmBF$_3$-PEG$_7$-TOC ([^{18}F]**12.3**) 1,4-DHPs were detected with retention times of 20.6 min and 20.2 min as peak clusters, but the identification between tautomers was not possible with this method. The lipophilicities of separated TOC isomers were [^{18}F]AmBF$_3$-PEG$_7$-TOC ([^{18}F]**12.3**, oxidized, t_R = 17.3 min) Log$D_{7.4}$ -0.73 ± 0.12 (n = 4), [^{18}F]AmBF$_3$-PEG$_7$-TOC ([^{18}F]**12.3**, **A+B**, t_R = 20.2 – 20.6) Log$D_{7.4}$ -0.04 ± 0.02 (n = 3), [^{18}F]AmBF$_3$-PEG$_7$-TOC ([^{18}F]**12.3**, **A**, t_R = 20.6 min) Log$D_{7.4}$ -0.21 ± 0.19 (n = 3), [^{18}F]AmBF$_3$-PEG$_7$-TOC ([^{18}F]**12.3**, **B**, t_R = 20.2 min) Log$D_{7.4}$ 0.28 ± 0.16 (n = 3).(**III**, **IV**) Most of the peptides radiolabeled with IEDDA, except for [^{18}F]**12.3**, **B**, demonstrated promising hydrophilicity after conjugation with the zwitterionic prosthetic group [^{18}F]**10.6** (**Figure 8 B**).

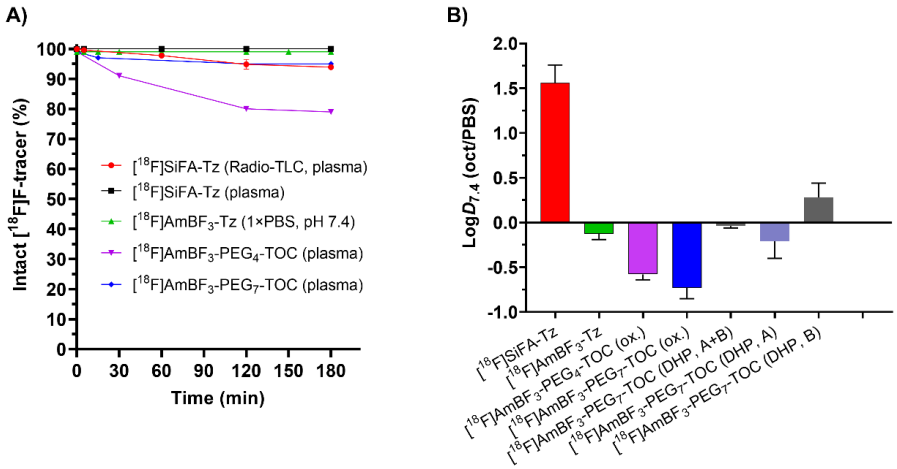

Figure 8. A) *In vitro* PBS and plasma stability of prosthetic groups and peptides, analyzed by radio-HPLC, unless otherwise noted. [^{18}F]AmBF$_3$-Tz **B)** Log$D_{7.4}$ evaluated by octanol-PBS distribution of selected radiotracers [^{18}F]SiFA-Tz ([^{18}F]**9.6**), [^{18}F]AmBF$_3$-Tz [^{18}F]**9.6**, [^{18}F]AmBF$_3$-PEG$_4$-TOC(ox.) ([^{18}F]**12.2**), [^{18}F]AmBF$_3$-PEG$_7$-TOC(ox) ([^{18}F]**12.3**) and DHP. ox; oxidized.

5.4.2 CELLULAR UPTAKE STUDIES

The specific receptor binding of the radiolabeled TOC analogs was studied in rat pancreatic adenocarcinoma cell line, AR42J, that overexpresses SSTR2. As a demonstration of specific, receptor mediated uptake, [^{18}F]AmBF$_3$-PEG$_7$-TOC(ox.) ([^{18}F]**12.3**) presented a high tumor uptake that was efficiently blocked with native octreotide throughout the study (**Figure 9**). The two other PEGylated radiopeptides demonstrated notably lower tumor uptakes, with [^{18}F]AmBF$_3$-PEG$_4$-TOC(ox.) ([^{18}F]**12.2**) demonstrating the lowers efficacy in blocking. The ability to block the uptake of each analog, demonstrated that the uptake was specific and receptor mediated. Low uptake in [^{18}F]AmBF$_3$-PEG$_4$-TOC(ox.) ([^{18}F]**12.2(ox.)**) and [^{18}F]AmBF$_3$-PEG$_{11}$-mTOC(ox.) ([^{18}F]**12.5(ox.)**) was likely due to lower A_m, and also low stability for [^{18}F]AmBF$_3$-PEG$_4$-TOC(ox.) ([^{18}F]**12.2**). The tumor uptake of [^{18}F]AmBF$_3$-PEG$_{11}$-mTOC(ox.) ([^{18}F]**12.5(ox.)**) most likely suffered from non-optimized RCYs and the incorporation yields would likely increase after more experimental repetitions.

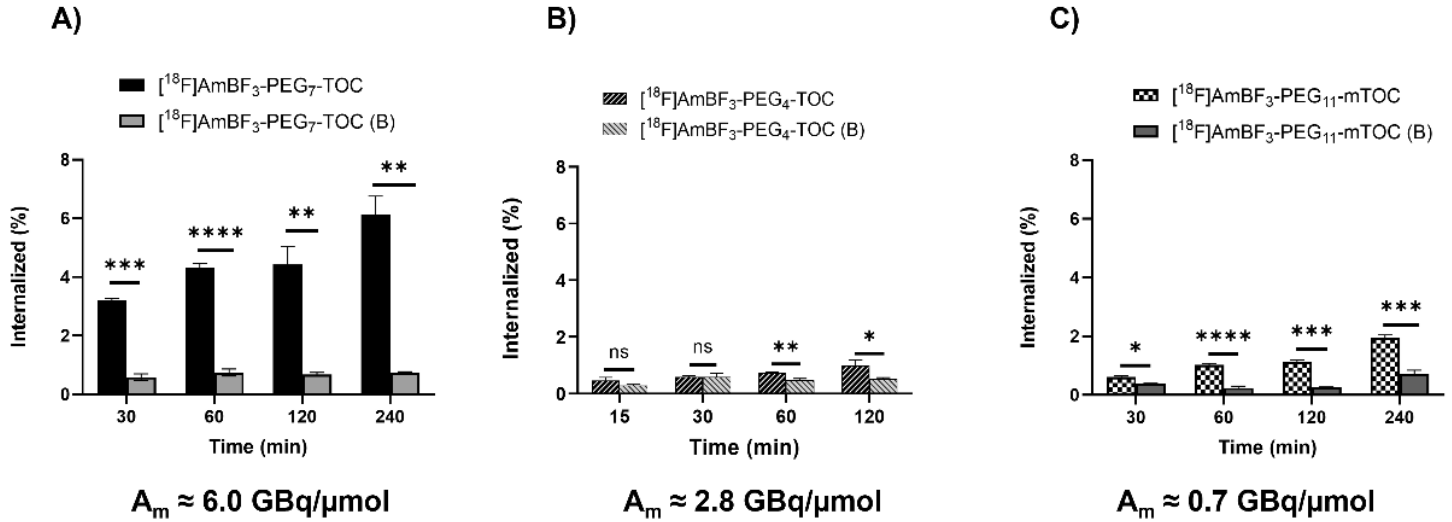

Figure 9. Cell uptake of oxidized forms of [^{18}F]AmBF$_3$-PEG$_7$-TOC(ox.) ([^{18}F]**12.3**), [^{18}F]AmBF$_3$-PEG$_4$-TOC (ox.) ([^{18}F]**12.2**) and [^{18}F]AmBF$_3$-1-PEG$_{11}$-mTOC(ox.) ([^{18}F]**12.5**) in AR42J, a rat pancreatic exocrine tumor cell line. Both tracers demonstrated receptor mediated uptake which were efficient blocking with octreotide. Data points represent mean ± standard deviation.

5.5 EX VIVO, PET/CT AND DOSIMETRY

5.5.1 PROSTHETIC GROUPS

In *ex vivo* biodistribution studies, in healthy CD-I mice, [^{18}F]**9.6** eliminated *via* hepatobiliary and urinary route with rapid clearance from blood.(**I**) The predominant elimination was into urine (229.5 ± 204.5 %ID/g) and gallbladder (143.9 ± 103.1 %ID/g) at 60 minutes post-injection (p. i.). Elimination into intestines increased as a function of time, peaking at 240 min p.i. Surprisingly, bone uptake was detected already 5 minutes p.i., which increased dramatically (13.4 ± 1.6 %ID/g) by 60 minutes p.i. and remained high (14 ± 4 %ID/g) up to 240 minutes p. i. (**Figure 10**). This was indicative of low stability of the radiolabel. The defluorination phenomenon of a [^{18}F]SiFA-derivatized radiotracer has been reported earlier in other studies.[98] Reliable quantitation of the brain uptake of [^{18}F]**9.6** was compromised due to the defluorination phenomenon, possibly accounting for some passage of radioactivity to the brain, but it was observed that radioactivity penetrated the blood-brain barrier (brain uptake 0.7 ± 0.2 %ID/g) 5 minutes after intravenous administration of [^{18}F]**9.6**, with the uptake declining steadily until 240 min p.i. (0.22 ± 0.04%ID/g), demonstrating an opposite trend to the detected bone uptake. The slow decline in brain uptake compared to simultaneously dramatically rising bone uptake, indicated that the passage through BBB was a separate phenomenon not arising from the free [^{18}F]fluoride. The lipophilic nature of [^{18}F]**9.6** resulted in slow clearance from liver and intestines, undesirable for PET imaging of targets located at the abdominal region. The structural modifications done in recent years to SiFAs, from diisopropyl-groups to *tert*-butyl substituents, enhanced the stability of the radiolabel. By adding a quaternary ammonium group attached to the *α*-carbon bonded to the aromatic ring in the para-position, resulted in SiFA*lin*-structure of high stability, simultaneously lowering the lipophilicity.[20] The downfall of using SiFA-groups is their lipophilicity and the anticipated low stability of the [^{18}F]fluoride, unless the aforementioned structural alterations are done. [^{18}F]**10.6** on the other hand, was designed as a universal *in vivo* and *in vitro* radiolabeling tool harbouring lower lipophilicity than [^{18}F]**9.6** and in the attempt to develop a tracer better in resisting defluorination. [^{18}F]**10.6** evaluated in healthy female C57BL7/6JRj and male SCID mice by PET/CT imaging followed by *ex vivo* biodistribution 270 minutes post-injection,(**III**) revealed the radioactivity exhibited low uptake in major organs, fast clearance from blood and negligible bone uptake (0.4 ± 0.1 %ID/g for C57BL/6JRj, 0.3 ± 0.1 %ID/g for SCID), indicating a stable prosthetic group was developed. The radioactivity of all background tissues, except for blood, spleen and pancreas, were lower for [^{18}F]**10.6** (t = 270 min) than [^{18}F]**9.6** (t = 240 min) (**Figure 10**).

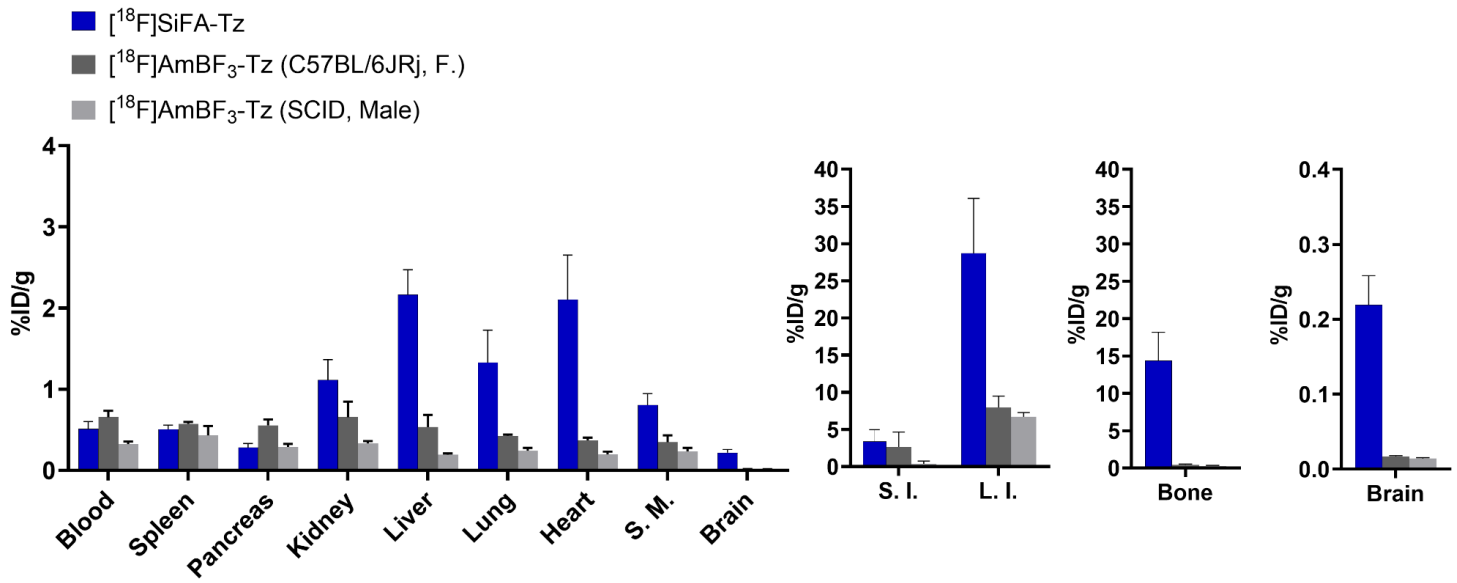

Figure 10. *Ex vivo* biodistribution of developed prosthetic groups after intravenous injection of the radiotracer. Blue; [^{18}F]SiFA-Tz ([^{18}F]**9.6**, CD-1 mice, female) at 240 minutes, dark grey; [^{18}F]AmBF$_3$-Tz ([^{18}F]**10.6**, C57BL/6Jrj, female) at 270 minutes and light grey; [^{18}F]AmBF$_3$-Tz ([^{18}F]**10.6**, SCID, male) at 270 minutes. S.M.; skeletal muscle, S.I.; small intestines (+content), L.I.; large intestines (+content), bone; tibia with bone marrow, F; female.

Based on the PET/CT image acquisition, [^{18}F]**10.6** cleared rapidly from blood as illustrated in the time-activity curve (TAC) of the heart left ventricle with low uptake in major organs or background tissue, such and fast clearance from blood (**Figure 11**). Elevated liver uptake, possibly due to the tetrazine moiety, that decreased steadily throughout the 50-minute dynamic image acquisition was also seen. The liver uptake, although at a reasonable level, could be further decreased by adding a hydrophilic group to the construct, that would direct the elimination mostly towards renal clearance. The elimination of radioactivity from the tissues during the PET/CT image acquisition presented as TACs indicated that the prosthetic group eliminated quickly, mainly through the kidneys (**Figure 11**).

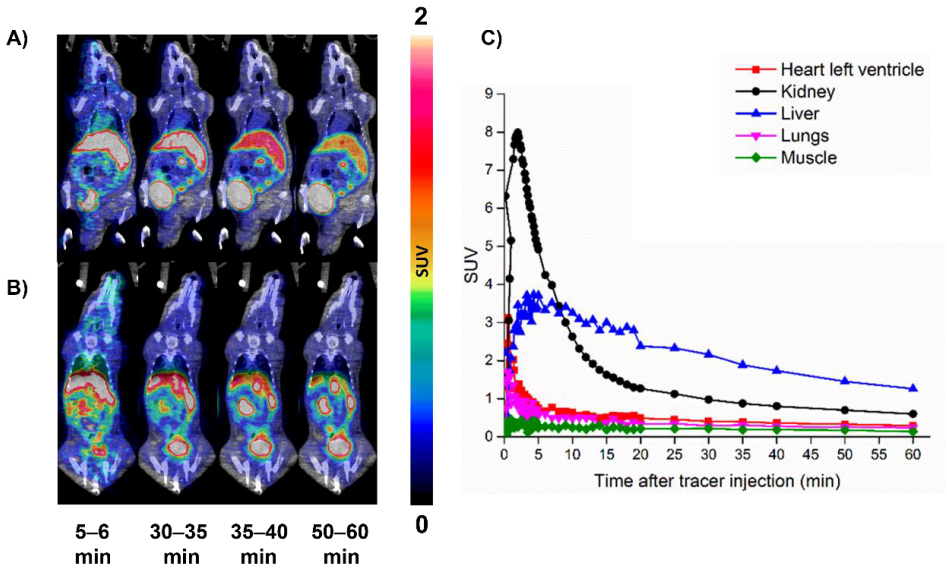

Figure 11. Single-slice coronal PET/CT images of [^{18}F]AmBF$_3$-Tz ([^{18}F]**10.6**) in **A**; CB.17 SCID (male) and **B**; C57BL/6J:Rj (female) mice 270 minutes post-injection.

5.5.2 RADIOFLUORINATED BIOMOLECULES

5.5.2.1 Ex vivo

[^{18}F]**12.1** demonstrated a typical elimination profile of a serum albumin tracer, dominated by prolonged blood-pool residence time. The plasma half-life of [^{18}F]**12.1** was determined as 49 minutes, a value comparable to other [^{18}F]SiFA–based radiolabeled serum albumin,[42] and was significantly higher ($p \leq 0.0001$) than the blood-pool residence time of [^{18}F]SiFA-Tz [^{18}F]**9.6**. However, it is evident that due to the declined biological half-life, some unbeneficial structural modifications have resulted from the excessive TCO modification on the protein.

The main elimination was into urine (54.7 ± 25.8 %ID/g) and gallbladder (275.3 ± 185.6 %ID/g), with some uptake in intestines and liver at 60 minutes post-injection. The *ex vivo* evaluation of the protein tracer [^{18}F]**12.1**, demonstrated that the Si-^{18}F bond in [^{18}F]**12.1** was noticeably more stable than when [^{18}F]**9.6** was evaluated as a standalone tracer (**Figure 12**). Recently, the development of a serum albumin tracer using organofluorophosphine fluoride acceptor for radiolabeling yielding a novel blood pool radiotracer, ^{18}F-DBPOF-HSA, was reported, that provided good visualization in the PET image of the heart and the arteries.[16] [^{18}F]**12.1** was conjugated with TCOs by targeting all available lysine residues in the protein, which were then radiolabeled with fluorine-18 by IEDDA. This strategy likely results in modification of the radiolabeled serum albumin protein and alteration in its natural *in vivo* behaviour. This obstacle might be circumvented by applying enzyme mediated site-specific pre-conjugation strategy for introducing the TCO.[66, 67] This would result in control over the conjugation-site and the number of TCO-conjugates per albumin protein. The influence of the lipophilic SiFA-group on the pharmacokinetics of the protein can be expected to be low if the conjugation number of TCOs is kept low.

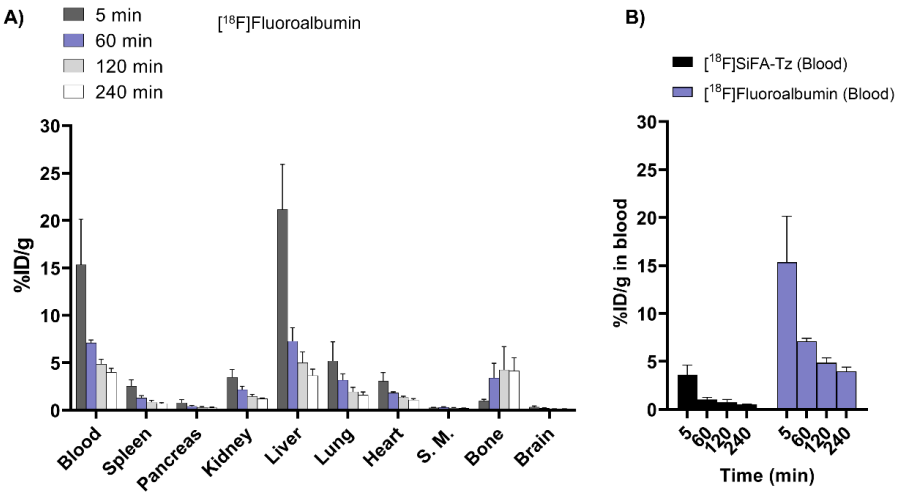

Figure 12. Biodistribution of radioactivity after intravenous administration of **A**) [^{18}F]Fluoroalbumin ([^{18}F]**12.1**) demonstrating a prolonged residence time in circulation, characteristic to a plasma protein. **B**) Enhanced blood pool cisculation was evident compared to [^{18}F]SiFA-Tz ([^{18}F]**9.6**).

In the attempt to produce a prosthetic group of more hydrophilic character, [^{18}F]**10.6** was used to radiolabel the TOC and α-MSH peptide derivatives. TOC analogs were evaluated *in vivo* for their biodistributions and specificity towards SSTR2 overexpressing AR42J tumor. TOC analog [^{18}F]**12.3** demonstrated slightly higher tumor uptake and better *in vivo* stability incomparison to [^{18}F]**12.2**. The relatively low tumor uptake likely arised from the moderate A_m achieved in this study. Nevertheless, the tumor uptake was blocked with significant differences ($p < 0.05$) visible for both peptide tracers **Figure 13** and

Table 9. The A_m of the PEGylated TOCs developed in this study, could be increased by pre-conjugation of the $AmBF_3$-group to the TCO-modified TOC peptides, followed by the radiolabeling with fluorine-18. This reversed method would benefit from shorter synthesis time as the redox species could be converted to one prior to start of the synthesis, resulting in shorter reaction time and likely in higher A_m. Furthermore, the preconjugation would result in higher total incorporation of [^{18}F]fluoride in the peptide, as no radiofluorinated precursor would be left unreacted, since in this study the TCO-peptide was used in excess mols compared to the radiolabeled prosthetic group [^{18}F]**10.6**. A possible down-fall for the reversed pre-conjugated method is that some biomolecules might not withstand the radiolabeling conditions but would benefit more from the milder two-step method. Using $AmBF_3$ for radiofluorinations has resulted in a radiopeptide tracer of high stability and of desirable pharmacokinetic profile. The general approach is to introduce the $AmBF_3$-group to the peptide stucture prior to radiolabeling, a method well-suited for structures withstanding heat.[76, 103] Using [^{18}F]**10.6** by IEDDA as a labeling strategy for a peptide, can result in an alteration of the elimination more towards hepatobiliary route, as the cycloaddition product increases the lipophilicity of the resulting radiopeptide. This added lipophilicity, if critical to the application, could likely be canceled when suitable hydrophilic linkers were introduced to the structure.

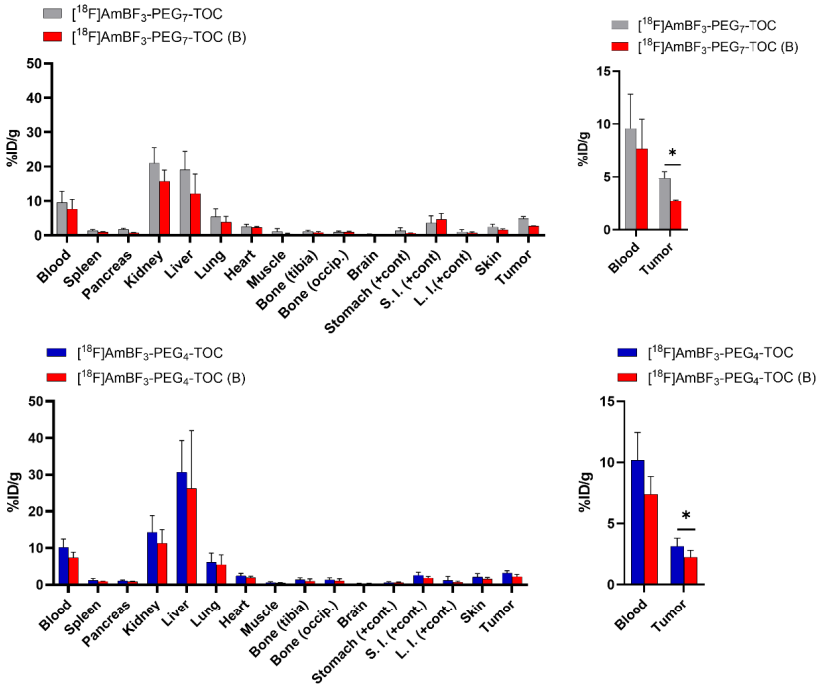

Figure 13. Biodistribution of radioactivity 60 minutes after intravenous administration of [^{18}F]$AmBF_3$-PEG_7-TOC ([^{18}F]**12.3**) and [^{18}F]$AmBF_3$-PEG_4-TOC ([^{18}F]**12.2**) demonstrating prolonged residence time in circulation, liver uptake and specific tumor uptake blocked (B) by non-modified octreotide.

The effect of A_m has been previously shown for a $AmBF_3$-derivatized α-MSH peptide with A_m near levels reported in this study, a tumor uptake and blocking efficacy, of comparable magnitude was reached.[77] Once the A_m was increased, both tumor uptake and blocking efficacy increased dramatically, explaining partly our findings of achievable tumor uptake and blocking efficacy.(**III**) The pharmacokinetics of the peptide tracers developed in this study suffer likely from the achieved moderate A_m and elevated lipophilicities, as the receptor-specific uptake in background tissue is masked by the accompanied blocking non-labeled peptide carrier and the liver scavenges the relatively lipophilic peptide tracers, thus resulting in altered apparent biodistribution profiles of the traditionally renally excreted peptide tracers. The lipophilicites would likely have a lower if any influence on biomacromolecule based tracers, where the bulky biomolecule would steer the elimination of the tracers. Several SSTR2-targeting radiotracers demonstrated in AR42J tumor bearing mice similar levels of tumor uptake as the tracers developed in this study; ^{18}F-FETE-PEG-TOCA (A_m = 5.9 GBq/µmol, 5.14%ID/g in tumor), ^{18}F-FETβAG[W-c-K] (A_m = 3.9 GBq/µmol, 8.23%ID/g in tumor), and ^{18}F-FET-βAG-TOCA (A_m = 12.3 GBq/µmol, 0.10%ID/ in tumor). [83] These reports corroborate that the A_m influences the tracer performance dramatically.

Table 9. Radiosynthesis times, A_m, and tumoruptakes with tumor-to-blood ratios of ^{18}F-labeled TOCs developed in this study.

Radiopeptide	Synthesis (min)	A_m (GBq/µmol)	Tumor t=60 min (%ID/g)	Tumor/Blood t=60 min (%ID/g)	Ref.
[^{18}F]$AmBF_3$-PEG_4-TOC ([^{18}F]**12.2**)	85 ± 8 min (n = 3)	2.8 ± 1.8	3.1 ± 0.7 2.2 ± 0.6 (blocked) *p<0.05	0.30, 0.30(B)	III
[^{18}F]$AmBF_3$-PEG_7-TOC ([^{18}F]**12.3**)	102 ± 29 min (n = 17)	6.0 ± 3.4	4.5 ± 1.0 3.1 ± 0.5 (blocked) *p<0.05	0.50, 0.40(B)	III
[^{18}F]$AmBF_3$-PEG_{11}-TOC ([^{18}F]**12.5**)	70	0.7	6.4 ± 4.2 3.5±0.6 (blocked) *p<0.05	0.30, 0.28(B)	IV**

**contains also unpublished biodistribution data

5.5.2.2 PET/CT imaging and dosimetry

The radiotracer with better overall biological performance was selected for further evaluation by PET/CT for neuroendocrine tumor and receptor imaging. [^{18}F]**12.3**, (0.2 nmol) was administered intravenously and the radioactivity in the subcutaneous AR42J tumor increased slowly and peaked at 20–30 minutes p. i., as demonstrated by the TACs. The tumor was well visualized as seen in the single-slice summed maximum intensity projection (MIP) PET/CT image (**Figure 14**).

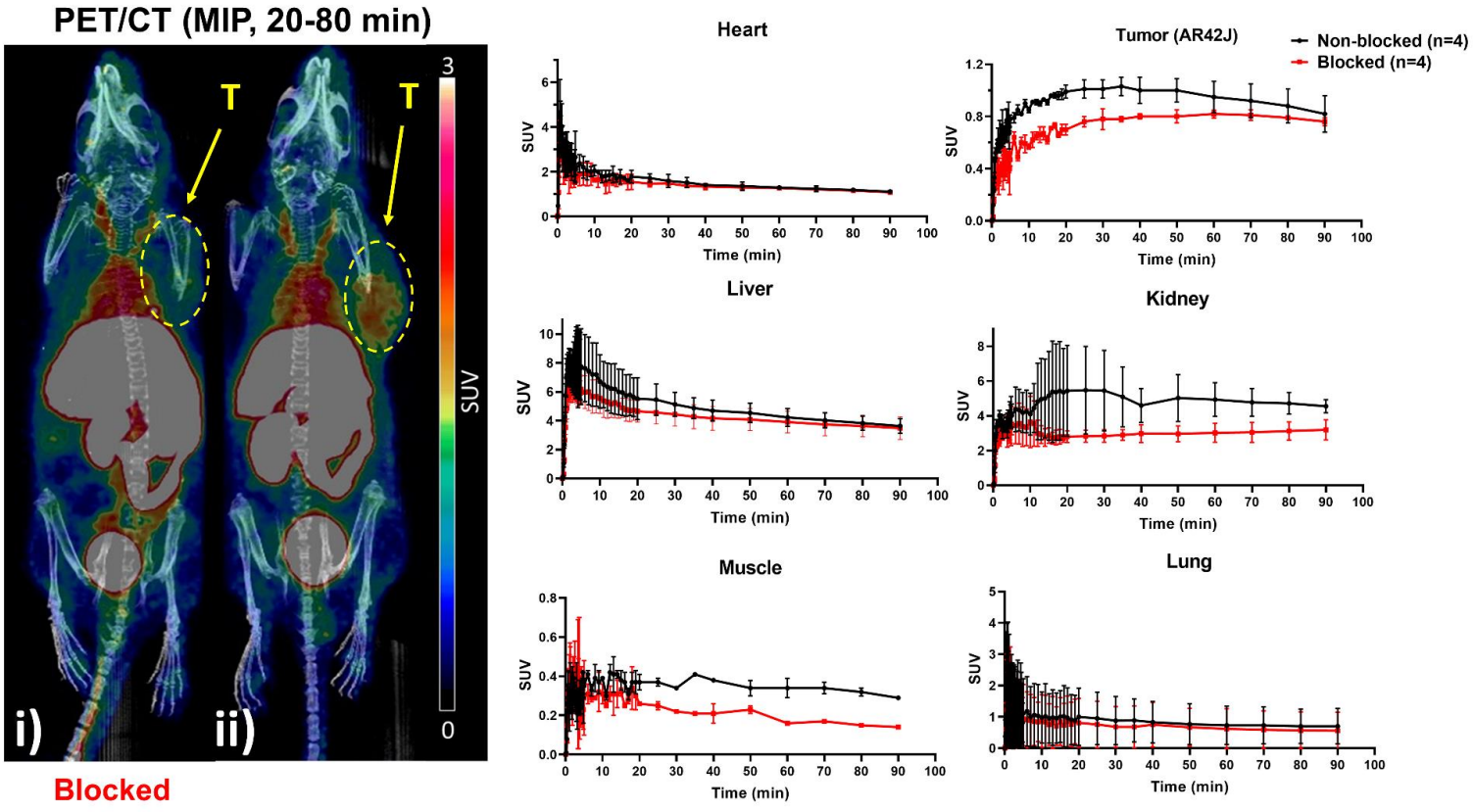

Figure 14. PET/CT image (**A**) depicting biodistribution of radioactivity after intravenous administration of [^{18}F]AmBF$_3$-PEG$_7$-TOC ([^{18}F]**12.3**) in blocked (**i**) and baseline (**ii**) conditions, with the kinetics in selected organs (**B**) presented as standardized-uptake values (SUVs). Data points represent mean ± standard deviation.

In the dosimetry calculations it was apparent that [^{18}F]**12.3** resulted in highest absorbed radiation dose to the kidneys and liver (kidney = 0.0366 mGy/MBq, liver = 0.0334 mGy/MBq) (**Table 10**), without meaningful differences between the baseline and the blocking conditions (kidney = 0.0337 mGy/MBq, liver = 0.0313 mGy/MBq). When compared to the closest SSTR targeting analogue, [^{18}F]AmBF$_3$-TATE, the urinary bladder (baseline = 0.0134, blocked = 0.0135) and pancreas (baseline = 0.0156, blocked = 0.0154) received lower absorbed dosed with [^{18}F]**12.3** than after administration of [^{18}F]AmBF$_3$-TATE (bladder = 0.027–0.030 mGy/MBq, pancreas = 0.018–0.028 mGy/MBq).[21] Furthermore, after administraton [^{18}F]AmBF$_3$-TATE, the kidneys received a higher radiation dose ([^{18}F]AmBF$_3$-TATE; female, 1.24 mGy/MBq, male, 1.13 mGy/MBq) than after intravenous administration of [^{18}F]**12.3** (0.0334 mGy/MBq. All organs except for kidneys and liver responsible for eliminating the radiotracer, received a dose of, or below, 0.02 mGy/MBq (**Table 10**).

Table 10. Dosimetry coparison between [^{18}F]AmBF$_3$-PEG$_7$-TOC and [^{18}F]AmBF$_3$-TATE.

Organ	**[^{18}F]AmBF$_3$-PEG$_7$-TOC** ([^{18}F]**12.3**)	**[^{18}F]AmBF$_3$-TATE**	
	Dose (mGy/MBq)	Dose (mGy/MBq)	
Kidney	0.0366	0.0288 / 0.0109	1.13–1.24
Liver	0.0334	0.0049 / 0.0042	-
Gallbladder	0.0194	0.0145 / 0.0380	-
Pancreas	0.0156	0.0052 / 0.0047	0.018–0.028
Adrenal glands	0.0190	0.0039 / 0.0044	n. d.
Lungs	0.0109	0.0022 / 0.0027	0.018–0.028
Bladder	0.0134	0.1060 / 0.1070	0.027–0.030
Ref.	**III**	**[111]**	**[21]**

5.6 METABOLISM STUDIES

5.6.1 DEFLUORINATION AND BONE UPTAKE (IN VIVO)

In biodistribution studies, it was noticed that the Si-^{18}F bond in [^{18}F]**12.1** was significantly ($p \leq 0.001$) more stable than the corresponding Si-^{18}F in [^{18}F]**9.6** at 60 minutes post-injection (**Figure 10, 12** and **15**). This was likely due to the bulky protein shielding the prosthetic group from oxidation and ^{18}F-hydrolysis. The defluorination detected in both radiotracers as accumulation of radioactivity in bone peaked around 120 minutes after i. v. administration, and the phenomenon persisted until the last time point at 240 minutes post-injection. In comparison, high bone uptake (13.4 ± 1.6%ID/g) of radioactivity was observed 60 minutes post-injection of [^{18}F]**9.6**.

This is a characteristic indication of fast defluorination and a subsequent accumulation of the free fluoride into the bone *in vivo,* as it accumulates into the hydroxyapatite $Ca_{10}(PO_4)6(OH)_2$, and forms fluorapatite ($Ca_{10}(PO_4)6F_2$).[94] After defluorination the free fluoride is sequestered rapidly from circulation and either binds into the surface of the bone or accumulates irreversibly into the hydroxyapatite.[94] The influence of the radiolabel stability in the prosthetic group was evident when comparing the bone uptake of radioactivity after intravenous administration of the peptide and protein tracers [^{18}F]**12.1** (**I**), TOC analogs [^{18}F]**12.3** and [^{18}F]**12.3** (**III**). [^{18}F]**12.1** demonstrated a typical defluorination pattern as the radiotracer accumulated to the bone rapidly without decline in the uptake, but rather at a steady rate (**Figure 15**). The bone uptake of the protein tracer [^{18}F]**12.1** was significantly lower than the bone uptake after administration of [^{18}F]**9.6** (***p < 0.001, n = 3) 60 minutes post-injection, indicating the protein construct shielded the small molecule partially from metabolism. [^{18}F]**12.2** (bone; 1.3 ± 0.6 %ID/g, n = 10) and [^{18}F]**12.3** (bone; 1.1 ± 0.4 %ID/g, n = 5) demonstrated low bone uptake that correlated with the values reported earlier for other SSTR2 tageting radiotracer developed with the same prosthetic group, [^{18}F]AmBF$_3$-TATE (femur = 1.5 - 1.7 %ID/g at 30 min).[21]

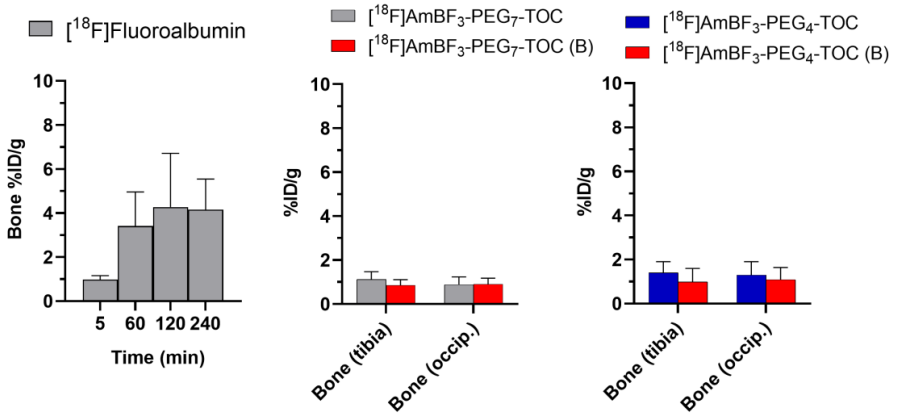

Figure 15. Defluorination and bone uptake *in vivo*. [18F]Fluoroalbumin ([^{18}F]**12.1**) demonstrated increasing defluorination from 60 minutes onwards. On the contraty [^{18}F]AmBF$_3$-PEG$_7$-TOC ([^{18}F]**12.3**) and [^{18}F]AmBF$_3$-PEG$_4$-TOC ([^{18}F]**12.2**) demonstrated good in vivo stability 60 minutes after administration of the peptide radiotracers.

5.6.2 RADIOMETABOLITES AND TRACER DISTRIBUTION IN BLOOD (IN VIVO)

Stability of the protein tracer [^{18}F]**12.1** was further investigated as a distribution of molecules of molecular weight ≥ 30 kDa by separating the components with ultrafiltration from plasma samples collected after intravenous administration. The proportion of radiolabeled molecules with a M_W of ≥30 kD, representing intact [^{18}F]**12.1**, was over 90% until 180 minutes post-injection, after which it decreased to 40% over the next 60 min (240 min incubation time in total). [^{18}F]**12.1** was detected in mouse blood and remained stable *in vivo*. When studied with ultrafiltration, fluoroalbumin presented a calculated biological half life of 49 minutes coinciding closely with the reported half-life or BSA in mice (60 min).[112] The difference in the *in vivo* half-lives is likely due to the extensive chemical modification of the plasma protein.

Ex vivo stability of the octreotide analog [^{18}F]**12.2**), that demonstrated lower stability, revealed radiometabolites in mouse blood samples at 5 and 30 minutes post-injection. In the radio-TLC, a slightly polar metabolite (4%) in blood with a position presented as retardation factor (R_f) of R_f = 40 mm was detected 5 minutes post-injection. At 30 minutes post-injection the radiometabolite at 40 mm had disappeared and instead a highly polar metabolite (2.8%) at R_f = 4.0 mm was visible, likely resulting from free [^{18}F]fluoride, and was accompanied by another metabolite (2.0%) eluting in the immediate vicinity of the tracer at R_f = 58 mm. At a sample taken 60 minutes post-injection, the tracer accounted for ≥99% of the radioactivity both in blood and urine (**Figure 16**).

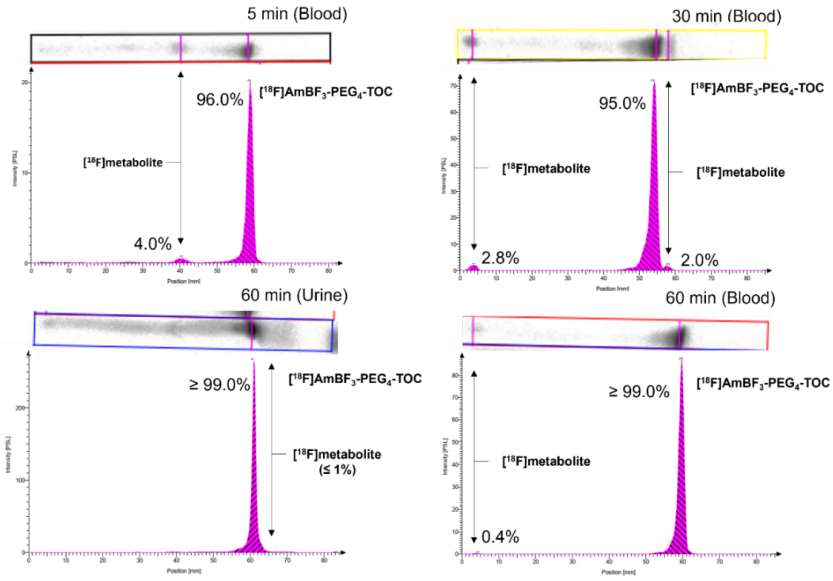

Figure 16. Radiometabolites of [^{18}F]AmBF$_3$-PEG$_4$-TOC ([^{18}F]**12.2**) indicating defluorination *in vivo* 30 minutes post-injection.

5.6.3 METABOLISM OF SIFA-TZ IN MOUSE LIVER MICROSOMES (IN VITRO) AND MOUSE LIVER (EX VIVO)

The metabolism pathway of **9.6** was studied in mouse liver microsomes (MLMs) with co-factors required for typical phase I metabolism, hypothesized to participate in ^{18}F-hydrolysis, as well as phase II metabolism by conjugation reactions, likely following the phase I metabolism *in vivo*. Specifically, the stability of the Si-F bond and the defluorination pathway of [^{19}F/^{18}F]**9.6** due to the bone uptake detected *in vivo*, was the focus of the MLM studies. The proposed structures of the metabolites were elucidated with non-targeted UHPLC-HRMS screening and by fragmenting the molecular ions found by their exact masses and elemental compositions.

A SiFA-derivatized-TOC ([^{18}F]SiFA-TOC) tracer containing the same oxime bond at the para-position of the SiFA aromatic ring, found also in **9.6**, has been reported.[96] In the study it was repoted that the *in vitro* stability during HPLC quality control of the [^{18}F]SiFA-TOC was good, but to date no reports was found regarding its *in vivo* stability, to corroborate or challenge the results presented in this study, possibly elucidating the participation of the oxime bond at the para position to the metabolism. Precursor **9.6** exists in two isomeric (*E*/*Z*) forms (**I**, **II**), due to the oxime bond generating a double bond.[113] The existence of the *E*- and *Z*-isomers was detected in radio-TLC during analysis of [^{18}F]**9.6**.(**I**) Prior to the metabolite screening studies, the presence of *E*- and *Z*-isomers of SiFA-Tz (**9.6**) was verified with HRMS.(**II**) Two distinct and well separated protonated molecule peaks were detected eluting at 4.37 min (*m/z* 509.24900, Δ= −0.20865 ppm) and 4.64 min (*m/z* 509.24905, Δ= 0.01860 ppm), with the elemental composition of $C_{26}H_{34}FN_6O_2Si^+$, corresponding to the geometric isomers of (*Z*)-SiFA–Tz ((*Z*)-**9.6**) and (*E*)-SiFA–Tz ((*E*)-**9.6**), respectively. The ratio of the dominating *E*-isomer was determined as 92 ± 0.7% (n = 2). The fragmentation pattern of (*Z*)-**9.6** and (*E*)-**9.6** was used to establish identification criteria of **9.6**, and to aid in identifying the fragmentation positions of the proposed metabolites. The reduced forms of (*Z*)-**9.6** and (*E*)-**9.6** were detected in the analytical standard with a ratio of 89 ± 7% (n = 2) of (*E*)-**9.6**, likely due to the spontaneous reduction of tetrazines in solution, as earlier reported.[114, 115]

Livers from healthy CD-1 mice were collected 5 min post-injection of [^{18}F]**9.6** after *ex vivo* biodistribution studies and stored in freezer (-20 °C) for HRMS analysis. The isomers had individual half-lives *in vivo*, and the *E*-isomer metabolized faster both *in vitro* in MLMs and *in vivo*, based on the extracted liver homogenate sample where a ratio of approximately 48:52% (*E*/*Z*) was detected.(**II**) The corresponding reduced SiFA-dihydrotetrazines (SiFA-H_2Tz) were detected in the analytical standard, in the *in vitro* in MLM samples and in *ex vivo* mouse liver homogenate. The silanol analogues, Si-OH-Tz and the reduced Si-OH-H_2Tz, produced from **9.6**, were found after incubation with NADPH.

The chemical structures SiFA-Tz, SiFA-H_2Tz, Si-OH-Tz and Si-OH-H_2Tz, together with extracted ion chromatograms of **9.6** and SiFA-H_2Tz in analytical standard and in mouse liver exctract are presented in **Figure 17**.

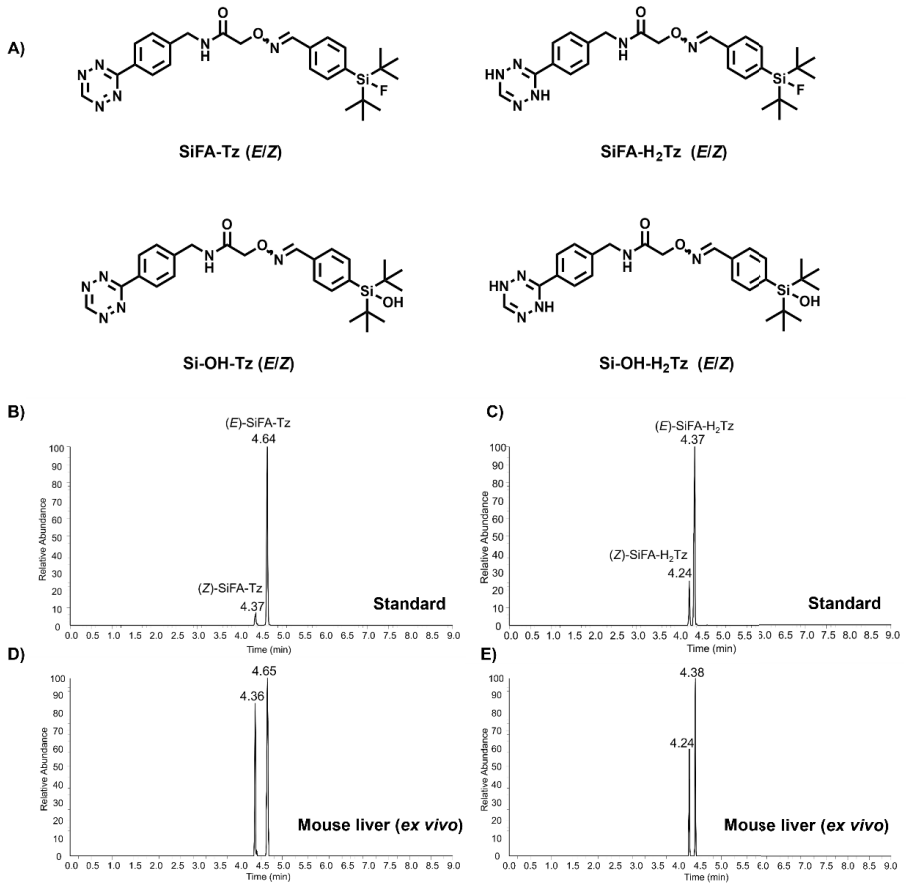

Figure 17. *Upper panel **A**)* Chemical structure of SiFA-Tz (**9.6**, *E*/*Z*) together with the proposed chemical structures of main phase I metabolites of SiFA–Tz (*E*/*Z*): reduced dihydrotetrazine SiFA–H_2Tz (*E*/*Z*), defluorinated silanol Si-OH–Tz (*E*/*Z*), and reduced dihydrotetrazine silanol Si-OH–H_2Tz (*E*/*Z*). *Lower panel* exctracted ion chromatograms of ***B***) analytical standard sample SiFA-Tz (**9.6**), **D**) SiFA-Tz (**9.6**) in *ex vivo* mouse live exctract, **C**) SiFA-H_2Tz present in analytical standard, and **E**) SiFA-H_2Tz in *ex vivo* mouse liver extract.

Based on the fragmentation patterns (**Figure 18 A, C**), the kinetics of metabolism formation and the substrate depletion patterns, it was hypothesized that first transformation was the hydroxylation to a *tert*-butyl group, followed by the proposed subsequent oxidation further to a carboxylic acid at the *tert*-butyl group, accompanied by oxidative defluorination providing in total nine proposed phase I metabolites of **9.6** and SiFA–H_2Tz. The proposed monohydroxylated metabolites were o-glucuronidated forming in total eight phase II metabolites. In all metabolite samples both fluorine-containing and defluorinated metabolites were detected. In summary, it was indicated, that the defluorination was a sligtly slower event, accelerated by CYP enzyme mediated oxidative defluorination process, likely accompanied by ^{18}F-hydrolysis, repoted for other SiFA-derivatives earlier. Also the slight loss of radioactivity (≤1%) as [^{18}F]fluoride from [^{18}F]**9.6** in PBS at 90 min, increased in human plasma (5%),(**I**) indicated some other participating factor, likely enzymatic phenomenon, in addition to ^{18}F-hydrolysis, influenced the phenomenon.

The HRMS results indicated, that the proposed metabolites were hydroxylated at a *tert*-butyl-carbon. Indeed, the phase I metabolism of two extensively studied *tert*-butyl group (Finasteride and Docetaxel), and aromatic ring (Docetaxel) containing compounds,[116, 117] demonstrated that the *tert*-butyl group underwent oxidation rather at the *tert*-butyl sp^3-carbons than an aromatic ring, supporting the findings and hypothesized metabolism sites presented in this study.(**II**) Also clear species-specific differences in the oxidation or hydroxylation sites has been reported, with *tert*-butyl groups hydroxylated in human and *para*-positioned methyl group or Ar-Me hydroxylated in rat, rabbit, and monkey, when studying butylated hydroxytoluene.[118] The metabolite formation and substrate consumption kinetics revealed that the *E*-isomers, in all instances, were metabolized more rapidly than the *Z*-isomer (**Figure 18**). Moreover, even though the reduced SiFA–H_2Tz was present in the analytical standard, also used as substrate in the metabolism studies, it was evident that the amount of SiFA–H_2Tz increased as a function of time (from t=0 min to t=5 min) in the phase I and phase II microsomal assays. The proposed metabolic pathway for phase I hydrolation, reduction and phase II o-glucuronidation is presented in **Scheme 16**.

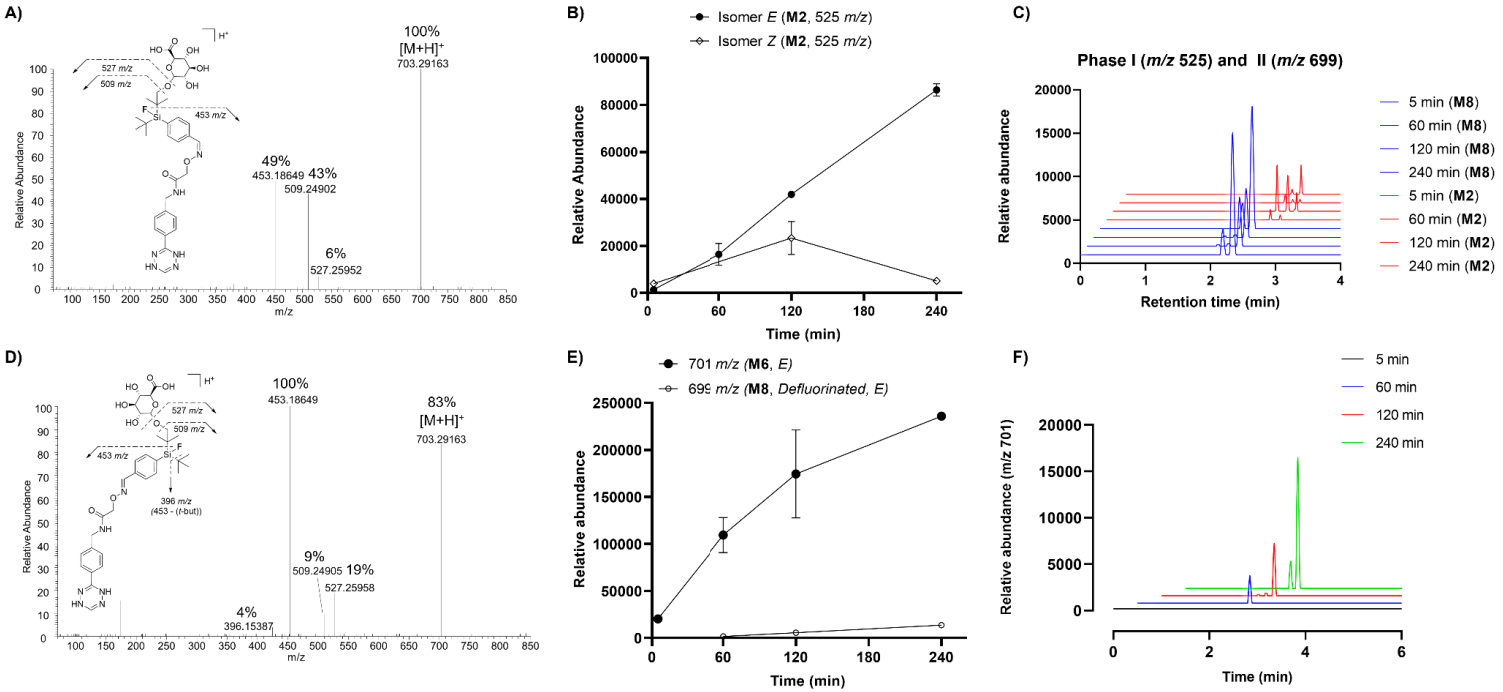

Figure 18. Fragmentation pattern of **A**) *E*- and **D**) *Z*-isomers of reduced and hydroxylated o-glucuronide conjugates of SiFA-Tz (**9.6**) from full scan screening. **B**) formation of metabolite **M2** (phase I) as isomers. **C**) Exctracted ion chromatograms formed metabolites **M2** (phase I) and **M8** (phase II). **E**) Formation of o-glucuronide phase II metabolites **M6** and **M8** in mouse liver microsomes. **F**) Formation of phase II metabolite **M6** (m/z 701).

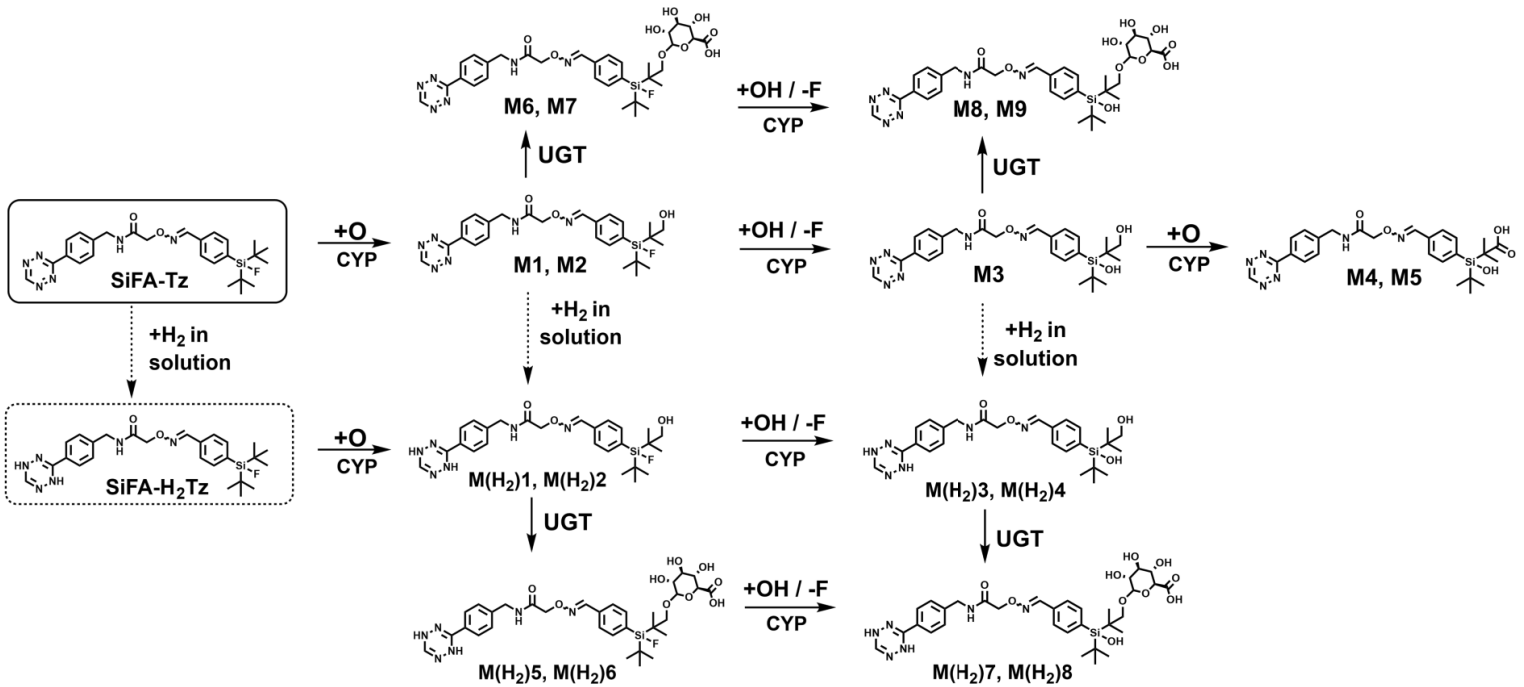

Scheme 16. Proposed phase I and phase II metabolic pathway of SiFA-Tz (**9.6**), based on HRMS studies and fragmentation patterns of found metabolites.

6 CONCLUSIONS

The incidence of cancer is on the rise presenting earlier onset in younger adults. Early detection, accurate evaluation of the disease state without delay, and identification of possible metastasis, is a prerequisite for efficient treatment with positive outcomes. Different cancer types require different approaches for identifying tumors from healthy tissue. Non-invasive molecular imaging methods, such as PET combined with a complementary anatomical modality, CT or MRI, offers a powerful tool for visualizing sites that are out of reach for biopsies. These non-invasive methods offer a robust tool for closely monitoring the disease progress and treatment response, with minimum discomfort for the patient. A clear contrast between background tissue, such as the bloodstream and the organs responsible for eliminating the radiotracer is required for accurate visualization of a tumor and its metastasis.

To meet these requirements, and to provide clear visualization of the pathology in question, radiolabeled molecules are required for the delivery of the imaging agent within the patient to the region-of-interest. Hence, the development of novel radiolabeled compounds called radiotracers, is a pivotal part of ensuring efficient and reliable cancer imaging with the sophisticated imaging modalities. In addition to general purpose radiotracers, such as [^{18}F]NaF used for bone metastasis imaging, or multipurpose [^{18}F]FDG used to image many targets, from inflammation to Alzheimer's disease and cancerous tumors, more selective tracers that can be used as markers for imaging receptor expression, and moreover, for receptor mediated therapeutics as well, are under feverish development. Radiolabeled biomolecules offer an innate targeting capability towards membrane-associated receptors, that once internalized to the tumor, enable a prolonged time-window for target visualization, as well as uptake of therapeutic radiopharmaceuticals into the cancerous cells for radiotherapy. This targeting capability is crucial also for patient selection of receptor-mediated treatments.

Biomolecules comprise a vast array of appealing and valuable alternatives as radiopharmaceuticals, from small to bulky biomacromolecules, but many of them are sensitive to the harsh conditions generally associated with nucleophilic radiofluorinations. Uncontrolled insertion of the radiolabel in unsuitable locations can destroy the targeting moiety of the biomolecule. Continuos attempts to provide biomolecule-based radioharmaceuticals rapidly and chemoselectively has influenced the ongoing developments of more sensitive radiofluorination techinques applicable for even the most sensitive biomolecules, facilitating the introduction of click-based chemistry, with broad utility in the world of bioconjugations.

In this thesis, novel chemoselective prosthetic groups, [^{18}F]SiFA-Tz and [^{18}F]AmBF$_3$-Tz, were designed and developed for mild radiofluorination of biomolecules. The prosthetic groups were evaluated for their suitability as universal radiofluorination agents to produce biomolecule-based molecular imaging agents. The prosthetic groups were radiolabeled by isotopic exchange and used successfully for radiofluorination of biomolecules by chemoselective IEDDA. The prosthetic group, [^{18}F]SiFA-Tz, with high liver uptake and low *in vivo* stability as a standalone tracer, was further investigated in MLMs for elucidating the metabolism pathway leading to pronounced *in vivo* defluorination, enabling future optimization of similar structures. The defluorination was still detected when the prosthetic group was bound to a biomacromolecule, serum albumin, suggesting further structural optimization was required for finding the potential universal radiolabeling tool. Motivated by the instability and relatively high lipophilicity of the first prosthetic group, structural modifications were done accordingly, and [^{18}F]AmBF$_3$-Tz was introduced. The novel prosthetic group met all the requirements set for the optimal radiotracer in the study aims. After investigating the stability of the prosthetic groups and the radiolabeled biomolecules *in vitro*, evaluation of the performance, stability and biodistribution of the ^{18}F-fluorinated prosthetic groups and ^{18}F-fluorinated biomolecules by *ex vivo* and *in vivo* methods, it was concluded that a novel potentially universal radiolabeling tool for radio-biopharmaceutical production was developed.

In summary, [^{18}F]AmBF$_3$-Tz developed in this work is a novel universal and bioorthogonal radiolabeling tool, with excellent *in vivo* stability, desirable hydrophilicity, main elimination by excretion *via* kidneys to urine, and low non-target background when studied in mice by PET/CT imaging. The prosthetic group was also used to radiolabel two SSTR2 targeting peptides, of which one demonstrated preferrable elimination and good *in vivo* stability. The peptide derivatives warrant further structural optimization due to the low stability of the other radiopeptide, prolonged blood circulation and the relatively high liver uptake of both radiopeptide tracers, likely due to the added lipophilicity of the cycloadduct on the resulting radiopeptide. The radiolabeled serum albumin protein would benefit from enzyme-mediated site-specific pre-conjugation of TCO, rather than traditional chemical modification, for ensuring better control over both the TCO-conjugation site and the number of incorporated TCO.

Due to the promising pharmacokinetics of [^{18}F]AmBF$_3$-Tz *in vivo*, it is currently under investigation, as a standalone tracer for pretargeted PET imaging, as well as a universal tool for kit-like radiolabeling of various biomolecules, ushering the radiopharmaceutical field one step closer to rapid and affordable development of biological radiotracers.

REFERENCES

[1] E. di Martino, L. Smith, S.H. Bradley, S. Hemphill, J. Wright, C. Renzi, R. Bergin, J. Emery, R.D. Neal, Incidence trends for twelve cancers in younger adults-a rapid review, Brit J Cancer, (2022),10.1038/s41416-022-01704-x.

[2] R.L. Siegel, L.A. Torre, I. Soerjomataram, R.B. Hayes, F. Bray, T.K. Weber, A. Jemal, Global patterns and trends in colorectal cancer incidence in young adults, Gut, 68 (2019) 2179-2185,10.1136/gutjnl-2019-319511.

[3] T. Hussain, Q.T. Nguyen, Molecular imaging for cancer diagnosis and surgery, Adv Drug Deliv Rev, 66 (2014) 90-100,10.1016/j.addr.2013.09.007.

[4] C. Xu, H. Zhang, Somatostatin receptor based imaging and radionuclide therapy, Biomed Res Int, 2015 (2015) 917968,10.1155/2015/917968.

[5] E. Pauwels, F. Cleeren, G. Bormans, C.M. Deroose, Somatostatin receptor PET ligands - the next generation for clinical practice, Am J Nucl Med Mol Imaging, 8 (2018) 311-331

[6] W. Yang, J. Soares, P. Greninger, E.J. Edelman, H. Lightfoot, S. Forbes, N. Bindal, D. Beare, J.A. Smith, I.R. Thompson, S. Ramaswamy, P.A. Futreal, D.A. Haber, M.R. Stratton, C. Benes, U. McDermott, M.J. Garnett, Genomics of Drug Sensitivity in Cancer (GDSC): a resource for therapeutic biomarker discovery in cancer cells, Nucleic Acids Res, 41 (2013) D955-961,10.1093/nar/gks1111.

[7] E.A. Collisson, A. Sadanandam, P. Olson, W.J. Gibb, M. Truitt, S. Gu, J. Cooc, J. Weinkle, G.E. Kim, L. Jakkula, H.S. Feiler, A.H. Ko, A.B. Olshen, K.L. Danenberg, M.A. Tempero, P.T. Spellman, D. Hanahan, J.W. Gray, Subtypes of pancreatic ductal adenocarcinoma and their differing responses to therapy, Nat Med, 17 (2011) 500-503,10.1038/nm.2344.

[8] M. Jamous, U. Haberkorn, W. Mier, Synthesis of peptide radiopharmaceuticals for the therapy and diagnosis of tumor diseases, Molecules, 18 (2013) 3379-3409,10.3390/molecules18033379.

[9] M. Fani, H.R. Maecke, S.M. Okarvi, Radiolabeled peptides: valuable tools for the detection and treatment of cancer, Theranostics, 2 (2012) 481-501,10.7150/thno.4024.

[10] M.E. Phelps, Positron emission tomography provides molecular imaging of biological processes, Proc Natl Acad Sci U S A, 97 (2000) 9226-9233,10.1073/pnas.97.16.9226.

[11] O. Jacobson, D.O. Kiesewetter, X. Chen, Fluorine-18 radiochemistry, labeling strategies and synthetic routes, Bioconjug Chem, 26 (2015) 1-18,10.1021/bc500475e.

[12] P. Krecisz, K. Czarnecka, L. Krolicki, E. Mikiciuk-Olasik, P. Szymanski, Radiolabeled Peptides and Antibodies in Medicine, Bioconjug Chem, 32 (2021) 25-42,10.1021/acs.bioconjchem.0c00617.

[13] B.P. Burke, G.S. Clemente, S.J. Archibald, Boron-^{18}F containing positron emission tomography radiotracers: advances and opportunities, Contrast Media Mol I, 10 (2015) 96-110,10.1002/cmmi.1615.

[14] W.J. McBride, R.M. Sharkey, H. Karacay, C.A. D'Souza, E.A. Rossi, P. Laverman, C.H. Chang, O.C. Boerman, D.M. Goldenberg, A novel method of ^{18}F radiolabeling for PET, J Nucl Med, 50 (2009) 991-998,10.2967/jnumed.108.060418.

[15] L. Gower-Fry, T. Kronemann, A. Dorian, Y. Pu, C. Jaworski, C. Wangler, P. Bartenstein, L. Beyer, S. Lindner, K. Jurkschat, B. Wangler, J.J. Bailey, R. Schirrmacher, Recent Advances in the Clinical Translation of Silicon Fluoride Acceptor (SiFA) ^{18}F-Radiopharmaceuticals, Pharmaceuticals (Basel), 14 (2021),10.3390/ph14070701.

[16] H. Hong, L. Zhang, F. Xie, R. Zhuang, D. Jiang, H. Liu, J. Li, H. Yang, X. Zhang, L. Nie, Z. Li, Rapid one-step ^{18}F-radiolabeling of biomolecules in aqueous media by organophosphine fluoride acceptors, Nat Commun, 10 (2019) 989,10.1038/s41467-019-08953-0.

[17] H. Ilhan, A. Todica, S. Lindner, G. Boening, A. Gosewisch, C. Wangler, B. Wangler, R. Schirrmacher, P. Bartenstein, First-in-human ^{18}F-SiFAlin-TATE PET/CT for NET imaging and theranostics, Eur J Nucl Med Mol Imaging, 46 (2019) 2400-2401,10.1007/s00259-019-04448-8.

[18] S. Lindner, M. Simmet, F.J. Gildehaus, K. Jurkschat, C. Wangler, B. Wangler, P. Bartenstein, R. Schirrmacher, H. Ilhan, Automated production of [^{18}F]SiTATE on a Scintomics GRP platform for PET/CT imaging of neuroendocrine tumors, Nucl Med Biol, 88-89 (2020) 86-95,10.1016/j.nucmedbio.2020.07.008.

[19] H. Ilhan, S. Lindner, A. Todica, C.C. Cyran, R. Tiling, C.J. Auernhammer, C. Spitzweg, S. Boeck, M. Unterrainer, F.J. Gildehaus, G. Boning, K. Jurkschat, C. Wangler, B. Wangler, R. Schirrmacher, P. Bartenstein, Biodistribution and first clinical results of ^{18}F-SiFAlin-TATE PET: a novel ^{18}F-labeled somatostatin analog for imaging of neuroendocrine tumors, Eur J Nucl Med Mol Imaging, 47 (2020) 870-880,10.1007/s00259-019-04501-6.

[20] S. Niedermoser, J. Chin, C. Wangler, A. Kostikov, V. Bernard-Gauthier, N. Vogler, J.P. Soucy, A.J. McEwan, R. Schirrmacher, B. Wangler, In Vivo Evaluation of ^{18}F-SiFAlin-Modified TATE: A Potential Challenge for ^{68}Ga-DOTATATE, the Clinical Gold Standard for Somatostatin Receptor Imaging with PET, J Nucl Med, 56 (2015) 1100-1105,10.2967/jnumed.114.149583.

[21] J. Lau, J. Pan, E. Rousseau, C.F. Uribe, S.R. Seelam, B.W. Sutherland, D.M. Perrin, K.S. Lin, F. Benard, Pharmacokinetics, radiation dosimetry, acute toxicity and automated synthesis of [^{18}F]AmBF$_3$-TATE, EJNMMI Res, 10 (2020) 25,10.1186/s13550-020-0611-9.

[22] C.D. Anderson, The positive electron, American Institute of Physics, Lancaster, Pa, 1933.

[23] F.P. Jansen, J.L. Vanderheyden, The future of SPECT in a time of PET, Nucl Med Biol, 34 (2007) 733-735,10.1016/j.nucmedbio.2007.06.013.

[24] A. Rahmim, H. Zaidi, PET versus SPECT: strengths, limitations and challenges, Nuclear Medicine Communications, 29 (2008) 193-207,DOI 10.1097/MNM.0b013e3282f3a515.

[25] M. Conti, L. Eriksson, Physics of pure and non-pure positron emitters for PET: a review and a discussion, Ejnmmi Phys, 3 (2016),ARTN 8 10.1186/s40658-016-0144-5.

[26] M. Sergeev, M. Lazari, F. Morgia, J. Collins, M.R. Javed, O. Sergeeva, J. Jones, M.E. Phelps, J.T. Lee, P.Y. Keng, R.M. van Dam, Performing radiosynthesis in microvolumes to maximize molar activity of tracers for positron emission tomography, Commun Chem, 1 (2018),ARTN 10 10.1038/s42004-018-0009-z.

[27] C. Ebook Central Academic, Cyclotron produced radionuclides : emerging positron emitters for medical applications : ^{64}Cu and ^{124}I, International Atomic Energy Agency, Vienna, Austria, 2016.

[28] G.J. Kemerink, M.G. Visser, R. Franssen, E. Beijer, M. Zamburlini, S.G. Halders, B. Brans, F.M. Mottaghy, G.J. Teule, Effect of the positron range of ^{18}F, ^{68}Ga and ^{124}I on PET/CT in lung-equivalent materials, Eur J Nucl Med Mol Imaging, 38 (2011) 940-948,10.1007/s00259-011-1732-1.

[29] A. Vértes, A. Vértes, S. Nagy, Z. Klencsár, R.G. Lovas, F. Rösch, SpringerLink, Handbook of Nuclear Chemistry : Vol. 1: Basics of Nuclear Science; Vol. 2: Elements and Isotopes: Formation, Transformation, Distribution; Vol. 3: Chemical Applications of Nuclear Reactions and Radiation; Vol. 4: Radiochemistry and Radiopharmaceutical Chemistry in Life Sciences; Vol. 5: Instrumentation, Separation Techniques, Environmental Issues; Vol. 6: Nuclear Energy Production and Safety Issues, 2nd 2011. ed., Springer US : Imprint: Springer, New York, NY, 2011.

[30] B.K. Park, N.R. Kitteringham, P.M. O'Neill, Metabolism of fluorine-containing drugs, Annu Rev Pharmacol Toxicol, 41 (2001) 443-470,10.1146/annurev.pharmtox.41.1.443.

[31] J.P. Holland, Y. Sheh, J.S. Lewis, Standardized methods for the production of high specific-activity zirconium-89, Nucl Med Biol, 36 (2009) 729-739,10.1016/j.nucmedbio.2009.05.007.

[32] R. Halder, T. Ritter, ^{18}F-Fluorination: Challenge and Opportunity for Organic Chemists, Journal of Organic Chemistry, 86 (2021) 13873-13884,10.1021/acs.joc.1c01474.

[33] C.G. Zhan, D.A. Dixon, Hydration of the fluoride anion: Structures and absolute hydration free energy from first-principles electronic structure calculations, J Phys Chem A, 108 (2004) 2020-2029,10.1021/jp0311512.

[34] E.L. Cole, M.N. Stewart, R. Littich, R. Hoareau, P.J.H. Scott, Radiosyntheses using Fluorine-18: The Art and Science of Late Stage Fluorination, Current Topics in Medicinal Chemistry, 14 (2014) 875-900,Doi 10.2174/1568026614666140202205035.

[35] K. Bratteby, V. Shalgunov, M.M. Herth, Aliphatic ^{18}F-Radiofluorination: Recent Advances in the Labeling of Base-Sensitive Substrates*, ChemMedChem, 16 (2021) 2612-2622,10.1002/cmdc.202100303.

[36] K. Bratteby, V. Shalgunov, U.M. Battisti, I.N. Petersen, S.L. van den Broek, T. Ohlsson, N. Gillings, M. Erlandsson, M.M. Herth, Insights into Elution of Anion Exchange Cartridges: Opening the Path toward Aliphatic ^{18}F-Radiolabeling of Base-Sensitive Tracers, ACS Pharmacol Transl Sci, 4 (2021) 1556-1566,10.1021/acsptsci.1c00133.

[37] O. Keinanen, X.G. Li, N.K. Chenna, D. Lumen, J. Ott, C.F. Molthoff, M. Sarparanta, K. Helariutta, T. Vuorinen, A.D. Windhorst, A.J. Airaksinen, A New Highly Reactive and Low Lipophilicity Fluorine-18 Labeled Tetrazine Derivative for Pretargeted PET Imaging, ACS Med Chem Lett, 7 (2016) 62-66,10.1021/acsmedchemlett.5b00330.

[38] O. Keinanen, D. Partelova, O. Alanen, M. Antopolsky, M. Sarparanta, A.J. Airaksinen, Efficient cartridge purification for producing high molar activity [^{18}F]fluoro-glycoconjugates via oxime formation, Nucl Med Biol, 67 (2018) 27-35,10.1016/j.nucmedbio.2018.10.001.

[39] M. Reivich, D. Kuhl, A. Wolf, J. Greenberg, M. Phelps, T. Ido, V. Casella, J. Fowler, E. Hoffman, A. Alavi, P. Som, L. Sokoloff, The [^{18}F]fluorodeoxyglucose method for the measurement of local cerebral glucose utilization in man, Circ Res, 44 (1979) 127-137,10.1161/01.res.44.1.127.

[40] J.L. Zeng, J. Wang, J.A. Ma, New strategies for rapid ^{18}F-radiolabeling of biomolecules for radionuclide-based in vivo imaging, Bioconjug Chem, 26 (2015) 1000-1003,10.1021/acs.bioconjchem.5b00180.

[41] A.J. Airaksinen, The Radiopharmaceutical Chemistry of Fluorine-18: Next-Generation Fluorinations., in: Radiopharmaceutical Chemistry, Springer, Cham, 2019, pp. 297–310.

[42] B. Wangler, G. Quandt, L. Iovkova, E. Schirrmacher, C. Wangler, G. Boening, M. Hacker, M. Schmoeckel, K. Jurkschat, P. Bartenstein, R. Schirrmacher, Kit-like ^{18}F-labeling of proteins: synthesis of 4-(di-tert-butyl[^{18}F]fluorosilyl)benzenethiol (Si[^{18}F]FA-SH) labeled rat serum albumin for blood pool imaging with PET, Bioconjug Chem, 20 (2009) 317-321,10.1021/bc800413g.

[43] Z. Liu, M. Pourghiasian, M.A. Radtke, J. Lau, J. Pan, G.M. Dias, D. Yapp, K.S. Lin, F. Benard, D.M. Perrin, An organotrifluoroborate for broadly applicable one-step ^{18}F-labeling, Angew Chem Int Ed Engl, 53 (2014) 11876-11880,10.1002/anie.201406258.

[44] F. Basuli, X. Zhang, M.R. Williams, J. Seidel, M.V. Green, P.L. Choyke, R.E. Swenson, E.M. Jagoda, One-pot synthesis and biodistribution of fluorine-18 labeled serum albumin for vascular imaging, Nuclear Medicine and Biology, 62-63 (2018) 63-70,10.1016/j.nucmedbio.2018.05.004.

[45] B.J. Walter N., Drewes B., Bahutski V., Timmer M., Schütz M. B., Kramer F., Neumaier F., Endepols H., Neumaier B., Zlatopolskiy B. D., Convenient PET-tracer production via SuFEx 18F-fluorination of nanomolar precursor amounts, European Journal of Medicinal Chemistry, 237 (2022),10.1016/j.ejmech.2022.114383.

[46] S.H. Wessmann, G. Henriksen, H.J. Wester, Cryptate mediated nucleophilic ^{18}F-fluorination without azeotropic drying, Nuklearmed-Nucl Med, 51 (2012) 1-8,10.3413/Nukmed-0425-11-08.

[47] A.P. Kostikov, J. Chin, K. Orchowski, S. Niedermoser, M.M. Kovacevic, A. Aliaga, K. Jurkschat, B. Wangler, C. Wangler, H.J. Wester, R. Schirrmacher, Oxalic acid supported Si-^{18}F-radiofluorination: one-step radiosynthesis of N-succinimidyl 3-(di-tert-butyl[^{18}F]fluorosilyl)benzoate ([^{18}F]SiFB) for protein labeling, Bioconjug Chem, 23 (2012) 106-114,10.1021/bc200525x.

[48] L.O. Dialer, S.V. Selivanova, C.J. Muller, A. Muller, T. Stellfeld, K. Graham, L.M. Dinkelborg, S.D. Kramer, R. Schibli, M. Reiher, S.M. Ametamey, Studies toward the development of new silicon-containing building blocks for the direct ^{18}F-labeling of peptides, J Med Chem, 56 (2013) 7552-7563,10.1021/jm400857f.

[49] D.M. Perrin, [^{18}F]-Organotrifluoroborates as Radioprosthetic Groups for PET Imaging: From Design Principles to Preclinical Applications, Accounts Chem Res, 49 (2016) 1333-1343,10.1021/acs.accounts.5b00398.

[50] Q.H. Zheng, H.T. Xu, H. Wang, W.G.H. Du, N. Wang, H. Xiong, Y. Gu, L. Noodleman, K.B. Sharpless, G. Yang, P. Wu, Sulfur [^{18}F]Fluoride Exchange Click Chemistry Enabled Ultrafast Late-Stage Radiosynthesis, Journal of the American Chemical Society, 143 (2021) 3753-3763

[51] J.J. Dong, L. Krasnova, M.G. Finn, K.B. Sharpless, Sulfur(VI) Fluoride Exchange (SuFEx): Another Good Reaction for Click Chemistry, Angew Chem Int Edit, 53 (2014) 9430-9448,10.1002/anie.201309399.

[52] H.J. Wester, K. Hamacher, G. Stocklin, A comparative study of NCA fluorine-18 labeling of proteins via acylation and photochemical conjugation, Nuclear Medicine and Biology, 23 (1996) 365-372,Doi 10.1016/0969-8051(96)00017-0.

[53] O. Tietz, S.K. Sharma, J. Kaur, J. Way, A. Marshall, M. Wuest, F. Wuest, Synthesis of three ^{18}F-labelled cyclooxygenase-2 (COX-2) inhibitors based on a pyrimidine scaffold, Organic & Biomolecular Chemistry, 11 (2013) 8052-8064

[54] Y.S. Chang, J.M. Jeong, Y.S. Lee, H.W. Kim, G.B. Rai, S.J. Lee, D.S. Lee, J.K. Chung, M.C. Lee, Preparation of ^{18}F-human serum albumin: a simple and efficient protein labeling method with ^{18}F using a hydrazone-formation method, Bioconjug Chem, 16 (2005) 1329-1333,10.1021/bc050086r.

[55] G. Vaidyanathan, M.R. Zalutsky, Synthesis of N-succinimidyl 4-[^{18}F] fluorobenzoate, an agent for labeling proteins and peptides with ^{18}F-18, Nature Protocols, 1 (2006) 1655-1661

[56] R.A. Carboni, R.V. Lindsey, Reactions of Tetrazines with Unsaturated Compounds - a New Synthesis of Pyridazines, Journal of the American Chemical Society, 81 (1959) 4342-4346,DOI 10.1021/ja01525a060.

[57] B.L. Oliveira, Z. Guo, G.J.L. Bernardes, Inverse electron demand Diels-Alder reactions in chemical biology, Chem Soc Rev, 46 (2017) 4895-4950,10.1039/c7cs00184c.

[58] F. Karaki, T. Kiguchi, K. Itoh, N. Sato, K. Konishi, H. Fujii, Catalyst-free photooxidation reaction from 1,4-dihydropyridazine to pyridazine under air, Tetrahedron, 97 (2021),ARTN 132411
10.1016/j.tet.2021.132411.

[59] A. Darko, S. Wallace, O. Dmitrenko, M.M. Machovina, R.A. Mehl, J.W. Chin, J.M. Fox, Conformationally Strained trans-Cyclooctene with Improved Stability and Excellent Reactivity in Tetrazine Ligation, Chem Sci, 5 (2014) 3770-3776,10.1039/C4SC01348D.

[60] B.M. Zeglis, K.K. Sevak, T. Reiner, P. Mohindra, S.D. Carlin, P. Zanzonico, R. Weissleder, J.S. Lewis, A pretargeted PET imaging strategy based on bioorthogonal Diels-Alder click chemistry, J Nucl Med, 54 (2013) 1389-1396,10.2967/jnumed.112.115840.

[61] R. Rossin, S.M. van den Bosch, W. Ten Hoeve, M. Carvelli, R.M. Versteegen, J. Lub, M.S. Robillard, Highly reactive trans-cyclooctene tags with improved stability for Diels-Alder chemistry in living systems, Bioconjug Chem, 24 (2013) 1210-1217,10.1021/bc400153y.

[62] C. Denk, D. Svatunek, T. Filip, T. Wanek, D. Lumpi, J. Frohlich, C. Kuntner, H. Mikula, Development of a ^{18}F-labeled tetrazine with favorable pharmacokinetics for bioorthogonal PET imaging, Angew Chem Int Ed Engl, 53 (2014) 9655-9659,10.1002/anie.201404277.

[63] E.J.L. Steen, J.T. Jorgensen, C. Denk, U.M. Battisti, K. Norregaard, P.E. Edem, K. Bratteby, V. Shalgunov, M. Wilkovitsch, D. Svatunek, C.B.M. Poulie, L. Hvass, M. Simon, T. Wanek, R. Rossin, M. Robillard, J.L. Kristensen, H. Mikula, A. Kjaer, M.M. Herth, Lipophilicity and Click Reactivity Determine the Performance of Bioorthogonal Tetrazine Tools in Pretargeted In Vivo Chemistry, ACS Pharmacol Transl Sci, 4 (2021) 824-833,10.1021/acsptsci.1c00007.

[64] G.J. Quinlan, G.S. Martin, T.W. Evans, Albumin: Biochemical properties and therapeutic potential, Hepatology, 41 (2005) 1211-1219,10.1002/hep.20720.

[65] J.P. Nicholson, M.R. Wolmarans, G.R. Park, The role of albumin in critical illness, Brit J Anaesth, 85 (2000) 599-610,DOI 10.1093/bja/85.4.599.

[66] S. Jeger, K. Zimmermann, A. Blanc, J. Grunberg, M. Honer, P. Hunziker, H. Struthers, R. Schibli, Site-specific and stoichiometric modification of antibodies by bacterial transglutaminase, Angew Chem Int Ed Engl, 49 (2010) 9995-9997,10.1002/anie.201004243.

[67] A. Fontana, B. Spolaore, A. Mero, F.M. Veronese, Site-specific modification and PEGylation of pharmaceutical proteins mediated by transglutaminase, Adv Drug Deliv Rev, 60 (2008) 13-28,10.1016/j.addr.2007.06.015.

[68] G. Niu, L. Lang, D.O. Kiesewetter, Y. Ma, Z. Sun, N. Guo, J. Guo, C. Wu, X. Chen, In Vivo Labeling of Serum Albumin for PET, J Nucl Med, 55 (2014) 1150-1156,10.2967/jnumed.114.139642.

[69] H.W. Hong, L. Zhang, F. Xie, R.Q. Zhuang, D.L. Jiang, H.H. Liu, J.D. Li, H.Z. Yang, X.Z. Zhang, L.M. Nie, Z.J. Li, Rapid one-step ^{18}F-radiolabeling of biomolecules in aqueous media by organophosphine fluoride acceptors, Nature Communications, 10 (2019),ARTN 989 10.1038/s41467-019-08953-0.

[70] K.G. Mountjoy, L.S. Robbins, M.T. Mortrud, R.D. Cone, The cloning of a family of genes that encode the melanocortin receptors, Science, 257 (1992) 1248-1251,10.1126/science.1325670.

[71] I. Gantz, Y. Konda, T. Tashiro, Y. Shimoto, H. Miwa, G. Munzert, S.J. Watson, J. DelValle, T. Yamada, Molecular cloning of a novel melanocortin receptor, J Biol Chem, 268 (1993) 8246-8250

[72] C. Zhang, Z. Zhang, K.S. Lin, J. Lau, J. Zeisler, N. Colpo, D.M. Perrin, F. Benard, Melanoma Imaging Using ^{18}F-Labeled alpha-Melanocyte-Stimulating Hormone Derivatives with Positron Emission Tomography, Mol Pharm, 15 (2018) 2116-2122,10.1021/acs.molpharmaceut.7b01113.

[73] C. Fottner, M. Ferrata, M.M. Weber, Hormone secreting gastro-entero-pancreatic neuroendocrine neoplasias (GEP-NEN): When to consider, how to diagnose?, Rev Endocr Metab Disord, 18 (2017) 393-410,10.1007/s11154-017-9438-8.

[74] R.P. Baum, A.K. Kluge, H.R. Kulkarni, M. Sayeg, U. Schorr-Neufing, K. Niepsch, N. Bitterlich, C.J.A. Van Echteld, [^{177}Lu-DOTA]-D-Phe1-Tyr3-octreotide (^{177}Lu-DOTATOC) for peptide receptor radiotherapy in patients with advanced neuroendocrine tumours: A retrospective phase II study of efficacy and safety, European Journal of Cancer, 51 (2015) S422-S423,Doi 10.1016/S0959-8049(16)31185-6.

[75] C.C. Zhang, Z.X. Zhang, K.S. Lin, J. Lau, J. Zeisler, N. Colpo, D.M. Perrin, F. Benard, Melanoma Imaging Using ^{18}F-Labeled alpha-Melanocyte-Stimulating Hormone Derivatives with Positron Emission Tomography, Mol Pharmaceut, 15 (2018) 2116-2122,10.1021/acs.molpharmaceut.7b01113.

[76] Z. Liu, M. Pourghiasian, F. Benard, J. Pan, K.S. Lin, D.M. Perrin, Preclinical evaluation of a high-affinity ^{18}F-trifluoroborate octreotate derivative for somatostatin receptor imaging, J Nucl Med, 55 (2014) 1499-1505,10.2967/jnumed.114.137836.

[77] C. Zhang, Z. Zhang, H. Merkens, J. Zeisler, N. Colpo, N. Hundal-Jabal, D.M. Perrin, K.S. Lin, F. Benard, ^{18}F-Labeled Cyclized alpha-Melanocyte-Stimulating Hormone Derivatives for Imaging Human Melanoma Xenograft with Positron Emission Tomography, Sci Rep, 9 (2019) 13575,10.1038/s41598-019-50014-5.

[78] S.R. Dubash, Clinical translation of a 'click' labeled ^{18}F-octreotate radioligand for imaging neuroendocrine tumors., Journal of Clinical Oncology, 34 (2016),10.1200/JCO.2016.34.15_suppl.e15645.

[79] P. Laverman, W.J. McBride, R.M. Sharkey, A. Eek, L. Joosten, W.J. Oyen, D.M. Goldenberg, O.C. Boerman, A novel facile method of labeling octreotide with ^{18}F-fluorine, J Nucl Med, 51 (2010) 454-461,10.2967/jnumed.109.066902.

[80] T. Tshibangu, C. Cawthorne, K. Serdons, E. Pauwels, W. Gsell, G. Bormans, C.M. Deroose, F. Cleeren, Automated GMP compliant production of [^{18}F]AlF-NOTA-octreotide, EJNMMI Radiopharm Chem, 5 (2020) 4,10.1186/s41181-019-0084-1.

[81] P. Laverman, C.A. D'Souza, A. Eek, W.J. McBride, R.M. Sharkey, W.J. Oyen, D.M. Goldenberg, O.C. Boerman, Optimized labeling of NOTA-conjugated octreotide with ^{18}F, Tumour Biol, 33 (2012) 427-434,10.1007/s13277-011-0250-x.

[82] F. Cleeren, J. Lecina, E.M. Billaud, M. Ahamed, A. Verbruggen, G.M. Bormans, New Chelators for Low Temperature Al^{18}F-Labeling of Biomolecules, Bioconjug Chem, 27 (2016) 790-798,10.1021/acs.bioconjchem.6b00012.

[83] J. Leyton, L. Iddon, M. Perumal, B. Indrevoll, M. Glaser, E. Robins, A.J. George, A. Cuthbertson, S.K. Luthra, E.O. Aboagye, Targeting somatostatin receptors: preclinical evaluation of novel ^{18}F-fluoroethyltriazole-Tyr^3-octreotate analogs for PET, J Nucl Med, 52 (2011) 1441-1448,10.2967/jnumed.111.088906.

[84] S. Maschauer, M. Heilmann, C. Wangler, R. Schirrmacher, O. Prante, Radiosynthesis and Preclinical Evaluation of ^{18}F-Fluoroglycosylated Octreotate for Somatostatin Receptor Imaging, Bioconjugate Chem, 27 (2016) 2707-2714.

[85] B. Shaker, S. Ahmad, J. Lee, C. Jung, D. Na, In silico methods and tools for drug discovery, Comput Biol Med, 137 (2021) 104851,10.1016/j.compbiomed.2021.104851.

[86] P. Uhl, G. Fricker, U. Haberkorn, W. Mier, Radionuclides in drug development, Drug Discov Today, 20 (2015) 198-208,10.1016/j.drudis.2014.09.027.

[87] N. Penner, L. Xu, C. Prakash, Radiolabeled absorption, distribution, metabolism, and excretion studies in drug development: why, when, and how?, Chem Res Toxicol, 25 (2012) 513-531,10.1021/tx300050f.

[88] B. Kluger, C. Bueschl, N. Neumann, R. Stuckler, M. Doppler, A.W. Chassy, A.L. Waterhouse, J. Rechthaler, N. Kampleitner, G.G. Thallinger, G. Adam, R. Krska, R. Schuhmacher, Untargeted Profiling of Tracer-Derived Metabolites Using Stable Isotopic Labeling and Fast Polarity-Switching LC-ESI-HRMS, Anal Chem, 86 (2014) 11533-11537,10.1021/ac503290j.

[89] J. Keller, M. Baradat, I. Jouanin, L. Debrauwer, F. Gueraud, "Twin peaks": Searching for 4-hydroxynonenal urinary metabolites after oral administration in rats, Redox Biol, 4 (2015) 136-148,10.1016/j.redox.2014.12.016.

[90] A. Johansen, H.D. Hansen, C. Svarer, S. Lehel, S. Leth-Petersen, J.L. Kristensen, N. Gillings, G.M. Knudsen, The importance of small polar radiometabolites in molecular neuroimaging: A PET study with [^{11}C]Cimbi-36 labeled in two positions, J Cerebr Blood F Met, 38 (2018) 659-668,10.1177/0271678x17746179.

[91] J. Münch, P. Püllmann, W. Zhang, M.J. Weissenborn, Enzymatic Hydroxylations of sp^3-Carbons, ACS Catalysis, 11 (2021) 9168-9203,10.1021/acscatal.1c00759.

[92] Q. Huang, X. Zhang, Q. Chen, S. Tian, W. Tong, W. Zhang, Y. Chen, M. Ma, B. Chen, B. Wang, J.-b. Wang, Discovery of a P450-Catalyzed Oxidative Defluorination Mechanism toward Chiral Organofluorines: Uncovering a Hidden Pathway, ACS Catalysis, 12 (2022) 265-272,10.1021/acscatal.1c05510.

[93] M. Kuchar, C. Mamat, Methods to Increase the Metabolic Stability of (18)F-Radiotracers, Molecules, 20 (2015) 16186-16220,10.3390/molecules200916186.

[94] M. Piert, T.T. Zittel, G.A. Becker, M. Jahn, A. Stahlschmidt, G. Maier, H.J. Machulla, R. Bares, Assessment of porcine bone metabolism by dynamic [^{18}F]fluoride ion PET: Correlation with bone histomorphometry, Journal of Nuclear Medicine, 42 (2001) 1091-1100

[95] L.O. Dialer, S.V. Selivanova, C.J. Muller, A. Muller, T. Stellfeld, K. Graham, L.M. Dinkelborg, S.D. Kramer, R. Schibli, M. Reiher, S.M. Ametamey, Studies toward the Development of New Silicon-Containing Building Blocks for the Direct ^{18}F-Labeling of Peptides, Journal of Medicinal Chemistry, 56 (2013) 7552-7563,10.1021/jm400857f.

[96] R. Schirrmacher, G. Bradtmoller, E. Schirrmacher, O. Thews, J. Tillmanns, T. Siessmeier, H.G. Buchholz, P. Bartenstein, B. Wangler, C.M. Niemeyer, K. Jurkschat, ^{18}F-labeling of peptides by means of an organosilicon-based fluoride acceptor, Angew Chem Int Ed Engl, 45 (2006) 6047-6050,10.1002/anie.200600795.

[97] A. Hohne, L. Yu, L.J. Mu, M. Reiher, U. Voigtmann, U. Klar, K. Graham, P.A. Schubiger, S.M. Ametamey, Organofluorosilanes as Model Compounds for ^{18}F-Labeled Silicon-Based PET Tracers and their Hydrolytic Stability: Experimental Data and Theoretical Calculations (PET = Positron Emission Tomography), Chem-Eur J, 15 (2009) 3736-3743,10.1002/chem.200802437.

[98] C. Gonzalez, A. Sanchez, J. Collins, K. Lisova, J.T. Lee, R. Michael van Dam, M. Alejandro Barbieri, C. Ramachandran, S.F. Wnuk, The 4-N-acyl and 4-N-alkyl gemcitabine analogues with silicon-fluoride-acceptor: Application to ^{18}F-Radiolabeling, Eur J Med Chem, 148 (2018) 314-324,10.1016/j.ejmech.2018.02.017.

[99] Y. Joyard, R. Azzouz, L. Bischoff, C. Papamicael, D. Labar, A. Bol, V. Bol, P. Vera, V. Gregoire, V. Levacher, P. Bohn, Synthesis of new ^{18}F-radiolabeled silicon-based nitroimidazole compounds, Bioorg Med Chem, 21 (2013) 3680-3688,10.1016/j.bmc.2013.04.029.

[100] S. Niedermoser, J. Chin, C. Wangler, A. Kostikov, V. Bernard-Gauthier, N. Vogler, J.P. Soucy, A.J. McEwan, R. Schirrmacher, B. Wangler, In Vivo Evaluation of ^{18}F-SiFAlin-Modified TATE: A Potential Challenge for ^{68}Ga-DOTATATE, the Clinical Gold Standard for Somatostatin Receptor Imaging with PET, Journal of Nuclear Medicine, 56 (2015) 1100-1105.

[101] Y. Li, Z. Liu, C.W. Harwig, M. Pourghiasian, J. Lau, K.S. Lin, P. Schaffer, F. Benard, D.M. Perrin, ^{18}F-click labeling of a bombesin antagonist with an alkyne-^{18}F-ArBF_3: in vivo PET imaging of tumors expressing the GRP-receptor, Am J Nucl Med Mol Imaging, 3 (2013) 57-70.

[102] J. Zhu, S. Li, C. Wangler, B. Wangler, R.B. Lennox, R. Schirrmacher, Synthesis of 3-chloro-6-((4-(di-tert-butyl[^{18}F]-fluorosilyl)-benzyl)oxy)-1,2,4,5-tetrazine ([^{18}F]SiFA-OTz) for rapid tetrazine-based ^{18}F-radiolabeling, Chem Commun, 51 (2015) 12415-12418,10.1039/c5cc03623b.

[103] Z. Liu, K.S. Lin, F. Benard, M. Pourghiasian, D.O. Kiesewetter, D.M. Perrin, X. Chen, One-step ^{18}F labeling of biomolecules using organotrifluoroborates, Nat Protoc, 10 (2015) 1423-1432,10.1038/nprot.2015.090.

[104] M. Pourghiasian, Z. Liu, J. Pan, Z. Zhang, N. Colpo, K.S. Lin, D.M. Perrin, F. Benard, ^{18}F-AmBF_3-MJ9: a novel radiofluorinated bombesin derivative for prostate cancer imaging, Bioorg Med Chem, 23 (2015) 1500-1506,10.1016/j.bmc.2015.02.009.

[105] A. Roxin, C. Zhang, S. Huh, M. Lepage, Z. Zhang, K.S. Lin, F. Benard, D.M. Perrin, A Metal-Free DOTA-Conjugated ^{18}F-Labeled Radiotracer: [^{18}F]DOTA-AMBF_3-LLP2A for Imaging VLA-4 Over-Expression in Murine Melanoma with Improved Tumor Uptake and Greatly Enhanced Renal Clearance, Bioconjug Chem, 30 (2019) 1210-1219,10.1021/acs.bioconjchem.9b00146.

[106] A. Roxin, C. Zhang, S. Huh, M.L. Lepage, Z. Zhang, K.S. Lin, F. Benard, D.M. Perrin, Preliminary evaluation of ^{18}F-labeled LLP2A-trifluoroborate conjugates as VLA-4 (α_4 β_1 integrin) specific radiotracers for PET imaging of melanoma, Nucl Med Biol, 61 (2018) 11-20,10.1016/j.nucmedbio.2018.02.005.

[107] D. Kwon, J. Lozada, Z. Zhang, J. Zeisler, R. Poon, C. Zhang, A. Roxin, K.S. Lin, D. Perrin, F. Benard, High-Contrast CXCR4-Targeted ^{18}F-PET Imaging Using a Potent and Selective Antagonist, Mol Pharm, 18 (2021) 187-197,10.1021/acs.molpharmaceut.0c00785.

[108] A.C. Knall, C. Slugovc, Inverse electron demand Diels-Alder (iEDDA)-initiated conjugation: a (high) potential click chemistry scheme, Chem Soc Rev, 42 (2013) 5131-5142,10.1039/c3cs60049a.

[109] M. Jiang, Y. Li, H.J. Yang, R.L. Zong, Y.H. Jin, H. Fu, Metal-free UV-Vis-light-induced aerobic oxidative hydroxylation of arylboronic acids in the absence of a photosensitizer, Rsc Advances, 4 (2014) 12977-12980,10.1039/c3ra46516k.

[110] R. Selvaraj, B. Giglio, S.L. Liu, H. Wang, M.Z. Wang, H. Yuan, S.R. Chintala, L.P. Yap, P.S. Conti, J.M. Fox, Z.B. Li, Improved Metabolic Stability for ^{18}F PET Probes Rapidly Constructed via Tetrazine trans-Cyclooctene Ligation, Bioconjugate Chem, 26 (2015) 435-442,10.1021/acs.bioconjchem.5b00089.

[111] K. Lisova, M. Sergeev, S. Evans-Axelsson, A.D. Stuparu, S. Beykan, J. Collins, J. Jones, M. Lassmann, K. Herrmann, D. Perrin, J.T. Lee, R. Slavik, R.M. van Dam, Microscale radiosynthesis, preclinical imaging and dosimetry study of [^{18}F]AMBF$_3$-TATE: A potential PET tracer for clinical imaging of somatostatin receptors, Nucl Med Biol, 61 (2018) 36-44,10.1016/j.nucmedbio.2018.04.001.

[112] Y. Matsumura, H. Maeda, A new concept for macromolecular therapeutics in cancer chemotherapy: mechanism of tumoritropic accumulation of proteins and the antitumor agent smancs, Cancer Res, 46 (1986) 6387-6392

[113] D.S. Bohle, Z. Chua, I. Perepichka, K. Rosadiuk, E/Z Oxime Isomerism in PhC(NOH)CN, Chem-Eur J, 19 (2013) 4223-4229

[114] S. Samanta, S. Ray, A.B. Ghosh, P. Biswas, 3,6-Di(pyridin-2-yl)-1,2,4,5-tetrazine (pytz) mediated metal-free mild oxidation of thiols to disulfides in aqueous medium, Rsc Advances, 6 (2016) 39356-39363,10.1039/c6ra01509c.

[115] L. Fritea, P. Audebert, L. Galmiche, K. Gorgy, A. Le Goff, R. Villalonga, R. Sandulescu, S. Cosnier, First Occurrence of Tetrazines in Aqueous Solution: Electrochemistry and Fluorescence, Chemphyschem, 16 (2015) 3695-3699,10.1002/cphc.201500544.

[116] A. Lundahl, M. Hedeland, U. Bondesson, H. Lennernas, In Vivo Investigation in Pigs of Intestinal Absorption, Hepatobiliary Disposition, and Metabolism of the 5 alpha-Reductase Inhibitor Finasteride and the Effects of Coadministered Ketoconazole, Drug Metabolism and Disposition, 39 (2011) 847-857,10.1124/dmd.110.035311.

[117] M.L. Tang, L. Zhou, J. Chang, Z.H. Hu, Y. Qin, X. Sun, Differential metabolism of 3FDT and docetaxel in RLMs, rats, and HLMs, European Journal of Medicinal Chemistry, 113 (2016) 81-91,10.1016/j.ejmech.2016.02.007.

[118] D.M. Conning, J.C. Phillips, Comparative Metabolism of Bha, Bht and Other Phenolic Antioxidants and Its Toxicological Relevance, Food Chem Toxicol, 24 (1986) 1145-1148,Doi 10.1016/0278-6915(86)90300-5.